Seismic Design of Energy Dissipation Systems for Optimal Structural Performance

Luis M. Moreschi

Dissertation submitted to the Faculty of the
Virginia Polytechnic Institute and State University
in partial fulfillment of the requirements for the degree of

Doctor of Philosophy
in
Engineering Mechanics

Mahendra P. Singh, Chair
Romesh C. Batra
David. Y. Gao
Muhammad R. Hajj
Scott L. Hendricks

July, 2000
Blacksburg, Virginia

Keywords: Passive Control, Seismic Design, Structural Optimization, Genetic Algorithms

Seismic Design of Energy Dissipation Systems for Optimal Structural Performance

Luis M. Moreschi

(ABSTRACT)

The usefulness of supplementary energy dissipation devices is now quite well-known in the earthquake structural engineering community for reducing the earthquake-induced response of structural systems. However, systematic design procedures for optimal sizing and placement of these protective systems in structural systems are needed and are not yet available. The main objective of this study is, therefore, to formulate a general framework for the optimal design of passive energy dissipation systems for seismic structural applications. The following four types passive energy dissipation systems have been examined in the study: (1) viscous fluid dampers, (2) viscoelastic dampers, (3) yielding metallic dampers and, (4) friction dampers. For each type of energy dissipation system, the study presents the (a) formulation of the optimal design problem, (b) consideration of several meaningful performance indices, (c) analytical and numerical procedures for seismic response and performance indices calculations, (d) procedures for obtaining the optimal design by an appropriate optimization scheme and, (e) numerical results demonstrating the effectiveness of the procedures and the optimization-based design approach.

For building structures incorporating linear damping devices, such as fluid and solid viscoelastic dampers, the seismic response and performance evaluations are done by a random vibration approach for a stochastic characterization of the earthquake induced ground motion. Both the gradient projection technique and genetic algorithm approach can be conveniently employed to determine the required amount of damping material and its optimal distribution within a building structure to achieve a desired performance criterion. An approach to evaluate the sensitivity of the optimum solution and the performance function with respect to the problem

parameters is also described. Several sets of numerical results for different structural configurations and for different performance indices are presented to demonstrate the effectiveness and applicability of the approach.

For buildings installed with nonlinear hysteretic devices, such as yielding metallic elements or friction dampers, the computation of the seismic structural response and performance must be performed by time history analysis. For such energy dissipation devices, the genetic algorithm is more convenient to solve the optimal design problem. It avoids the convergence to a local optimal solution. To formulate the optimization problem within the framework of the genetic algorithm, the study presents the discretization procedures for various parameters of these nonlinear energy dissipation devices. To include the uncertainty about the seismic input motion in the search for optimal design, an ensemble of artificially generated earthquake excitations are considered. The similarities of the optimal design procedure with yielding metallic devices and friction devices are clearly established. Numerical results are presented to illustrate the applicability of the proposed optimization-based approach for different forms of performance indices and types of building structures.

To my family in Argentina. To my family in Puerto Rico. To Aura and Rodrigo.

Acknowledgements

In the first place, I would like to give special thanks to my advisor Dr. M. P. Singh for his invaluable technical guidance and advice throughout my doctoral studies.

I would also like to express my appreciation to Dr. D. Y. Gao for sharing his brilliant thoughts and ideas. Thanks also to Dr. R. C. Batra, Dr. M. Hajj, and Dr. S. L. Hendricks for kindly serving in my committee and giving their valuable time to read this manuscript.

I am grateful to Loretta Tickle for her help with all administrative matters. Thanks to Christopher Bonadeo for facilitating the use of an entire computer laboratory to run some of the numerical simulations required in this dissertation.

I would like to thank all the people and friends I have met in Blacksburg during these years, specially to the members of the walleyball team, Raul, Aida, Tatiana, Virgilio, Diana and Azahar. I would also like to express my gratitude to Gustavo and Virna Molina, Sergio and Sandra Preidikman, Sarbjeet Singh, Luis Suárez, Alicia Almada, Ricardo and Cathia Burdisso, and Enrique and Yazmin Matheu. I will always treasure the moments shared during the past few years.

I am also particularly appreciative of the support and encouragement of my father José Luis, my sister Adriana and my brothers Gastón and Ariel. Mamá, you have always been at my side. Thanks to the Vallecillo-Moreschi family, in special to my aunt Monona, and to my parents in law Ivén, Aury and to my sister in law Aurimar. Heartfelt thanks to my friends Carlos, Daniel, Mario and Paco.

Most importantly, I would like to thank my wife Aura. This work would not have been possible without her love, patience and constant support.

This research was supported by the National Science Foundation through Grant No. CMS-9626850. This support is gratefully acknowledged.

Contents

List of Tables

List of Figures

Chapter 1

Introduction

1.1 Passive Control of Civil Structures

A large amount of energy is imparted into a structure during earthquake ground motions. Conventional design philosophy seeks to prevent collapse by allowing structural members to absorb and dissipate the transmitted earthquake energy by inelastic cyclic deformations in specially detailed regions. As sketched in Figure 1.1, this strategy implies that some damage may occur, possibly to the extent that the structure is no longer repairable.

In the last two decades, special protective systems have been developed to enhance safety and reduce damage of structures during earthquakes. These alternative approaches aim to control the structural seismic response and energy dissipation demand on the structural members by modifying the dynamic properties of the system.

Currently, the most practical and reliable method of reducing seismic structural response is the use of passive response control systems. They can be classified according to the approaches employed to manage the input earthquake energy as [32; 87; 165]: (1) seismic isolation systems and, (2) passive energy dissipation systems.

The seismic isolation systems, illustrated in Figure 1.2(a), deflect or filter out the earthquake energy by interposing a layer with low horizontal stiffness between the structure and the foundation. These schemes are suitable for a large class of structures that are short to medium height, and whose dominant modes are within a certain frequency range. Several building and bridges have now been installed with base isolation systems [95; 163]. The passive

energy dissipation systems, on the other hand, act as energy sinks and absorb some of the vibration energy so that less is available to cause deformation of structural elements. They consist of strategically placed dampers (viscous, viscoelastic or friction dampers) or replaceable yielding elements that link various parts of the framing system, as portrayed in Figure 1.2(b). Dynamic vibration absorbers also belong to this category. The reduction in the structural response is accomplished by transferring some of the structural vibration energy to auxiliary oscillators attached to the main structure. Figure 1.2(c) shows a typical implementation of a tuned mass damper in a building structure.

Highly convincing analytical and experimental studies performed on these protective systems strongly affirm their suitability for applications in structures subjected to seismic disturbances [35; 71; 72; 77]. These passive devices have been shown to be reliable and sturdy for implementation. The formulation of design guidelines and building code requirements for structural implementation of energy dissipation devices has been significant in promoting the use of this emerging technology [43; 191]. The professionals involved in the seismic design of structures have started to feel comfortable with their use in practice. As such, they are being considered for the design of new structures as well as for retrofitting a large inventory of existing deficient structures. More will be said about the passive control devices to be considered in this study in a later section.

1.2 Research Motivation, Objectives, and Scope

Analytical methods are now available to analyze and evaluate structures installed with these devices. However, to design a structure with energy dissipation devices, that is to calculate the required size of a device to achieve a desired response reduction, or to extract a desired performance at a certain design intensity level of earthquake motion is not a trivial task. Furthermore, to get the most out of a device, the optimal decisions about its placement location and its size are quite important. Even with linear energy dissipation devices such as viscous or viscoelastic dampers, the optimal placement and sizing of the devices is not a straightforward task. That is, it is difficult to calculate the size and placement of a linear device to achieve a desired performance; such procedures are necessarily iterative and based on trial and error.

Some of the passive devices possess highly nonlinear hysteretic characteristics. Their installation in a structure would render it to behave nonlinearly even if all other structural members were designed to remain linear. For such devices, the design procedure becomes very complex, and remains highly iterative.

Obviously, there is a need to develop systematic and quantitative approaches to popularize the use of these very effective devices in the practice of earthquake structural engineering. With the currently available computing facilities and developments in the area of structural optimization, it now seems quite possible to design building structures installed with supplemental passive devices in an optimal manner. Also, it is quite important to know the sensitivity of an optimal design with respect to the design input and system parameter, as these parameters can vary in practice. This calls for an investigation of the post-optimal design analysis. This study is planned to address these important research issues in a comprehensive manner.

The main objective of this research is, thus, to formulate a general framework for the optimal design of passive energy dissipation devices for seismic structural applications. The methods will be developed to determine the optimum size and optimum placement location of the chosen protective systems within a building structure. The sensitivity of the optimal design solution to changes in the parameters of the problem will also be investigated by post-optimality analysis methods.

Four different types of energy dissipation systems have been selected for study in this research. They are viscous dampers, viscoelastic dampers, yielding metallic dampers, and friction dampers. The special characteristics of these systems, along with special research issues involved in the their optimal design are briefly described in the following sections. The research activities to achieve the objectives involve the following steps:

- Specialization of the general optimization-based framework for the design of each of the selected protective systems.
- Development and implementation of accurate and efficient analytical and numerical techniques for seismic response calculations of structural systems installed with energy dissipation systems.

- Establishment of meaningful performance indices to measure the improvement in the seismic structural performance.
- Use of suitable optimization procedures to obtain the optimal design solution.

1.3 Passive Energy Dissipation Systems to be Considered

The passive energy dissipation systems that will be considered for their optimal design in this study are: viscous fluid and viscoelastic dampers, friction dampers, and yielding metallic devices. Each of these passive devices has its own attributes and limitations. The design of these devices is strongly affected by their force-deformation characteristics and those of the building structure in which they are installed. Normally structural system designed according to current code provisions will go in the inelastic range when subjected to the design level ground motion. However, to avoid damage associated with inelastic behavior, the added damping devices may be designed such that the main structural elements (beams and columns) remain elastic. In this study, it will be assumed that the addition of passive devices to the framing system allows the main structural elements to remain within their elastic range of action and free of damage under earthquake disturbances. Commonly used force-deformation models as well as some refined models will be considered to represent the behavior of the different protective systems.

In the sequel, a brief description of the passive energy dissipation devices to be considered in this study is presented. The research issues relevant to their optimal use for seismic design of building structures are also highlighted.

1.3.1 Viscoelastic Devices

Fluid Viscoelastic Devices: These devices, originally used as shock and vibration isolation systems in the aerospace and automotive industries, operate on the principle of resistance of a viscous fluid to flow through a constrained opening. The input energy is dissipated by viscous heating due to the friction between fluid particles and device components [106; 107; 114]. Different viscous materials have been considered to enhance stiffness and damping properties of the main structure [36; 128; 137; 185]. Viscous fluid dampers can be designed to have linear or

nonlinear viscous behavior [155; 177], and be insensitive to significant temperature changes. Another advantage attributed to the viscous fluid dampers is that their viscous forces are out of phase with other displacement dependent forces, and do not directly add to the maximum forces developed in the main structural elements. This is a desirable attribute since it prevents the possibility of compression failure of weak columns in retrofit applications using viscous fluid dampers [33; 147].

Different mathematical models have been proposed to predict the behavior of these devices. A classical Maxwell model, in which dashpot and spring elements are joined in series, is adequate to capture the dependence of the mechanical properties of the viscous devices on the deformation frequency throughout the frequency range of interest [34]. A generalized Maxwell model has also been proposed based on the concept of fractional-derivative [108-112]. However, for typical structural applications the viscous fluid damper can be modeled as a simple dashpot element in which the damping force is directly proportional to the velocity of the piston.

Solid Viscoelastic Devices: Typical viscoelastic dampers consist of polymeric material layers bonded between steel plates. These devices are designed to dissipate vibration energy in the form of heat when subjected to cyclic shear deformations. Viscoelastic dampers have been successfully employed to suppress wind-induced response in high-rise buildings [94; 104]. Recently, further analytical and experimental studies have demonstrated the effectiveness of viscoelastic dampers in reducing seismic structural response over a wide range of operating conditions [17; 20; 71; 78; 86; 153; 179; 199]. Viscoelastic dampers have been proposed and used to retrofit buildings against earthquakes [38; 73; 91; 141] and in the construction of new facilities [42; 121].

Extensive tests have now been conducted on these dampers to define their force-deformation and their energy dissipation characteristics [3; 11; 22; 24; 52; 74; 99; 101; 102]. The mechanical properties of viscoelastic polymers are rather complex and depend on different factors. The effect of the ambient temperature and temperature rise within the viscoelastic material due to cyclic motion has been investigated and quantified [4; 23; 180]. The dependence of the stiffness and damping properties of the viscoelastic devices on the excitation frequency and shear strain has been considered with different levels of accuracy and sophistication.

Several authors have addressed the modeling problem by considering Kelvin-Voight, Maxwell and linear-hysteretic elements [79; 81; 82; 84; 105; 113]. The concepts of fractional derivatives [8; 93; 181], and Boltzman superposition principle [156], have also been proposed to predict the dampers behavior. Although these refined models can serve a very useful purpose in research applications, simplified models are necessary for usual design implementations. In this regard, the development of practical design guidelines and procedures concerning the implementation of viscoelastic devices for structural seismic performance enhancement have received the attention of researchers and the engineering professionals [1; 21; 92; 157].

Optimization of Structures with Supplemental Viscous and Viscoelastic Devices: In the past, several studies have been concerned with the problem of optimal distribution of viscous and viscoelastic materials for noise and vibration problems in engineering. Earlier attempts considered different classes of distributed parameters systems such as beams [41], and vibrating frames [103]. For linear MDOF systems, the optimal positioning of a viscous damper has been considered based on an energy criterion [66]. In aerospace applications, several authors have investigated the optimal locations of dampers for the vibration control of space structures [25; 120; 189].

For seismic applications, however, only a limited number of studies have been conducted to obtain the optimal placement of viscous and viscoelastic devices. In one case, analytical studies suggested that the optimal distribution of the supplemental damping should be the one that maximizes the damping ratio of the fundamental mode, as this mode contribution to the structure's overall response is often significant [5]. Parametric optimization analyses have been carried out to determine the optimum damping coefficient for a damping device placed on the first story of a building [37], and to establish the effect of different dampers distributions throughout the building height [70]. From a somewhat different perspective, topological optimization has been applied to obtain the optimal layout of a structure with viscoelastic devices [125]. A heuristic criterion for optimal placement of passive devices has also been proposed in the literature based on the concept of controllability index [200]. The idea behind this simple methodology is that a device is optimally located if it is placed at a position where the relative displacement across the damper is the largest. Therefore, a sequential procedure is adopted to

successively incorporate the devices in a building. Extensions of this approach have been used to study the effect of modeling of viscoelastic devices and the effect of earthquake excitation frequencies content [159], and to investigate the behavior of three-dimensional structures with supplemental damping [194]. A different attempt utilizes concepts of optimal control theory to find the best locations and damping coefficients of viscoelastic devices [58]. A fully populated optimal gain matrix is obtained by minimizing a quadratic performance index (LQR) and the parameters corresponding to the passive devices coefficients are derived using several approximations. Another study has considered both the optimal distribution of story stiffness and dampers for a shear building subjected to a set of spectrum-compatible earthquakes [186]. Recently, gradient-based optimization techniques have been applied to minimize the amplitudes of a structural system transfer functions [170-173].

1.3.2 Hysteretic Devices

Yielding Metallic Dampers: Inelastic deformation of structural members can dissipate a significant amount of the input earthquake energy. The current seismic design procedures of building structures make use of this fact by prescribing design loads that are significantly less than the elastically calculated loads. However, the controlled yielding of structural members may result in permanent deformations. To resist strong earthquakes and suffer only minor repairable damage, an alternative strategy was first proposed in the earlier seventies to reduce the energy dissipation demand in the main load-carrying elements [96; 162]. In this approach, a substantial portion of the vibration energy is absorbed or consumed at selected locations within a structure through the yielding of metallic elements specially designed for this purpose. Since these protective systems are separated from the main structure, they act as structural fuses that can be replaced after a severe seismic event occurs if damaged. Different devices have been proposed in the literature, including: lead extrusion [149], torsional beam [161], and flexural deformation dampers (X-shaped [166], triangular-shaped [10], U-shaped [2]).

The ADAS (Added Damping and Stiffness) and TPEA (Triangular Plate Energy Absorbers) devices incorporate X-shaped or triangular steel plates respectively to spread the yielding uniformly throughout the material. These devices exhibit stable hysteretic behavior; they are insensitive to thermal effects, and extremely reliable. The suitability of such damping

elements for retrofitting existing structures as well as the construction of new ones is confirmed and advocated by several authors [12; 59; 184; 192]. Yielding devices have been installed as part of seismic retrofit projects in concrete buildings in San Francisco [44; 138; 198] and in Mexico City [115]. Similar devices have also been tested in Japan with regard to their application in industrial piping [124; 158].

To design these devices for a particular application, it is necessary to characterize their expected force-deformation responses under arbitrary cyclic loading. Several levels of approximations can be made to develop these relationships. Idealized models, such as elastic-perfectly plastic or bilinear with post-yielding strain-hardening behavior have been adopted in some studies [88; 123; 152; 174-176; 193]. The Ramberg-Osgood formulas [142] have been used to fit the experimental data obtained from testing of the devices [167; 196]. An extension of the Özdemir model has also been developed to address situations involving multi-axial loadings conditions [62]. The modeling of these devices has been taken to another level of refinement by introducing a mechanics based approach [39]. An inelastic constitutive model combined with large deformation theories have been used to develop the force-deformation model of a device. A finite element formulation based on a two-surface plasticity model has been adopted to predict the device behavior under wind and earthquake loadings [140; 182]. The great advantage of these mechanics-based approaches is that they can be used to define the hysteretic models rationally for any suitable geometric configuration of the device reducing the requirements for component testing.

The effectiveness of the yielding devices in improving the earthquake resistance of a structure depends on the proper selection of the parameters governing their behavior. The results of numerical and analytical investigations have revealed that the key parameters involved in the design of these dampers are: the ratios of bracing stiffness to device stiffness, brace-device assemblage stiffness to device stiffness, and assemblage stiffness to that of the corresponding story [28; 154; 183; 195].

Friction Devices: These devices rely on the resistance developed between two solid interfaces sliding relative to one another. During severe seismic excitations, the device slips at a predetermined load, providing the desired energy dissipation by friction while at the same time

shifting the structural fundamental mode away from the earthquake resonant frequency. Although friction has been used effectively to control motion for centuries, the development of friction devices for use in civil structures to control seismic response was pioneered in the late seventies [132]. Several design variations of these dampers have been studied in the literature, and different forms of patented hardware, now available commercially are: (1) X-braced friction damper [131], (2) slotted bolted connection [50; 63-65; 65; 178; 197], (3) Sumitomo friction damper [168], (4) energy dissipating restraint [83; 85; 126; 127], and (5) Tekton friction devices [147]. These devices differ in their mechanical complexity and in the materials used for the sliding surfaces. To date, several buildings have already been built or retrofitted using friction devices[133-135].

Friction dampers are not susceptible to thermal effects, have a reliable performance and possess a stable hysteretic behavior for a large number of cycles under a wide range of excitation conditions [3; 27; 45]. The latter characteristic is a desired feature for a device aimed to protect a structural system during long duration earthquake loadings.

A number of models have been employed to characterize the hysteretic behavior of friction dampers. One of the most common is the bilinear model, in which the force-deformation relationship is given in terms of an elastic-perfectly plastic idealization [46; 47; 51; 53; 53; 136]. A multiple-stages stiffening model has also been proposed to describe the passages from stick to slip states in a device with varying degrees of stiffness [30; 150]. Other studies [6; 147] have incorporated the smooth Özdemir's form [130] of the Bouc-Wen uni-dimensional model [190]. Based on principles of viscoplasticity, this evolutionary type model provides continuous transitions from elastic to sliding phases. Besides facilitating the computations since there is no need to keep track of transitional rules under arbitrary cyclic motions, the parameters of this model are physically motivated and can be established via a curve fitting procedure from the experimental data [15].

Issues of importance in the efficient design of friction devices involve the determination of the slip load distribution that minimize the structural response and the ratio of bracing stiffness to stiffness of the corresponding structural story [29; 48].

Optimization of Structures with Supplemental Friction and Yielding Devices: The questions about the optimum selection of the design parameters and location for the placement of the displacement-dependent devices to meet some performance objectives have been addressed partially in the literature. The answers to such question are at the core of a good design. Most of the papers discussing the applications of these devices recommend that the distribution of the slip/yield load to be similar to the story stiffnesses [71; 72]. In most cases, such placements will reduce the displacements along the building height, but may not be very effective in reducing the accelerations near the top.

In particular, the optimum slip load distribution for friction devices has been obtained based on a parametric nonlinear dynamic analysis [49]. In this study, a performance index to quantify response reduction is defined as a function of the strain-energy of the original and damped structural systems, and the slip load is assumed the same for all the devices along the building height. The results are presented in the form of a simplified spectrum for the rapid evaluation of the optimum design slip load. In a different approach, an optimization-based design methodology of earthquake-resistant structures [9; 13; 14; 145] has been extended to the design of friction damped braced frames. Here, the design of a building with added friction devices is formulated as a constrained optimization problem, and a nonlinear programming technique is used to find the best solution for various objective functions [7].

Direct enumeration studies involving multiple nonlinear analyses have also been used for the determination of optimum properties of yielding dampers [92]. Recently, a design method for ADAS devices has been presented using optimal control theory [148]. To make use of this framework, an idealized linear model of the device is assumed by comparing the energy dissipated through viscocity and elastoplastic action of the material in a linear and nonlinear device respectively.

1.4 Thesis Organization

This thesis is organized into seven chapters. A brief description of the contents of each chapter is presented here.

Chapter 2 describes the general framework for the optimal design of energy dissipation devices for seismic structural applications. A basic review of the gradient projection technique and genetic algorithm search procedures is presented. This chapter ends with a description of the different structural building models and earthquake loading characterizations employed in this study.

The general formulation presented in Chapter 2 is then specialized for the optimal design of linear viscoelastically-damped building structures. The fluid viscoelastic devices, considered in Chapter 3, and the solid viscoelastic devices, studied in Chapter 4, are characterized by mechanical models consisting of various arrangements of linear springs and viscous dashpots. The linear velocity dependent behavior exhibited by both fluid and solid viscoelastic devices permits their optimal design within a unified performance-based approach. The details of such implementation are provided in Chapter 3. This chapter also presents the development of a generalized modal-based random vibration approach valid for the estimation of the response of general linear systems with arbitrary damping characteristics. Explicit expressions are provided for the calculation of gradient information required by the search procedures and post-optimality analysis. An approach to evaluate the sensitivity of the optimal solution to the excitation parameters is presented. Numerical examples are given to illustrate the applicability of both gradient-based and genetic algorithm optimization approaches, and to establish their convergence characteristics.

Chapters 3 and 4 considered the optimal design of linear viscoelastically-damped structural system. The linearity of the system facilitates the analysis and subsequent application of the optimization procedures. The incorporation of devices with highly hysteretic characteristics, on the other hand, causes an original linear system to become nonlinear. Consequently, time history analyses of real and/or simulated earthquake acceleration records have to be performed for the calculation of the required response quantities. In this case, the optimization procedure not only has to deal with the cumbersome calculation of gradient information but also has to properly handle the presence of multiple local minima solutions. These shortcomings motivate the implementation of a genetic algorithm approach for the solution of the optimal design problem. Chapter 5 presents the details of such implementation for the optimal design of yielding metallic devices. Friction devices, considered in Chapter 6,

present similar behavior characteristics and design challenges. Therefore, these two chapters essentially follow the same design approach. The mechanical parameters governing the behavior of the devices are first identified, and a hysteretic model is then validated for appropriate assessment of the system response. The improvement in the seismic structural performance is evaluated by a number of alternate performance indices. Several sets of numerical results are presented to demonstrate the usefulness of the proposed optimization-based design approach.

Finally, Chapter 7 summarizes the findings of the previous chapters. Recommendations for future research topics are also provided.

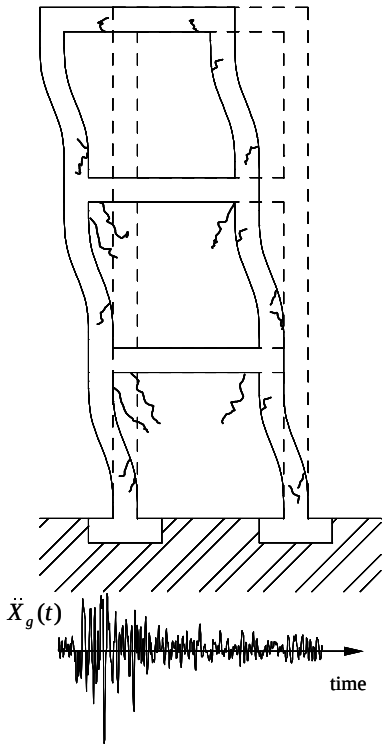

Figure 1.1: Conventional design of seismic resistant building structures.

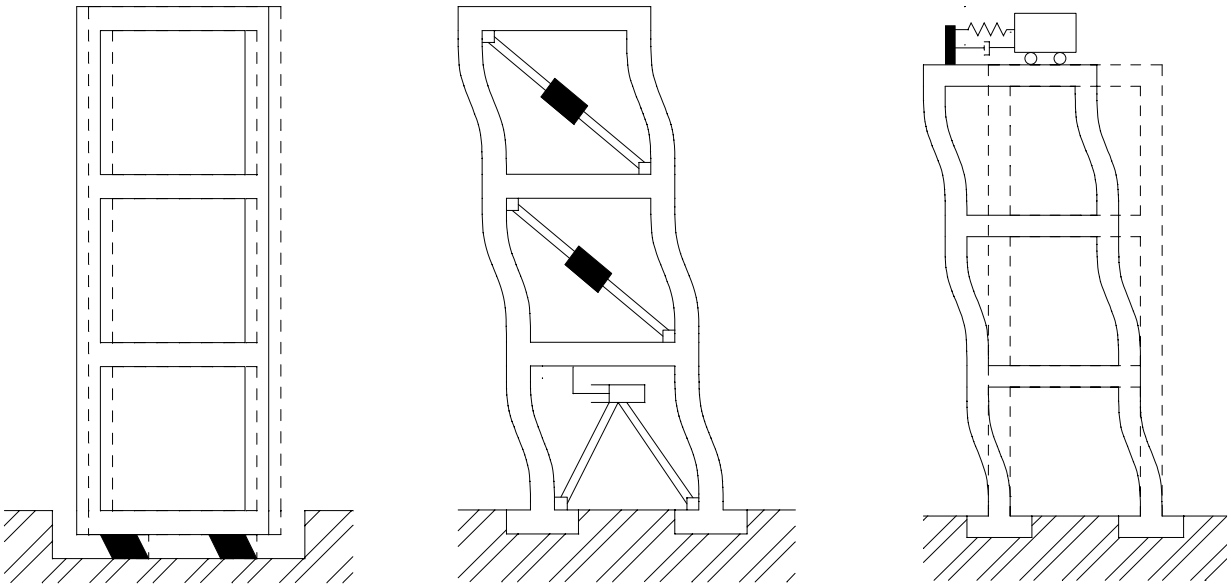

Figure 1.2: Passive response control systems: (a) seismic isolation, (b) energy dissipation devices, (c) dynamic vibration absorbers.

Chapter 2

Basic Concepts and Elements

2.1 Introduction

The main purpose of this chapter is to provide the basic concepts and elements used in this study. In Section 2.2, the formulation of a general optimization-based approach for the design of energy dissipation devices for seismic structural applications is presented. The various concepts and techniques are introduced by means of general expressions for specialization in subsequent chapters. The selection of an optimization procedure depends on the characterization of the problem design variables. For a continuous representation, Section 2.3 presents the basic concepts of the gradient projection method, while Section 2.4 describes a genetic algorithm optimization approach for the case in which the design variables are better described as discrete. Finally, Sections 2.5 and 2.6 introduce, respectively, the structural building models and the ground motion representation used in this study.

2.2 Problem Definition

The equations of motion of an *N* degree of freedom building structure with supplemental energy dissipation devices subjected to ground excitations at its base during an interval of time $[0,t_f]$, can be written in the following standard form:

$$\mathbf{M}\,\ddot{\mathbf{u}}(t)+\mathbf{C}_s\,\dot{\mathbf{u}}(t)+\mathbf{K}_s\,\mathbf{u}(t)+\sum_{d=1}^{n_l}\mathbf{r}_d\,n_d\,P_d(t)=-\mathbf{M}\,\mathbf{E}\,\mathbf{f}(t);\qquad t\in[0,t_f] \tag{2.1}$$

where **M,** $\mathbf{K}_s$ and $\mathbf{C}_s$ represent, respectively, the $N \times N$ mass, structural stiffness and inherent structural damping matrices; $\mathbf{f}(t)$ is an l-dimensional vector representing the seismic excitation; **E** is a $N \times l$ matrix of ground motion influence coefficients; $\mathbf{u}(t)$ is the N-dimensional relative displacement vector with respect to the base, and a dot over a symbol indicates differentiation with respect to time. The local force $P_d(t)$ due to a passive damper installed at the d^{th} location is considered through the N-dimensional influence vector $\mathbf{r}_d$, with n_d being the number of identical dampers and n_l the number of possible locations for a device in the structure. The forces of the energy dissipation devices considered in this study can be expressed through an algebraic or differential operator as:

$$P_d[d_1, \ldots, d_n, h_d(t), \Delta_d(t), \dot{\Delta}_d(t), t] = 0 \tag{2.2}$$

where d_i represents the mechanical parameters characterizing the behavior of the devices, $h_d(t)$ is an internal variable of the element, and the local deformations $\Delta_d(t)$ and deformations rate $\dot{\Delta}_d(t)$ experienced by the d^{th} device are related to those of the main structure by

$$\Delta_d(t) = \mathbf{r}_d^T\, \mathbf{u}(t); \qquad \dot{\Delta}_d(t) = \mathbf{r}_d^T\, \dot{\mathbf{u}}(t) \tag{2.3}$$

The main purpose of installing energy dissipation devices in structures is to control the structural seismic response in order to enhance safety and to reduce structural damage. It is clear form Eqs. (2.1) and (2.2) that the effectiveness of these protective systems in improving the seismic performance of a structure is a function of several variables including their number, their location in the structure, and their physical parameters. One design approach usually employed in practice is to assume a reasonable placement pattern for the devices and to vary their parameters until the structural system satisfies certain performance requirements. However, as the structure becomes more complex and the number of dampers increases such approach may not be efficient for design purposes.

In this study, the problem of determining the proper design parameters of the damping devices and the best places to locate them in a structure in order to get the most out of each device is posed as an optimization problem. The effectiveness of a device arrangement can be measured in terms of how much it reduces a particular response of interest, or how much it minimizes or maximizes a performance function index. This effectiveness could be expressed in terms of an optimality criterion as follows:

$$\underset{\mathbf{d},\,\mathbf{n}}{\text{minimize}} \quad f\left[\mathbf{R}(\mathbf{d},\mathbf{n},t)\right]; \qquad t\in[0,t_f] \tag{2.4}$$

subject to

$$g_j(\mathbf{d},\mathbf{n},t)\le 0 \qquad j=1,\ldots,m; \qquad t\in[0,t_f] \tag{2.5}$$

where $\mathbf{R}(\mathbf{d},\mathbf{n},t)$ is the desired structural response vector in terms of which the performance function $f(\ )$ is defined, $\mathbf{d}$ is the vector of design variables representing the parameters of the added damping elements, $\mathbf{n}$ is the vector of number of identical devices n_d, and m is the number of inequality constraints g_j which may include upper and lower bounds on the design variables.

A number of alternate performance indices can be used to evaluate the improvement in the seismic performance of a building structure. Depending upon the chosen criteria, different design solutions can be obtained for the same problem. Moreover, a solution obtained by reducing some measure of the structural response may increase some other response quantities. It is clear that there is no unique way of defining an optimal problem. Therefore, several forms of performance indices are defined in this study in order to determine the design that produces the best overall behavior.

The design space of the general optimization problem formulated by Eqs. (2.4) and (2.5) may be considered as continuous or discrete. For the placement problem of a given number of devices, the mechanical properties $\mathbf{d}$ are held fixed while the damper locations are optimized. The variables $\mathbf{n}$ defining the number of devices at different locations are of a discrete nature since only an integer number of devices can be placed at any given location. On the other hand, by fixing the number of devices and their locations, the mechanical properties of the devices $\mathbf{d}$ can be regarded as continuous and able to take on any real value within the specified bounds. Alternatively, the parameters $\mathbf{d}$ can also be restricted to take on only a list of permissible values obtained by a proper discretization of the design variables.

The optimization problem given by Eqs. (2.4) and (2.5) may be solved by any general numerical search procedure. Many design optimization methods assume that the design variables are continuous. If an integer solution is desired, the continuous solutions can be rounded to the nearest discrete value. However, one must often select energy dissipation devices from those that are already commercially available and a simple roundup from the continuous values may result in a solution far from the original optimum value. In addition, the round-off

solution may violate some of the constraints. Therefore, a gradient-based technique is implemented in this study for the solution of problems involving only continuous design variables, and a genetic algorithm is used for those cases in which the design variables are considered as discrete. In what follows, a brief but relevant description of these optimization techniques is presented.

2.3 Gradient Projection Method

In the nonlinear design optimization problem encountered in this study, the constraints given by Eqs. (2.5) are linear in the design variables **d**. In general, they can be expressed as:

$$g_j(\mathbf{d}) = \sum_{i=1}^{n} a_{ij} d_i - b_j \leq 0, \qquad j = 1, \ldots, m \tag{2.6}$$

The Rosen's gradient projection method provides an effective yet simple technique for the numerical solution of such optimization problems involving linear constraints [151]. Although the details of this optimization procedure can be found elsewhere [68; 69; 143], a basic theoretical background and computational algorithm is included here for completeness and convenience.

This optimization algorithm is based on the following general iterative scheme:

$$\mathbf{d}_{k+1} = \mathbf{d}_k + \alpha_k \mathbf{s} \tag{2.7}$$

where the subscript k represents the iteration number, $\mathbf{d}_k$ is the current estimate of the optimum design, α_k is a step size and **s** is a search direction. Eq. (2.7) can be separated in two basic problems: determination of a direction search **s**, and determination of the scalar parameter α_k.

Direction-Search:

The basic assumption of the gradient projection technique is that the search direction is confined to the subspace defined by the active constraints. The gradients of the active constraints at any point are given by

$$\nabla g_j(\mathbf{d}) = \left[\frac{\partial g_j}{\partial d_1} \quad \frac{\partial g_j}{\partial d_2} \quad \ldots \quad \frac{\partial g_j}{\partial d_n} \right]^T, \qquad j = 1, \ldots, q \tag{2.8}$$

Define a matrix **N** of order $n \times q$ as

$$\mathbf{N} = \left[\nabla g_1 \quad \nabla g_2 \quad \cdots \quad \nabla g_q \right] \tag{2.9}$$

where q is the number of active constraints at any point. This number can change as the number of active constraints that are engaged changes from one step to another. We would like to approach the minimum of the function in the direction of the steepest descent. That is, the direction $\mathbf{s}_k$ must be such that it minimizes its dot product with the gradient vector of the performance function of Eq. (2.4) under the constraints of Eqs. (2.5). If there were no constraints, then this steepest descent direction will be opposite of the gradient vector of the function. However, since there are constraints on the design variables, the steepest descent direction finding problem can be posed as follows:

$$\text{Find } \mathbf{s} \text{ which minimizes } \mathbf{s}^T \nabla f(\mathbf{d}) \tag{2.10}$$

subject to

$$\mathbf{N}^T \mathbf{s} = 0 \tag{2.11}$$

$$\mathbf{s}^T \mathbf{s} - 1 = 0 \tag{2.12}$$

Equation (2.11) forces the direction $\mathbf{s}$ to be normal to the constraint gradients, and Eq. (2.12) normalizes it to a unit vector of direction. To solve this equality-constrained problem, the Lagrangian function can be constructed by introducing the multipliers $\boldsymbol{\lambda}$ and β as

$$L(\mathbf{s}, \boldsymbol{\lambda}, \boldsymbol{\beta}) = \mathbf{s}^T \nabla f(\mathbf{d}) + \boldsymbol{\lambda}^T \mathbf{N}^T \mathbf{s} + \beta \left(\mathbf{s}^T \mathbf{s} - 1 \right) \tag{2.13}$$

The necessary conditions for the minimum are given by

$$\frac{\partial L}{\partial \mathbf{s}} = \nabla f(\mathbf{d}) + \mathbf{N}^T \boldsymbol{\lambda} + 2\beta \mathbf{s} = \mathbf{0} \tag{2.14}$$

$$\frac{\partial L}{\partial \boldsymbol{\lambda}} = \mathbf{N}^T \mathbf{s} = \mathbf{0} \tag{2.15}$$

$$\frac{\partial L}{\partial \beta} = \mathbf{s}^T \mathbf{s} - 1 = 0 \tag{2.16}$$

Premultiplication of Eqs. (2.14) by $\mathbf{N}^T$, and consideration of Eqs. (2.15) leads to

$$\mathbf{N}^T \nabla f(\mathbf{d}) + \mathbf{N}^T \mathbf{N} \boldsymbol{\lambda} = \mathbf{0} \tag{2.17}$$

or

$$\boldsymbol{\lambda} = -\left(\mathbf{N}^T \mathbf{N} \right)^{-1} \mathbf{N}^T \nabla f \tag{2.18}$$

Substitution of Eqs. (2.18) in Eqs. (2.14) gives

$$\mathbf{s} = -\frac{1}{2\beta}\left[\mathbf{I} - \mathbf{N}\left(\mathbf{N}^T\mathbf{N}\right)^{-1}\mathbf{N}^T\right]\nabla f \tag{2.19}$$

Since **s** defines only the direction of search, the scaling factor 2β can be disregarded. The matrix in the bracket is called the projection matrix **P**. That is,

$$\mathbf{P} = \mathbf{I} - \mathbf{N}\left(\mathbf{N}^T\mathbf{N}\right)^{-1}\mathbf{N}^T \tag{2.20}$$

The normalized direction **s** resulting from this equality-constrained problem can be finally expressed as

$$\mathbf{s} = -\frac{\mathbf{P}\nabla f}{\left\|\mathbf{P}\nabla f\right\|} \tag{2.21}$$

It is clear form Eqs (2.20) and (2.21) that if no constraints are active, the projection matrix **P** reduces to the identity matrix **I** and the search direction **s** becomes the steepest descent direction.

Determination of Step-Length:

After the search direction **s** has been determined, the maximum permissible step α along this direction must be determined. The step length has to be large enough to achieve the best improvement in the performance function while avoiding any violation of the previously inactive constraints.

The effect of an increase in the value of α on the constraints can be investigated by expressing Eqs. (2.6) in the following form:

$$g_j(\mathbf{d} + \alpha\mathbf{s}_i) = g_j(\mathbf{d}) + \alpha\sum_{i=1}^{n} a_{ij}s_i \le 0, \qquad j = 1,\ldots,m \tag{2.22}$$

In particular, the step length that makes an originally inactive constraint, say the k^{th}, to become active can be determined as

$$g_k(\alpha_k) = g_k(\mathbf{d}) + \alpha_k\sum_{i=1}^{n} a_{ik}s_i = 0 \tag{2.23}$$

or

$$\alpha_k = -\frac{g_k(\mathbf{d})}{\sum_{i=1}^{n} a_{ik}s_i} \tag{2.24}$$

The maximum permissible step value is then limited by the minimum value of α_k. That is,

$$\alpha = \min_{\alpha_k > 0} (\alpha_k) \tag{2.25}$$

A Fortran 90 subroutine has been written for optimization studies based on the above presented gradient projection technique. The computational algorithm involved the following steps [143]:

1. Start with an initial feasible design $\mathbf{d}_i$.
2. Evaluate the problem constraints $g_j(\mathbf{d}_i)$ for $j=1,\ldots,m$ to determine active constraints.
3. Compute the gradient of the performance function, $\nabla f(\mathbf{d}_i)$.
4. Compute the gradients of the active constraints $\nabla g_j(\mathbf{d}_i)$ for $j=1,\ldots,q$, and form the **N** matrix of Eq. (2.9).
5. Calculate the projection matrix **P** from Eq. (2.20), and find the normalized search direction $\mathbf{s}_i$ using Eq. (2.21).
6. Test if $\mathbf{s}_i = \mathbf{0}$. If $\mathbf{s}_i = \mathbf{0}$, compute the Lagrange multipliers $\boldsymbol{\lambda}$ from Eq. (2.18). Stop the iterative procedure.
7. If $\mathbf{s}_i \neq \mathbf{0}$, determine the maximum step length α_k that is permissible without violating any of the constraints, using Eqs. (2.24) and (2.25).
8. Calculate the new design point as $\mathbf{d}_{i+1} = \mathbf{d}_i + \alpha_i \mathbf{s}_i$.
9. Set the new value of i as $i = i+1$, and go to step 2.

2.4 Genetic Algorithms

The basic principles of genetic algorithms were first proposed by Holland [76]. Since then, many different applications of genetic algorithms have been explored, and several books are now available on this subject [40; 56; 61; 119]. Significant applications of this technique have been made in structural engineering [18; 19; 26; 55; 56; 67; 89; 98]. Several researches have used genetic algorithms in the context of placement of control actuators in aerospace applications [54; 129; 144]. A brief outline of the approach, as it is applied to the problem of optimal placement of dampers in a building structure, is given in this section.

The genetic algorithms are based on the mechanism of natural selection where the stronger individuals are likely to be the winners in a competing environment. They employ the analogy of natural evolution of a population of individuals through generations where the fittest survive and dominate. The genetic algorithms differ from gradient-based optimization techniques in the following ways: (1) They consider simultaneously many designs points in the search space and therefore have a reduced chance of converging to local optima. (2) They do not require any computations of gradients of complex functions to guide their search; the only information needed is the response of the system to calculate the objective or fitness function. (3) They use probabilistic transition rules (genetic operators) instead of deterministic transition rules.

In the context of the problem of optimal placement of supplemental damping devices in a structure, the feasible designs of the structure represent the individuals in the search space of all possible designs. A design is considered the best (fittest individual) if an objective function or a performance index associated with this design has the highest value. The objective is to search for the best design in this search space. In a genetic algorithm, a generation of population undergoes successive evolution into future generations through the process of genetic operators such as mating for reproduction with crossover and mutations. The selection of pairs for reproduction exploits the current knowledge of the solution space by propagating the better designs (individuals) and discouraging the poorer ones. The crossover and mutation operators are the two basic mechanisms of a genetic algorithm; they create new designs for further exploration in the search space. As a new population is created, the performance index is evaluated for each new design to determine its fitness with respect to other designs in the population. This process is repeated for a number of cycles (generations) until no further improvement is observed in the best individual in the subsequent generations.

Figure 2.1 shows all the basic elements of the genetic algorithm used in this study. To start the genetic algorithm search, first an initial population of a chosen size is randomly generated (Step 1, Figure 2.1). This population consists of unique individuals. In the context of placement of devices, each individual represents a design with a particular scheme of placement of the devices. To illustrate this, consider the placement of fifteen devices in a ten story building structure. One possible arrangement of these fifteen devices is {1, 5, 2, 5, 10, 2, 8, 1, 2, 9, 7, 6,

4, 3, 1}, which represents an individual of the population. In this particular arrangement, the first device is placed in the first story, the second in the fifth story, and so on. In genetic terms, these device locations represent the genes, and when collectively arranged together in a string they form a chromosome identifying an individual of the population. Thus, in this particular case, a gene (floor location of each device) in a chromosome (devices arrangement) will be a real number between 1 and 10 (possible floor locations).

For the problem of placement of fifteen devices in ten locations, there are 1.31×10^6 possible different design solutions that define the search space. To start the genetic search process, however, only a few of these are selected to form the population. There is no set rule to select the size of a population. A larger population may converge to the final solution in less number of iterations than a smaller population. On the other hand, a larger population will also require a larger number of performance index calculations per iteration.

After selecting a population size, the next step is to operate on the genetic information contained in this population by the genetic operators of the reproduction process. For this, first the suitability of each individual member of the chosen population is evaluated by calculating its performance index. The higher the performance index the better the individual. The individuals are then rank-ordered from the best to the worst in the population. Next, they are paired for reproduction, according to the roulette-wheel scheme explained below (see Step 3, Figure 2.1). In this scheme, individual with a higher performance index is likely to be selected more than the one with a lower index. However, to avoid a complete domination in the pairing process by the individuals with highest performance indices, and thus causing a rapid convergence to a possible sub-optimal solution, the performance indices are mapped into a fitness function that modulates the relative dominance of the performance index values. This fitness function depends on the rank of the individuals sorted according to their raw performance index values. In this paper, the fitness function $F(i)$ for the i^{th} ranked individual in a population of size N is defined as follows [60]:

$$F(i) = F(i-1) + \frac{2(N+1-i)}{(N+1)N} \tag{2.26}$$

with $F(0) = 0$.

In the well-known roulette-wheel scheme employed in this paper, a candidate is assigned a sector of the roulette in proportion to its fitness interval value I_i defined as:

$$I_i = F(i) - F(i-1) \tag{2.27}$$

The sum of all I_i is of course equal to 1.0. To select a pair, two random numbers between 0 and 1 are generated. The individuals associated with these random numbers are identified by the fitness intervals in which the selected random numbers fall. To further illustrate this pairing scheme further, consider a population of six individuals ranked according to their objective function values f_i shown in Table 2.1. The table also shows the corresponding values of the fitness function and fitness interval for these individuals, defined according to Eqs. (1) and (2). Figure 2.2 shows the sectors of a simulated roulette wheel, the areas of which are proportional to the individual fitness interval values given in Table 2.1. The next row in Table 2.1 shows six randomly generated numbers between 0 and 1. The individuals associated with these numbers are shown in the following row of this table. The pairs are then formed for mating sequentially. That is, for this particular example, the three pairs are (A, C), (B, E), and (D, A). In the random generation of numbers, it is quite possible that two consecutive random numbers will be associated with the same individual for pairing. To avoid in-breeding, such pairing is not accepted; a new random number is generated until a different individual is found for pairing.

The next step (see Step 4 in Figure 2.1) is reproduction of two new offspring (new designs) by the each pair. The crossover scheme is used to produce offspring that share the genetic information of the parents. For this, a gene location (device location) is randomly selected for each pair of individuals, above which the genes are interchanged to create new offspring. More complex crossover schemes with multiple point crossovers have also been considered. Figure 2.3(a) illustrates this one-point crossover scheme for individuals A and C previously selected for breeding. In this case, children a and c are created by simple switching of the genes after the sixth parental gene. This crossover operation is not necessarily performed on all the individuals in the population. Instead, it is applied only to a fraction p_c of the population when the pairs are chosen for mating. This fraction is usually a large number to allow for exploration of a larger part of the solution space to avoid convergence to a local optimum. The pairs subjected to crossover were selected on a random basis to satisfy this crossover fraction criterion.

A small fraction p_m of the chromosomes is also mutated to introduce new designs. The mutation introduces new genes in the population for further trials. This fraction p_m controls the rate at which new genes are introduced in the population. This factor is usually kept low to avoid too many offspring losing the resemblance to their parents, and thus losing their ability to learn from their gene history. In the context of the search for the optimal solution, a higher mutation might delay the convergence of the process. The mutation operator alters the individual genetic representation (chromosome) according to a simple probabilistic rule. Figure 2.3(b) illustrates a one-point mutation carried out on the child chromosome c. A randomly selected gene in a randomly selected chromosome is changed to take on a new value from the set of other possible values.

Often, the newly generated population is also subjected to an elitist selection scheme to retain the best individual characteristics of the previous generation (see Step 6, Figure 2.1). For this, the new generation is ranked according to their performance index values. The last ranked individual is then dropped from the population and replaced by the best individual from the parental population. This is shown in Figure 2.1 where the N^{th} individual in Box (6) has been shown to be replaced by the 1^{st} individual from Box (3). More complex elitist policies, involving more than one individual have also been used in the literature.

This recently formed population is subjected to rank-ordering, pairing, reproduction through crossover and mutation as before to start the new cycle of population generation. The process is repeated until a convergence to the optimal solution is reached. For the genetic search outlined in Figure 2.1, a Fortran 90 program has been written which used a genetic algorithm module previously developed [116; 117]. For a further in-depth discussion of the operation of the genetic algorithms, the reader is referred to the cited references.

2.5 Structural Building Models

Several building models have been used in this study for optimal placement of energy dissipation systems. In this section, the basic properties and dynamic characteristics of these models are described. Each building is identified for reference in subsequent chapters.

The first three structures are modeled as planar shear buildings. In this idealization, the building is considered as a system of masses connected by means of linear springs and viscous dampers to represent, respectively, the lateral stiffness and energy dissipation of the structure. Associated to each lumped mass there is one-degree-of freedom defining its displaced position relative to the original equilibrium position. Often the floor and stories of a building structure will exhibit some eccentricity between their mass and stiffness centers. These structures will respond in coupled lateral-torsional vibration modes. The fourth model used in this study is intended to represent such structures. In this case, each floor diaphragm, assumed to be rigid in its own plane, has three DOFs defined at the center of mass to describe the translations along the x and y axes and torsional rotation about the vertical axis.

The first structure, which will be referred to as Building 1, is a 10-story building with uniform mass and stiffness properties along its height as shown in Figure 2.4(a). The natural frequencies are provided in Column (4) of Table 2.2.

The second structure, hereafter referred to as Building 2, is a variation of Building 1 in which the floor stiffnesses vary linearly as depicted in Figure 2.4(b), with ratio 1:3 between the stiffness at the upper floor k_s^{10} and at the lower floor k_s^1. The mass is uniformly distributed, and the mechanical properties of this building are enumerated in Table 2.2.

The third structure, identified as Building 3, is a 24-story building. This structure represents a slight modification of a 24-story concrete frame structure [16]. The mass and stiffness properties of this structure, presented in Table 2.3, are not uniform along its height.

The fourth structure considered in this study is a 6-story building. The schematic of this building, referenced as Building 4, is given in Figure 2.5. Table 2.4 shows the mass, mass moment of inertia and stiffness distribution along the x and y longitudinal axes.

2.6 Ground-Motion Representation

To arrive at an optimal design of a structure to be retrofitted with energy dissipation devices, one must consider several earthquake excitations that are likely to occur at the site. In earthquake engineering, the seismic input for design of structures is commonly defined in the form of smoothed response spectra curves. This input model of earthquake can be directly used in the

analysis and design of linear structural systems. For this, the modal properties of the system are first identified and then they are used in estimating structural response by superimposing the responses of all contributing modes. For linear structural systems that also remain linear after the installation of the passive devices, this form of input or its equivalent spectral density function can be directly used. However, if the structure or the installed device behaves inelastically, one must resort to a step-by-step time history analysis to calculate the response and performance index for the optimization study.

The uncertainty about the seismic input motion can be incorporated in the response analysis by considering an ensemble of actual earthquake records that characterize the construction site geology and seismicity. Another option is to generate artificial earthquake excitations with characteristics compatible with those of past-observed earthquakes, or with similar spectral characteristics. The spectral characteristics of earthquake motions are often defined in terms of power spectral density functions. A commonly adopted stochastic model for ground acceleration is a zero-mean stationary process with power spectral density function $\Phi_l(\omega)$ of the Kanai-Tajimi form [90; 169]:

$$\Phi_l(\omega) = S \frac{\omega_g^4 + 4\,\beta_g^2\,\omega_g^2\,\omega^2}{(\omega_g^2 - \omega^2)^2 + 4\,\beta_g^2\,\omega_g^2\,\omega^2} \tag{2.28}$$

The parameters ω_g, β_g and S can be established from a site-specific ground motion study and correspond, respectively, to the natural frequency and damping ratio of the site, and intensity of an ideal white noise input from the bedrock. For a given set of parameters, Figure 2.6 shows the corresponding Kanai-Tajimi power spectral density function. If desired, a synthetic ground acceleration $\mathbf{f}_l(t)$ compatible to a power spectral density function can be generated as the sum of k harmonics with frequencies ω_k and random phase angles δ_k,

$$\mathbf{f}_l(t) = \kappa(t)\sqrt{4\Delta\omega}\,\mathrm{Re}\left\{\sum_k \left[\sqrt{\Phi_l(\omega_k)}\,e^{i\delta_k}\right] e^{i\omega_k t}\right\} \tag{2.29}$$

where $\kappa(t)$ is a deterministic envelope function. In this study, this function is defined as follows:

$$\kappa(t) = \begin{cases} (t/3)^2 & 0\text{ s} \le t \le 3\text{ s} \\ 1 & 3\text{ s} \le t \le 10\text{ s} \\ e^{-0.26(t-10)} & t > 10\text{ s} \end{cases} \tag{2.30}$$

The time series presented by Eqs. (2.29) and (2.30), compatible with the power spectral density function of Eq. (2.28), are used in this study for the design of nonlinear hysteretic devices considered in Chapters 5 and 6. However, for the case in which the response of the combined building structure and added energy dissipation devices is linear, such as those described in Chapters 3 and 4, a modal-based random vibration approach is used for the evaluation of the performance indices required by the optimization procedures.

2.7 Chapter Summary

This chapter has introduced the basic concepts and elements used in this study. This material was presented in a general format adequate for specialization in subsequent chapters. The basic properties and dynamic characteristics of various building models were described. Commonly used models of input earthquake ground motion were presented. The next chapters will be referring to this material repeatedly.

Table 2.1: Individuals parameters for selection procedure.

Individual	A	B	C	D	E	F
Objective function f_i	0.92	0.33	0.17	0.12	0.09	0.05
i^{th} best individual	1	2	3	4	5	6
Fitness $F(i)$	0.29	0.52	0.71	0.86	0.95	1.00
Interval I_i	0.29	0.23	0.19	0.15	0.09	0.05
Random number	0.25	0.63	0.49	0.87	0.79	0.18
Individual chosen	A	C	B	E	D	A

Table 2.2: Mechanical properties of Building 1 and Building 2.

Story Mode (1)	Mass [kg $\times 10^5$] (2)	Building 1		Building 2	
		Stiffness [N/m $\times 10^8$] (3)	Frequencies [rad/sec] (4)	Stiffness [N/m $\times 10^7$] (5)	Frequencies [rad/sec] (6)
1	2.50	4.50	6.34	9.26	2.51
2	2.50	4.50	18.88	8.57	6.66
3	2.50	4.50	31.00	7.88	10.78
4	2.50	4.50	42.43	7.20	14.66
5	2.50	4.50	52.90	6.51	18.18
6	2.50	4.50	62.20	5.83	21.29
7	2.50	4.50	70.11	5.14	24.15
8	2.50	4.50	76.45	4.45	27.07
9	2.50	4.50	81.08	3.77	30.30
10	2.50	4.50	83.90	3.08	34.16

Note: 3% modal damping ratio for all modes.

Table 2.3: Mechanical properties of Building 3.

Story Mode (1)	Mass [kg $\times 10^5$] (2)	Stiffness [N/m $\times 10^8$] (3)	Frequencies [rad/s] (4)
1	74.26	20.98	3.43
2	74.26	19.77	8.30
3	69.18	18.55	13.39
4	69.70	18.55	18.26
5	58.49	17.41	23.14
6	55.87	17.29	28.27
7	55.69	17.29	32.96
8	40.63	16.09	37.74
9	36.78	15.81	41.34
10	36.78	15.81	45.76
11	36.78	15.67	50.01
12	34.15	15.55	54.30
13	34.15	15.55	57.59
14	28.55	14.92	61.60
15	24.69	14.75	64.97
16	24.69	14.75	68.89
17	23.29	14.55	74.26
18	17.69	14.34	78.24
19	17.69	14.34	83.06
20	15.24	13.45	87.97
21	12.78	13.38	93.24
22	12.61	13.45	98.51
23	9.28	13.43	107.43
24	7.71	13.96	116.54

Note: 3% modal damping ratio for all modes.

Table 2.4: Mechanical properties of Building 4.

Story	Mass	Mass Moment of Inertia	Story Stiffness	
			k_x	k_y
	[kg × 10^4]	[kg-m^2 × 10^5]	[N/m × 10^7]	[N/m × 10^7]
(1)	(2)	(3)	(4)	(5)
1	4.80	8.00	8.34	8.34
2	4.80	8.00	8.34	8.34
3	4.32	7.20	5.34	5.34
4	4.32	7.20	5.34	5.34
5	3.84	6.40	3.24	3.24
6	3.84	6.40	3.24	3.24

Note: radius of gyration r = 10 m; 3% modal damping ratio for all modes.

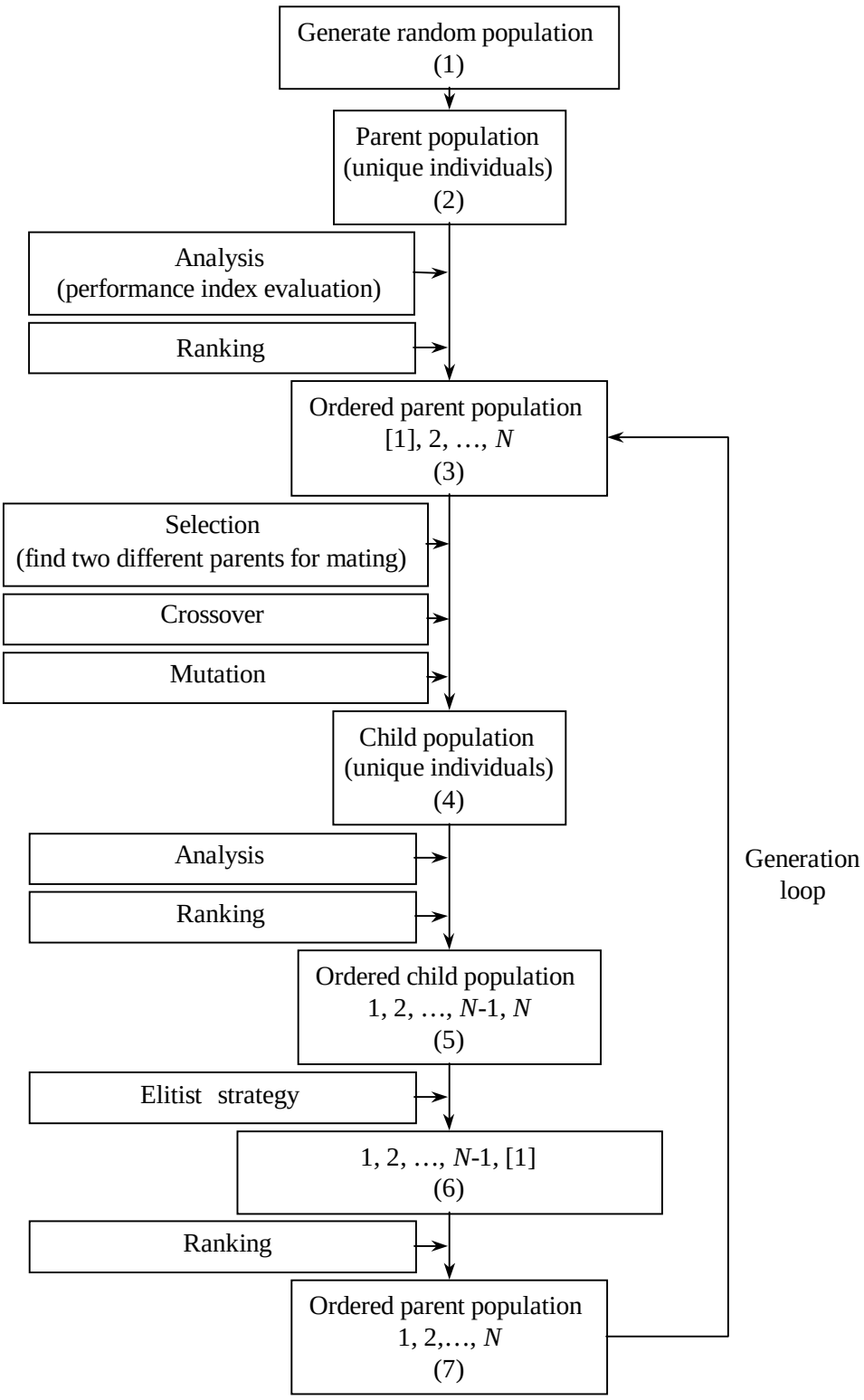

Figure 2.1: Genetic algorithm flow chart.

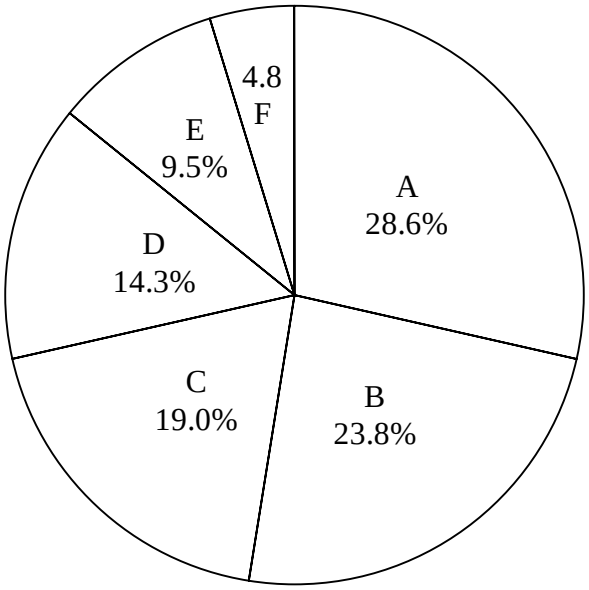

Figure 2.2: Roulette wheel selection procedure.

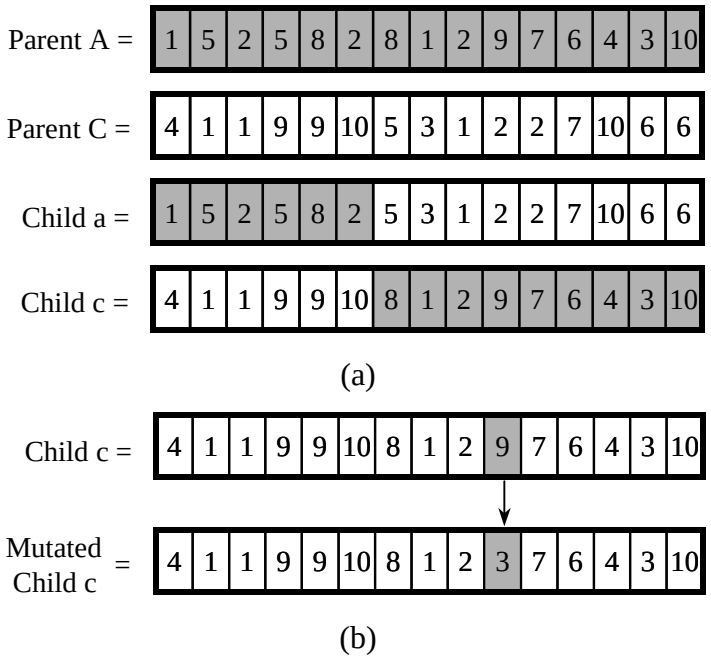

Figure 2.3: Example of genetic operators: (a) one point crossover, (b) one point mutation.

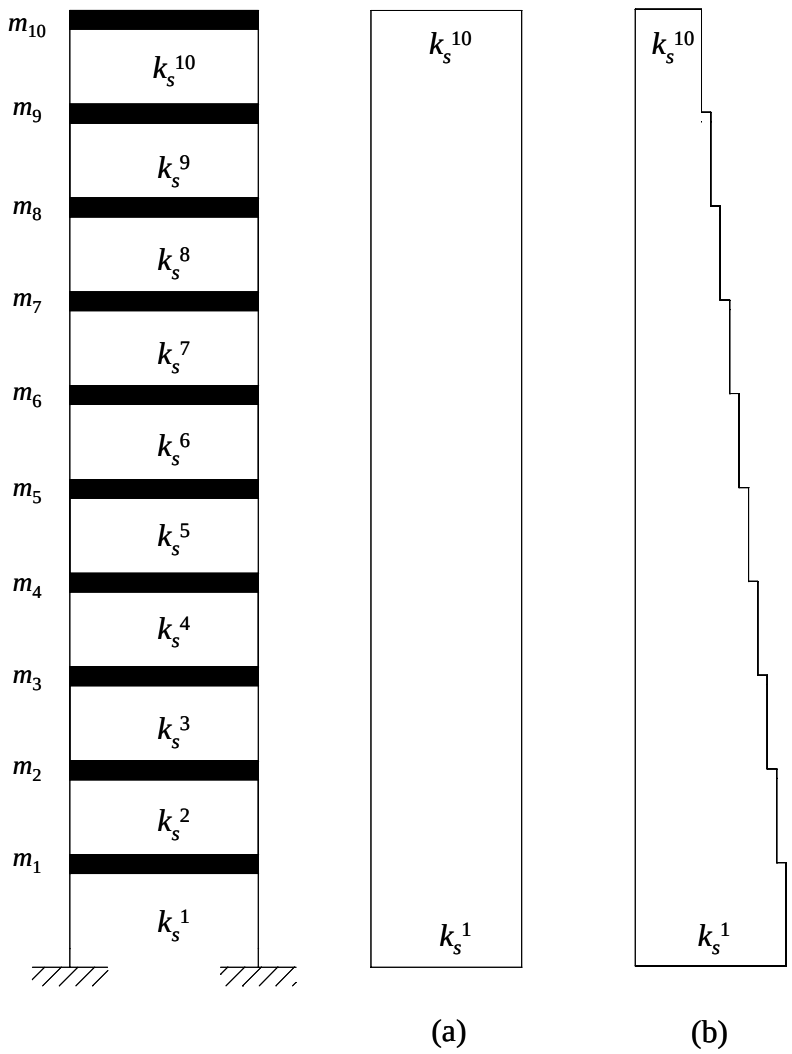

Figure 2.4: Schematic representation of ten story plane shear buildings used in the study, (a) Building 1 with uniform mass and stiffness distribution, (b) Building 2 with uniform mass and linear stiffness distribution.

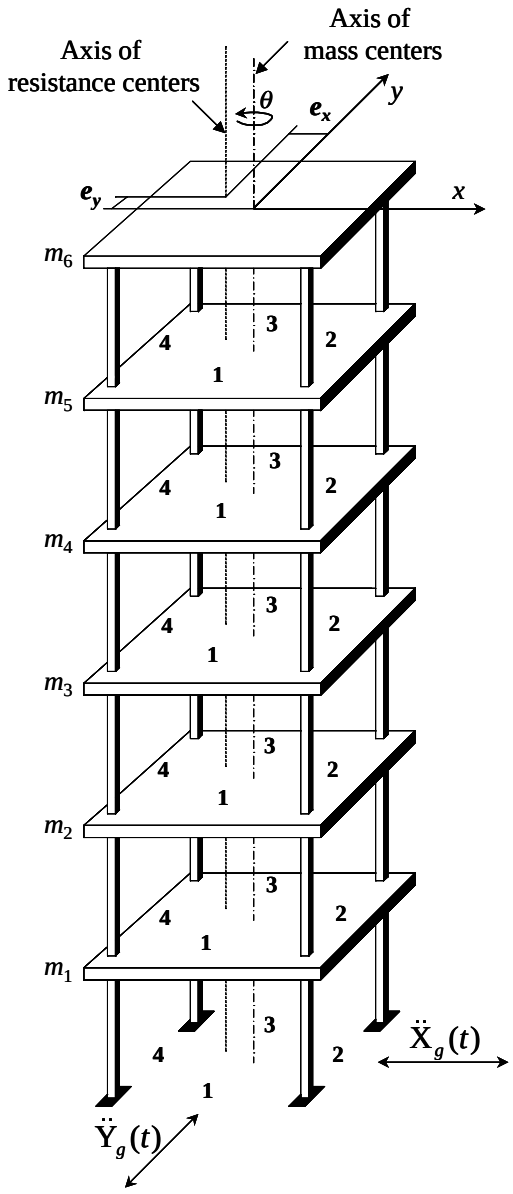

Figure 2.5: Schematic representation of six story torsional Building 4 used in the study.

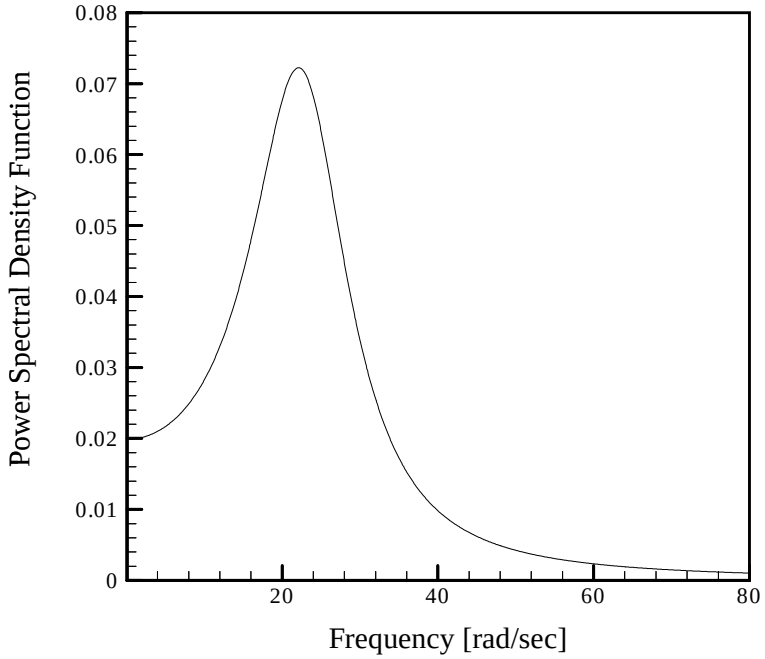

Figure 2.6: Power spectral density function of the Kanai-Tajimi form (ω_g=23.96 rad/s, β_g=0.32, and S=0.020 m^2/s^3/rad).

Chapter 3

Fluid Viscoelastic Devices

3.1 Introduction

In the previous chapter, a general framework for the optimization problem of structural systems with supplemental energy dissipation devices was formulated. In this chapter, this general framework is specialized for the fluid viscoelastic devices installed in buildings for seismic performance enhancement.

Fluid viscoelastic devices, widely used as shock and vibration isolation systems for aerospace and military applications, operate on the principle of resistance of a viscous fluid to flow through a constrained opening. These devices have been adapted for seismic structural applications due to their abilities to dissipate large amounts of the input earthquake energy by viscous heating. Another advantage attributed to the fluid viscoelastic devices is that their rate dependent viscous forces are out of phase with other displacement dependent forces, and do not directly adds to the maximum forces developed in the main structural members. Figure 3.1 shows a schematic of a typical fluid viscoelastic damper.

The fluid viscoelastic dampers can be designed to exhibit linear behavior over a broad range of operating frequencies. They can be designed to be nearly unaffected by the changes in the ambient temperature or internal temperature rise due to the heat generated during earthquake excitations. Moreover, if the added damping devices are designed such that the main structural elements remain elastic and free of damage during a seismic event, the response of the overall

structural system can also be considered as linear. In this chapter, it is assumed that it is, indeed, the case.

In practice, the design of structures with viscous dampers follows the traditional iterative trial and error process. A reasonable placement pattern is assumed for the devices and their parameters are varied until a desired level of the critical damping ratio is achieved. Once the mechanical properties of the dampers are chosen, the level of response reduction achieved for this installation can be easily computed. However, for design or retrofit of a deficient structure one is more interested in knowing the required amount of viscoelastic damping material and its distribution in the structure in order to achieve a desired level of reduction in the response and improvement in the performance. Therefore, in this chapter a level of response reduction is first established and the number of devices and their best locations are determined by coupling the analysis and design process with an optimization procedure. Section 3.3 presents the details of implementing a performance-based approach for the design of fluid viscoelastic devices.

Basic steps required in an optimization solution are the evaluation of the performance index and the determination of search direction. The numerical procedures for calculating the required response quantities and gradient information are made simpler by the assumed linear behavior of the structural system. Since the addition of viscous dampers renders a structure nonclassically damped, the development of a modal-based random vibration technique for dynamic analysis of general nonclassically linear systems is presented in Section 3.4. For efficient computation of search direction and post-optimality analysis, analytical expressions for the rates of change of responses quantities with respect to the design variables are provided in Section 3.5. Once an optimal design solution is found, it is of practical interest to determine how the solution is affected when the parameters of the problem changes. An approach to evaluate the sensitivity of the optimum solution and the performance function is described in Section 3.6. Finally, numerical results are presented in Section 3.7 to demonstrate practical applications and effectiveness of the proposed performance-based design approach. A brief discussion of some of the available models to represent the linear behavior exhibited by the fluid viscoelastic devices is presented next.

3.2 Analytical Modeling of Fluid Viscoelastic Devices

The linear force-deformation response of the fluid viscoelastic device has commonly been characterized by mechanical models consisting of combinations of linear springs and dashpots. The cyclic response of fluid viscoelastic devices is generally dependent on the deformation frequency and can be adequately captured by the use of a classical Maxwell model in which dashpot and spring are joined in series, as shown in Figure 3.2(a). For this model, the general relation given by Eq. (2.2) for the resistance force $P_d(t)$ in the d^{th} damping element takes the following form [33],

$$P_d(t) + \frac{c_d}{k_d}\dot{P}_d(t) = c_d\,\dot{\Delta}_d(t) \tag{3.1}$$

where k_d is the stiffness of the device at infinitely large frequency, and c_d is the damping coefficients at zero frequency. The ratio $\tau_d = c_d/k_d$ is referred in the literature as the relaxation time constant. Figure 3.2(b) shows the typical dependency of the damping and stiffness coefficients with respect to the deformation frequency for this mechanical model. Figure 3.2(c) illustrates the force-deformation responses for different loading frequencies. It is observed that for a low deformation frequency the fluid device exhibits a purely viscous behavior contributing to the energy dissipation capabilities of the building structure by dampening the lower modes of vibration. As the frequency increases, the damper also develops significant stiffness resulting in a suppression of the contribution of higher modes to the structural response. In design practice, this model is recommended to characterize the response of fluid viscoelastic devices that may exhibit some stiffening behavior at high frequencies of cyclic loading. This model can be further simplified when considering low frequencies range of operation for the device. In this case, the contribution of stiffness may be negligible and a purely viscous dashpot model, as illustrated in Figure 3.3(a), is sufficient to estimate the device force $P_d(t)$ as

$$P_d(t) = c_d\,\dot{\Delta}_d(t) \tag{3.2}$$

Combinations of linear springs and dashpots have also been proposed to model linear damping devices that exhibit stiffening at very low frequencies such as bituminous fluid dampers. Figure 3.3(b) shows the Wiechert model, in which the force in the device is obtained as:

$$P_d(t) + \tau_d \dot{P}_d(t) = \tau_d k_g \dot{\Delta}_d(t) + k_e \Delta_d(t) \tag{3.3}$$

where k_g and k_e are, respectively, the "glossy" and "rubbery" material stiffness, and τ_d is the previously defined relaxation time constant. Although this mechanical model is not used in this study, is presented here to demonstrate the different levels of refinement that can be obtained by increasing the number of springs and dashpots elements, and by considering their varied configurations.

The discussion so far has been concerned with the description of the models available to characterize the force-deformation relation of a fluid viscoelastic device. In a typical application, it is also necessary to consider the flexibility of attachments and brace elements used to support and link the device to the various parts of the main framing system. Figure 3.4 illustrates different arrangements of bracings and devices.

To account for the effect of the flexibility of the brace, consider a linear viscous device located on top of the chevron bracing of Figure 3.4(a). The force exerted by the device on the structure is modeled by Eq. (3.2), while the local force in the bracing system $f_b(t)$ can be expressed as a function of its inherent stiffness k_b ($=2AE\cos^2\theta_b/l_b$) and deformation of the bracing $\Delta_b(t)$ as:

$$f_b(t) = k_b \Delta_b(t) \tag{3.4}$$

The local deformations experienced by the device $\Delta_d(t)$ and bracing element $\Delta_b(t)$ are related to the global structural deformation, or interstory drift $\Delta_s(t)$ by

$$\Delta_s(t) = \Delta_b(t) + \Delta_d(t) \tag{3.5}$$

The global force applied by the damping element $F_d(t)$ on the structure satisfies $F_d(t)=f_b(t)=P_d(t)$. Thus from Eq. (3.5),

$$F_d(t) + \frac{c_d}{k_b}\dot{F}_d(t) = c_d \dot{\Delta}_s(t) \tag{3.6}$$

Therefore, the behavior of the damper-brace assembly can also be described by a spring and dashpot connected in series, where the stiffness and deflections of the brace can influence the performance of the damper. It is clear that if the brace is considered as rigid, the deformation

experienced by the damper is the same as the one in the structure. In this case, Eq. (3.6) reduces to Eq. (3.2) with $k_b = \infty$, $\Delta_b = 0$, and $\Delta_d = \Delta_s$.

In the case in which the damper is connected through a diagonal bracing to the structure, as depicted in Figure 3.4(b), the global force $F_d(t)$ acting on the structure is obtained by considering the angle θ_d of the damping element with respect to the horizontal axis. For a rigid bracing, it can be written as:

$$F_d(t) = P_d(t)\cos\theta_d = c_d\,\dot{\Delta}_s(t)\cos^2\theta_d \tag{3.7}$$

For a flexible bracing, the global force $F_d(t)$ is given by

$$F_d(t) + \frac{c_d}{k_b}\dot{F}_d(t) = c_d\,\dot{\Delta}_s\cos^2\theta_d \tag{3.8}$$

It is noticed that the damper deformation is reduced due to the inclination angle, with the consequent reduction in its energy dissipation capability. Figure 3.4(c) presents an alternate toggle brace mechanism in which the structural drift Δ_s is amplified causing a much larger deformation at the damper level.

3.3 Performance-Based Design of Fluid Viscoelastic Devices

In this study, performance-based design of energy dissipation devices refers to the design of the supplemental damping elements such that the structural seismic response is reduced to a desired level, or the performance of the main structure satisfies certain prescribed criteria. This requires the determination of the level of damping or number of devices required to satisfy the stipulated design goals, and the corresponding distribution or placement pattern of the damping elements within a building structure. In this regard, two different treatments of the design variables are contemplated in this chapter. First, the details of implementing a performance-based approach are presented for the case in which the design variables can be described by real continuous values. Next, a more versatile approach is described in which a discrete representation of the properties of the devices is considered.

3.3.1 Continuous Design Variables

As previously discussed, the objective in the design of a viscoelastically-damped structure is to achieve a prescribed seismic structural performance by optimally distributing a given amount of viscous damping material within the structure. In the following development, it is assumed that there is one fluid viscoelastic device at every bay of the building frame. The damping coefficient values of the devices are considered as continuous. Under this assumption, the general optimization problem previously formulated in Chapter 2 can be restated as:

$$\underset{\mathbf{d}}{\text{minimize}} \quad f\left[\mathbf{R}(\mathbf{d},t)\right] \tag{3.9}$$

subject to

$$\sum_{d=1}^{n_l} c_d - C_T = 0 \tag{3.10}$$

$$0 \le c_d \le c_d^u \qquad d = 1,\ldots,n_l \tag{3.11}$$

where **d** is the vector of design variables c_d representing the coefficients of the added damping elements, $c_d{}^u$ denotes the upper bound value of the damping coefficient for the d^{th} location; and C_T is the total amount of damping coefficient values to be distributed in the building.

To solve the optimization problem stated in Eqs. (3.9) through (3.11), the gradient projection technique can be employed. Using the Lagrange multipliers method, it can be shown that the following necessary conditions must be satisfied by the optimum solution:

$$f_{,d}(\mathbf{d}^*) + \sum_{j\in A} \lambda_j = 0 \qquad d = 1,\ldots,n_l \tag{3.12}$$

$$\sum_{d=1}^{n_l} c_d - C_T = 0 \tag{3.13}$$

$$c_j = 0, \qquad j \in \mathcal{A} \tag{3.14}$$

$$c_j - c_j^u = 0, \qquad j \in \mathcal{A} \tag{3.15}$$

$$\lambda_j > 0, \qquad j \in \mathcal{A} \tag{3.16}$$

where $\mathcal{A}$ denotes the set of active constraints with associated Lagrange multipliers λ_j, and $\mathbf{d}^*$ is the vector of design variables that minimizes the performance function. Here, and in the rest of the chapter, $()_{,d}$ denotes partial differentiation with respect to the damping coefficient c_d, and the

superscript * identifies the optimal value of a design variable. These necessary conditions, known as the Kuhn-Tucker conditions, are implemented in the gradient projection algorithm to check whether a design candidate is an optimal solution of the design problem. Notice that in general, the optimization problem may have several local minima and that Eqs. (3.12) to (3.16) only give the necessary conditions to be satisfied by these locally optimal solutions. In order to find the globally optimal solution, the optimization procedure must be restarted from different initial guesses to select the solution that gives the least value to the performance index.

For a given amount of viscous damping material C_T, the solution of the optimization problem determines its best distribution throughout the building height. However, this amount of material may not be adequate to comply with the established performance criteria, such as the reduction of the acceleration response of the top story of a building by a given percentage. One way to determine the necessary damping material is to solve a series of new optimization problems in which the C_T quantity is varied in the constraint Eq. (3.10). However, the extra computational effort could be avoided if an explicit dependency of the performance index function with respect to the damping material quantity C_T could be determined. Although such an expression is not available, it is possible to implicitly relate $f[\mathbf{R}(\mathbf{d},t)]$ with the constraint parameter C_T through the solution of the optimization problem. The constraint sensitivity theorem provides such an analysis tool. It can be shown that the rate of change of the performance function with respect to C_T is equal to the λ_1^* Lagrange multiplier associated with the equality constraint of Eq. (3.10) as follows:

$$\left\{ f\left[\mathbf{R}(\mathbf{d}^*,t)\right]\right\}_{,C_T} = -\lambda_1^* \tag{3.17}$$

where $\mathbf{d}^*$ is the optimal solution describing the distribution of C_T. Equation (3.17) can be used to estimate the amount of damping coefficient value ΔC_T to be added or extracted from the building to obtain the desired reduction in the optimum performance function value. Since the optimum performance index value depends implicitly on C_T, it is possible to use a first-order Taylor expansion about this point as,

$$f(C_T + \Delta C_T) = f(C_T) + \frac{\partial f(C_T)}{\partial C_T}\Delta C_T \tag{3.18}$$

Let $f_d[\mathbf{R}(\mathbf{d}^*,t)]$ be the desired value for the optimum performance index. Substituting Eq. (3.17)

in (3.18), the following result is obtained for the quantity ΔC_T,

$$\Delta C_T = \frac{f_d\left[\mathbf{R}(\mathbf{d}^*, t)\right] - f(C_T)}{-\lambda_1^*} \tag{3.19}$$

Therefore, the performance-based design of viscoelastically-damped structures can be summarized as follows:

- Specify a desired level of response reduction or a change in the performance index of the uncontrolled structure $f_d[\mathbf{R}(\mathbf{d}^*, t)]$.
- Select a value for the total damping coefficient C_T and assume an initial distribution of the damping elements along the building height.
- Use the gradient projection technique with this initially assumed distribution of damping guess to find the optimal design parameters $\mathbf{d}^*$ and Lagrange multipliers $\boldsymbol{\lambda}^*$.
- If the value of the performance index at the optimal solution satisfies the target reduction level, then stop. Otherwise, determine the amount of damping coefficient value ΔC_T to be added or extracted from Eq. (3.19).
- Solve a new optimization problem with the total damping coefficient set to the value $C_T + \Delta C_T$.
- Repeat the previous steps until the prescribed performance criteria are satisfied.

3.3.2 Discrete Design Variables

In the previous subsection, the mechanical properties of the damping devices were determined considering that they could take on any admissible real value. The assumption of continuous design variables permitted the use of analytical techniques of differential calculus in locating the optimum design solutions as well as the determination of the relations between the design variables, performance index function and constraints parameters. However, this solution may not be practically feasible due to the limited availability of the commercial products. In this regard, a more convenient and practical solution will be the one involving the selection of dampers from those that can be supplied by the industry. Therefore, in the following development, the characteristics of a unitary device (i.e. damper capacity) are specified, or a device with predetermined mechanical properties is chosen from a catalog of commercial

products for optimization purposes. Since the parameters of the devices are fixed, the problem of finding the number of devices and their locations within the building can be viewed as a combinatorial optimization problem with a discrete design space. Thus, the general optimal design problem can now be expressed as:

$$\underset{\mathbf{n}}{\text{minimize}} \quad f\left[\mathbf{R}(\mathbf{n},t)\right] \tag{3.20}$$

subject to

$$\sum_{d=1}^{n_l} n_d = n_T \tag{3.21}$$

where **n** is the vector of design variables n_d, and n_T is the total number of dampers to be placed in a structure. Although, in principle, the optimal solution to such a finite problem can be found by an exhaustive or enumerative search of every possible combination of dampers locations, practical implementation of this search is impossible due to the high number of feasible design solutions. For example, for optimal placement of 50 different damper devices in ten possible stories of a building structure, one will have to examine 10^{50} possible combinations. For m identical devices to be placed in n possible stories, there are $(m+n-1)!/m!(n-1)!$ different combinations. For $m = 50$ and $n = 10$, this number is 1.25×10^{10}. Searching each possible combination is obviously a daunting task even for the current computing facilities and, therefore, a more systematic and an efficient approach must be used.

A genetic algorithm is employed to find the best design solution of problems involving discrete design variables. For a given number of devices, one can obtain their locations in a structure by solving the optimization problem given by Eqs. (3.20) and (3.21), and compute the level of response reduction achieved for this installation. On the other hand, the problem of obtaining the least number of devices to reduce the response by a determined amount has to be solved by a series of trial optimization iterations. In this case, the lack of an analytical result, such as the constraint sensitivity theorem presented in the previous subsection, precludes the determination of a relationship between the performance index function and the total number of devices. Therefore, the dependence of $f[\mathbf{R}(\mathbf{n}^*,t)]$ on n_T has to be determined numerically. This can be done by varying the total number of devices in the vicinity of n_T and solving a new optimization problem using the value of $n_T+\Delta n_T$ in the constraint Eq. (3.21). The obtained

variation can then be used for extrapolation purposes, and the total number of devices required to accomplish the target design goal can be estimated.

3.4 Response Calculations

To calculate the performance index to evaluate a particular design, one must analyze the structure. Usually the focus of a performance-based design is to reduce the maximum values of the response or a norm. For a linear structural system, these response quantities can be estimated using a linear analysis technique combined with a stochastic or a response spectrum description of the site input earthquake excitation. This methodology lessens the computational effort required in the evaluation of the performance indices since it obviates the need to numerically integrate the differential equations of motion of the structural system. Furthermore, this approach facilitates the inclusion of the variability of the input excitation in the optimization design process by considering collectively in a single analysis the population of ground motions that represent the site geology and seismicity.

For the present research, a modal analysis based random vibration approach is adopted. In this methodology, the equations of motion of the combined structural system must be solved by a modal analysis approach to properly identify the natural frequencies, natural modes, and modal damping ratios of the system. The maximum modal response is first computed for each mode, and the total structural response can then be estimated by superimposing the responses of all contributing modes.

For illustration, consider an *N*-degree of freedom model shear building model installed with fluid viscoelastic devices, as shown in Figure 3.5. The equations of motion for this can be written as:

$$\mathbf{M}\,\ddot{\mathbf{x}}(t) + \mathbf{C}_s\,\dot{\mathbf{x}}(t) + \mathbf{K}_s\,\mathbf{x}(t) + \sum_{d=1}^{n_l} \mathbf{r}_d\, n_d P_d(t) = -\mathbf{M}\,\mathbf{E}\,\ddot{X}_g(t) \tag{3.22}$$

where $\ddot{X}_g(t)$ the seismic disturbance at the base of the structure, and $\mathbf{x}(t)$ is the vector of relative displacements along the excitation direction. If the force exerted by the d^{th} fluid viscoelastic device is characterized by a simple dashpot model, the following kinematic relations can be established between the local deformations at the damper element and those of the main

structural members:

$$\left.\begin{aligned} P_d(t) &= c_d\,\dot{\Delta}_d(t) \\ \dot{\Delta}_d(t) &= \mathbf{r}_d^T\,\dot{\mathbf{x}}(t) \end{aligned}\right\} \quad P_d(t) = c_d\,\mathbf{r}_d^T\,\dot{\mathbf{x}}(t) \tag{3.23}$$

where for the building model depicted in Figure 3.5, the influence vectors $\mathbf{r}_d{}^T$ are given by:

$$\mathbf{r}_1^T = \begin{bmatrix} 1 & 0 & 0 \end{bmatrix}; \qquad \mathbf{r}_2^T = \begin{bmatrix} -1 & \cos\theta_2 & 0 \end{bmatrix}; \qquad \mathbf{r}_3^T = \begin{bmatrix} 0 & -\cos\theta_2 & \cos\theta_3 \end{bmatrix} \tag{3.24}$$

Substitution of Eq. (3.23) in Eqs. (3.22) leads to,

$$\mathbf{M}\,\ddot{\mathbf{x}}(t) + \left(\mathbf{C}_s + \sum_{d=1}^{n_l} \mathbf{r}_d\, n_d\, c_d\, \mathbf{r}_d^T \right) \dot{\mathbf{x}}(t) + \mathbf{K}_s\,\mathbf{x}(t) = -\mathbf{M}\,\mathbf{E}\,\ddot{X}_g(t) \tag{3.25}$$

Therefore, the damping matrix of the overall system, defined as **C**, is obtained by adding the inherent structural damping matrix $\mathbf{C}_s$ and the damping contribution from the devices. That is,

$$\mathbf{C} = \mathbf{C}_s + \sum_{d=1}^{n_l} \mathbf{r}_d\, n_d\, c_d\, \mathbf{r}_d^T \tag{3.26}$$

It can be noticed from Eqs. (3.25) and (3.26) that by adding several damping devices at different locations of a structure, the resultant modified structure can become a non-classically damped system. This non-classically damped system can also be overdamped in certain modes, depending upon the amount of supplemental damping introduced.

To analyze a case of a non-proportional or non-classical damping matrix **C**, it is convenient to rewrite the equations of motion (3.25) as a system of first order state equations,

$$\mathbf{A}_s\,\dot{\mathbf{z}}(t) + \mathbf{B}_s\,\mathbf{z}(t) = -\mathbf{D}_s \begin{Bmatrix} \mathbf{0} \\ \mathbf{E} \end{Bmatrix} \ddot{X}_g(t) \tag{3.27}$$

where, for an N-degree of freedom dynamic system $\mathbf{z}(t)$ is the $2N$-state vector consisting of the relative velocity vector $\dot{\mathbf{x}}(t)$ in its first N elements and the relative displacement vector $\mathbf{x}(t)$ in the remaining N elements. The symmetric system matrices $\mathbf{A}_s$, $\mathbf{B}_s$ and $\mathbf{D}_s$ of dimension $2N \times 2N$ are defined as:

$$\mathbf{A}_s = \begin{bmatrix} \mathbf{0} & \mathbf{M} \\ \mathbf{M} & \mathbf{C} \end{bmatrix}; \quad \mathbf{B}_s = \begin{bmatrix} -\mathbf{M} & \mathbf{0} \\ \mathbf{0} & \mathbf{K}_s \end{bmatrix}; \quad \mathbf{D}_s = \begin{bmatrix} \mathbf{0} & \mathbf{0} \\ \mathbf{0} & \mathbf{M} \end{bmatrix} \tag{3.28}$$

In the case where the fluid viscoelastic device is modeled by a dashpot and spring in series, the force exerted by the d^{th} damper on the structure is described by the first order differential equation relationship of Eq. (3.1). It is rewritten here for convenience of solution as:

$$\tau_d \, \dot{P}_d(t) + P_d(t) - c_d \, \mathbf{r}_d^T \, \dot{\mathbf{x}}(t) = 0; \qquad d = 1, \ldots, n_l \tag{3.29}$$

The equations of motion (3.22) combined with the equation (3.29) of the linear damping device can be written in the similar state space format given for Eq. (3.27) as,

$$\mathbf{A}_s \, \dot{\mathbf{z}}(t) + \mathbf{B}_s \, \mathbf{z}(t) = -\mathbf{D}_s \begin{Bmatrix} \mathbf{E} \\ \mathbf{0} \\ \mathbf{0} \end{Bmatrix} \ddot{X}_g(t) \tag{3.30}$$

where the system matrices $\mathbf{A}_s$, $\mathbf{B}_s$ and $\mathbf{D}_s$ are now of dimension $(2N + n_l) \times (2N + n_l)$, and defined as:

$$\mathbf{A}_s = \begin{bmatrix} \mathbf{M} & \mathbf{0} & \mathbf{0} \\ \mathbf{0} & \mathbf{I} & \mathbf{0} \\ \mathbf{0} & \mathbf{0} & \boldsymbol{\Gamma} \end{bmatrix}; \quad \mathbf{B}_s = \begin{bmatrix} \mathbf{C} & \mathbf{K}_s & \mathbf{L} \\ -\mathbf{I} & \mathbf{0} & \mathbf{0} \\ -\mathbf{D} & \mathbf{0} & \mathbf{I} \end{bmatrix}; \quad \mathbf{D}_s = \begin{bmatrix} \mathbf{M} & \mathbf{0} & \mathbf{0} \\ \mathbf{0} & \mathbf{0} & \mathbf{0} \\ \mathbf{0} & \mathbf{0} & \mathbf{0} \end{bmatrix}; \quad \mathbf{z}(t) = \begin{Bmatrix} \dot{\mathbf{x}}(t) \\ \mathbf{x}(t) \\ \mathbf{P}_d(t) \end{Bmatrix} \tag{3.31}$$

$$\mathbf{L} = \begin{bmatrix} n_1 \mathbf{r}_1 & \cdots & n_{n_l} \mathbf{r}_{n_l} \end{bmatrix}; \qquad \mathbf{D} = \begin{bmatrix} c_1 \mathbf{r}_1^T \\ \vdots \\ c_{n_l} \mathbf{r}_{n_l}^T \end{bmatrix}; \qquad \boldsymbol{\Gamma} = \begin{bmatrix} \tau_1 & \cdots & 0 \\ \vdots & \ddots & \vdots \\ 0 & \cdots & \tau_{n_l} \end{bmatrix} \tag{3.32}$$

It can be seen from Eqs. (3.31) that the system matrix $\mathbf{B}_s$ is not longer symmetric, and that the extended state vector $\mathbf{z}(t)$ now includes the damping devices forces in the column vector $\mathbf{P}_d(t)$.

In the foregoing discussion, the equations of motion of the overall structural system were obtained for a shear-building model of a viscoelastically-damped structure. The fluid viscoelastic devices were characterized either as simple viscous elements or by dashpots and linear springs in series. However, more refined models may be needed to accurately represent and predict the behavior of the dampers and of the building structure. Therefore, the remainder of this section is devoted to the development of a generalized modal-based random vibration approach valid for the analysis of general linear structural systems with arbitrary linear damping characteristics.

The analysis of a linear viscoelastically-damped structure with force-deformation characterization of the devices described by a set of linear algebraic or differential equation relationships can be done by expressing the general equations of motion (2.1) in the following state space format:

$$\dot{\mathbf{z}}(t) = \mathbf{A} \, \mathbf{z}(t) + \mathbf{B} \, \mathbf{f}(t) \tag{3.33}$$

where the description of the dynamic behavior of the overall structural system is done in terms of a unique $(2N+n_l)\times(2N+n_l)$ non-symmetric system matrix **A**,

$$\mathbf{A}=\begin{bmatrix} -\mathbf{M}^{-1}\mathbf{C}_s & -\mathbf{M}^{-1}\mathbf{K}_s & \mathbf{L}_{N\times n_l} \\ \mathbf{I}_{N\times N} & \mathbf{0}_{N\times N} & \mathbf{0}_{N\times n_l} \\ \boldsymbol{\Gamma}_{\dot{u}(n_l\times N)} & \boldsymbol{\Gamma}_{u(n_l\times N)} & \boldsymbol{\Gamma}_{P(n_l\times n_l)} \end{bmatrix} \tag{3.34}$$

and

$$\mathbf{z}(t)=\begin{Bmatrix} \dot{\mathbf{u}}(t) \\ \mathbf{u}(t) \\ \mathbf{P}_d(t) \end{Bmatrix} \tag{3.35}$$

is the extended $(2N+n_l)$-dimensional state vector $\mathbf{z}(t)$ that includes the damping devices forces in the n_l-dimensional vector $\mathbf{P}_d(t)$. The influence matrices **L** and **B** specifying, respectively, the locations and number of linear passive devices and *l*-components of the seismic excitation in the state space are given by:

$$\mathbf{L}=\begin{bmatrix} -n_1\mathbf{M}^{-1}\mathbf{r}_1 & \cdots & -n_{n_l}\mathbf{M}^{-1}\mathbf{r}_{n_l} \end{bmatrix}_{N\times n_l}; \qquad \mathbf{B}=\begin{Bmatrix} -\mathbf{E}_{N\times l} \\ \mathbf{0}_{N\times l} \\ \mathbf{0}_{n_l\times l} \end{Bmatrix} \tag{3.36}$$

The matrices **M**, **C**, **K**, **E** and vectors $\mathbf{u}(t)$, and $\mathbf{f}(t)$ were defined in Chapter 2. The matrices $\boldsymbol{\Gamma}_{\dot{u}}$, $\boldsymbol{\Gamma}_u$ and $\boldsymbol{\Gamma}_P$ characterize the dynamic properties of the damping devices. It can be easily shown that for a building structure incorporating fluid viscoelastic devices modeled by first-order differential equations of the Maxwell type, the matrices $\boldsymbol{\Gamma}_{\dot{u}}$, $\boldsymbol{\Gamma}_u$ and $\boldsymbol{\Gamma}_P$ reduce to:

$$\boldsymbol{\Gamma}_{\dot{u}}=\begin{bmatrix} \frac{c_1}{\tau_1}\mathbf{r}_1^T \\ \vdots \\ \frac{c_{n_l}}{\tau_{n_l}}\mathbf{r}_{n_l}^T \end{bmatrix}; \qquad \boldsymbol{\Gamma}_u=\mathbf{0}; \qquad \boldsymbol{\Gamma}_P=-\begin{bmatrix} \frac{1}{\tau_1} & \cdots & 0 \\ \vdots & \ddots & \vdots \\ 0 & \cdots & \frac{1}{\tau_{n_l}} \end{bmatrix} \tag{3.37}$$

Since the system matrix **A** is not symmetric, a generalized modal analysis approach has to be used to transform the set of simultaneous ordinary differential equations (3.33) into a set of independent equations [118]. The previously developed generalized response spectrum approach such as the one proposed by Singh [160] can be extended to include this case as well. To

uncouple Eq. (3.33) using a similarity transformation, the eigenproperties of the following adjoint eigenvalue problem are used:

$$\mathbf{A}\boldsymbol{\varphi}_j = \mu_j \boldsymbol{\varphi}_j; \qquad \mathbf{A}^T\boldsymbol{\psi}_j = \mu_j \boldsymbol{\psi}_j; \qquad j = 1,\ldots,2N+n_l \tag{3.38}$$

where μ_j is the j^{th} eigenvalue, and $\boldsymbol{\varphi}_j$ and $\boldsymbol{\psi}_j$ are the corresponding right and left eigenvectors. Usually, the eigenvalues, and the corresponding eigenvectors, will occur in complex conjugate pairs. However, some of them could also be real if the corresponding modes are critically or overdamped. For a stable structural system, the eigenvalues must also have negative real parts. The two sets of eigenvectors satisfy the following biorthonormality relations

$$\boldsymbol{\psi}_j^T \mathbf{A}\boldsymbol{\varphi}_i = \mu_i \delta_{ij}; \qquad \boldsymbol{\psi}_j^T \boldsymbol{\varphi}_i = \delta_{ij}; \qquad i, j = 1,\ldots,2N+n_l \tag{3.39}$$

where δ_{ij} is the Kronecker delta. By using the following standard transformation of coordinates in Eq. (3.33)

$$\mathbf{z}(t) = \boldsymbol{\Phi}\boldsymbol{\xi}(t) \tag{3.40}$$

in which $\boldsymbol{\xi}(t)$ is the vector of modal coordinates and $\boldsymbol{\Phi}$ is the modal matrix containing the right eigenvectors $\boldsymbol{\varphi}_j$, and pre-multiplication by the modal matrix of left eigenvectors $\boldsymbol{\Psi}^T$, one obtains $2N + n_l$ uncoupled equations for the principal coordinates $\xi_j(t)$ as follows:

$$\dot{\xi}_j(t) - \mu_j \xi_j(t) = -\boldsymbol{\psi}_j^T \mathbf{B}\mathbf{f}(t); \qquad j = 1,...,2N+n_l \tag{3.41}$$

The solution of Eq. (3.41) for a given ground motion and zero initial conditions, can be obtained for $\xi_j(t)$ directly in the form

$$\xi_j(t) = \int_0^t e^{\mu_j(t-\tau)}\, \boldsymbol{\psi}_j^T \mathbf{B}\mathbf{f}(\tau)\, d\tau \tag{3.42}$$

For a given installation of devices, any response quantity can be obtained as a linear combination of the states of the system as:

$$\mathbf{R}(\mathbf{d},\mathbf{n},t) = \mathbf{T}\,\mathbf{z}(t) \tag{3.43}$$

where **T** is a transformation matrix of appropriate dimensions. For a force related response quantity, the elements of the transformation matrix **T** will consist of stiffness related quantities. For calculating the absolute acceleration vector of the structure, one can define such a response transformation matrix in the following form:

$$\mathbf{T} = \begin{bmatrix} -\mathbf{M}^{-1}\mathbf{C} & -\mathbf{M}^{-1}\mathbf{K} & \mathbf{0} \end{bmatrix} \tag{3.44}$$

Equations (3.40) and (3.43) relate the solution in the principal coordinates $\xi_j(t)$ to any desired response quantity as follows:

$$\mathbf{R}(\mathbf{d},\mathbf{n},t) = \mathbf{T}\boldsymbol{\Phi}\boldsymbol{\xi}(t) \tag{3.45}$$

Equation (3.45) can be used to define the mean square response for a stochastic description of the input, and to obtain the design response for a response spectrum description of the input. In this chapter, the maximum values of the structural response vector $\mathbf{R}(\mathbf{d},\mathbf{n},t)$, denoted as $\mathbf{R}(\mathbf{d},\mathbf{n})$, are utilized to evaluate the performance indices of Eqs. (3.9) or (3.20). For a stochastic input, these quantities can be expressed as an amplified value of the root mean square response. That is,

$$\mathbf{R}(\mathbf{d},\mathbf{n}) = \max_t \left|\mathbf{R}(\mathbf{d},\mathbf{n},t)\right| \cong F\sqrt{E\left[\mathbf{R}^2(\mathbf{d},\mathbf{n},t)\right]} \tag{3.46}$$

where F is a peak factor. It can be shown that for a stationary stochastic input defined by l-uncorrelated stationary random processes with spectral density functions $\Phi_l(\omega)$, the stationary mean square value of the response vector in Eq. (3.46) can be expressed as follows:

$$E\left[\mathbf{R}^2(\mathbf{d},\mathbf{n},t)\right] = \int_{-\infty}^{\infty} \sum_l \Phi_l(\omega) \left[\sum_{j=1}^{2N+n_l} \sum_{k=1}^{2N+n_l} \left(\frac{\{\mathbf{q}_l\}_j}{\mu_j - i\omega} \right)\left(\frac{\{\mathbf{q}_l\}_j}{\mu_k + i\omega} \right) \right] d\omega \tag{3.47}$$

where the vector $\{\mathbf{q}_l\}_j$ is the j^{th} column of the complex matrix $\mathbf{Q}_l$, defined as

$$\mathbf{Q}_l = \mathbf{T}\boldsymbol{\Phi}\boldsymbol{\Psi}^T\mathbf{b}_l \tag{3.48}$$

and the vector $\mathbf{b}_l$ is the l^{th} column of the $\mathbf{B}$ matrix. On the other hand, if the devices are modeled by algebraic relationships, such as the viscous dashpot models, the analysis can be done more conveniently using the pair of symmetric matrices $\mathbf{A}_s$ and $\mathbf{B}_s$ given by Eq. (3.28). The eigenproperties required for the evaluation of the different modal response quantities can be now obtained by solving the reduced $2N \times 2N$-symmetrical eigenvalue problem,

$$-\mu_j \mathbf{A}_s \boldsymbol{\varphi}_j = \mathbf{B}_s \boldsymbol{\varphi}_j; \qquad j = 1,\ldots,2N \tag{3.49}$$

In this case, the left eigenvectors coincide with the right eigenvectors and the eigenvalue problem is said to be self-adjoint. The complex matrix $\mathbf{Q}_l$ is now defined as:

$$\mathbf{Q}_l = \mathbf{T}\boldsymbol{\Phi}\boldsymbol{\Phi}^T\mathbf{M}\mathbf{E}_l \tag{3.50}$$

For a given spectral density function, one can evaluate the integral in Eq. (3.47) by

residue analysis. However, if one wants to express the integral in terms of the ground response spectra of the input motion, then Eq. (3.47) must be explicitly expressed in terms of the conventional frequencies ω_j and damping ratios β_j of the system modes.

Let the number of real eigenvalues be n_r and the number of complex conjugate eigenvalues be $2n_c$. Also, let the real and complex eigenvalues and their corresponding modal coefficients $\{\mathbf{q}_l\}_j$ and $\{\mathbf{g}_l\}_j$, be defined as:

$$\alpha_j = -\mu_j; \qquad \{\mathbf{e}_l\}_j = \{\mathbf{q}_l\}_j \qquad j = 1,...,n_r \tag{3.51}$$

$$\mu_j = -\beta_j \omega_j + i\,\omega_j \sqrt{1-\beta_j}; \qquad j = 1,\ldots,n_c \tag{3.52}$$

$$\omega_j = \left|\,\mu_j\,\right|; \qquad \beta_j = -\frac{\text{Real}\,(\mu_j)}{\omega_j}; \qquad j = 1,\ldots,n_c \tag{3.53}$$

$$\{\mathbf{q}_l\}_j = \{\mathbf{a}_l\}_j + i\{\mathbf{b}_l\}_j; \qquad j = 1,\ldots,n_c \tag{3.54}$$

$$\{\mathbf{g}_l\}_j = 2\,\omega_j \left[\{\mathbf{b}_l\}_j \sqrt{1-\beta_j^2} - \{\mathbf{a}_l\}_j\,\beta_j\right]; \qquad j = 1,\ldots,n_c \tag{3.55}$$

Of course, there are equal numbers of complex conjugate quantities corresponding to the quantities in Eqs. (3.52) to (3.55).

Consideration of the summation terms in Eq. (3.47) as a function of the real and complex quantities given by Eqs. (3.51) to (3.55), one can simplify the expression for the mean square value as follows

$$E\left[\mathbf{R}^2(\mathbf{d},\mathbf{n},t)\right] = \mathbf{S}_1 + \mathbf{S}_2 + \mathbf{S}_3 \tag{3.56}$$

where the components of the quantities $\mathbf{S}_1$, $\mathbf{S}_2$ and $\mathbf{S}_3$ are defined as follows:

$$\mathbf{S}_{1i} = \sum_l \sum_{j=1}^{n_r} \{\mathbf{e}_{li}\}_j^2\, J_{lj} + 2 \sum_l \sum_{j=1}^{n_r-1} \sum_{k=j+1}^{n_r} \frac{\{\mathbf{e}_{li}\}_j \{\mathbf{e}_{li}\}_k}{(\alpha_j + \alpha_k)} \left(\,\alpha_j J_{lj} + \alpha_k J_{lk}\,\right) \tag{3.57}$$

$$\mathbf{S}_{2i} = 2 \sum_l \sum_{j=1}^{n_r} \sum_{k=1}^{n_c} \{\mathbf{e}_{li}\}_j \left(\,A_{lijk}\; J_{lj} + B_{lijk}\; I_{1lk} + C_{lijk}\; I_{2lk}\,\right) \tag{3.58}$$

$$\mathbf{S}_{3i} = 2 \sum_l \sum_{j=1}^{n_c-1} \sum_{k=j+1}^{n_c} \left[W_{lijk} \left(I_{1lj} - \frac{I_{1lk}}{\Omega^4} \right) + Q_{lijk} \left(I_{2lj} - I_{2lk} \right) + \frac{\{\mathbf{g}_{li}\}_j \{\mathbf{g}_{li}\}_k}{\Omega^2} I_{1lk} + 4\{\mathbf{a}_{li}\}_j \{\mathbf{a}_{li}\}_k\, I_{2lk} \right] \tag{3.59}$$

where the explicit expressions for A_{jk}, B_{jk}, C_{jk}, W_{jk}, and Q_{jk} required in Eqs. (3.57) to (3.59) are given in Appendix. Equations (3.57) to (3.59) require the following frequency integrals

$$J_{lj} = \int_{-\infty}^{\infty} \frac{\Phi_l(\omega)}{(\alpha_j{}^2 + \omega^2)} d\omega \tag{3.60}$$

$$I_{1lj} = \int_{-\infty}^{\infty} \frac{\Phi_l(\omega)}{(\omega_j{}^2 - \omega^2)^2 + 4\,\omega_j{}^2 \beta_j{}^2 \omega^2} d\omega; \quad I_{2lj} = \int_{-\infty}^{\infty} \frac{\Phi_l(\omega)\,\omega^2}{(\omega_j{}^2 - \omega^2)^2 + 4\,\omega_j{}^2 \beta_j{}^2 \omega^2} d\omega \tag{3.61}$$

These integrals can be evaluated for a given spectral density function by any suitable method. It is noted that I_{1lj} and I_{2lj} are the mean square values of the relative displacement and relative velocity responses, respectively, of a single degree of freedom oscillator of parameters ω_j, β_j excited by ground motion component $\mathbf{f}_l(t)$. J_{lj} represents the mean square response $E[\nu^2(t)]$ of the following first order equation

$$\dot{\nu}(t) + \alpha_j \nu(t) = \mathbf{f}_l(t) \tag{3.62}$$

The mean square values defined by I_{1lj} and I_{2lj} can be expressed in terms of the usual response spectra used in seismic design practice. Similarly, J_{lj} can also be expressed in terms of a response spectrum input associated with Eq. (3.62). Such a spectrum can be easily developed for design purposes using an ensemble of time histories. This way, the response of the systems with augmented damping can be expressed in terms of the seismic input as defined by a response spectrum.

3.5 Gradients Calculations

In the gradient projection method, one moves along the direction of steepest descent that satisfies the problem constraints to reach at the optimum value. Therefore, it is necessary to calculate the rate of change of performance indices and constraint functions with respect to the design parameters at any design point of the search space. For a linear system, one can define the gradients more conveniently in terms of the rates of change of the modal quantities of the structural systems as explained below.

The mean square values of the response are defined in terms of the eigenproperties of the system through Eqs. (3.57) to (3.59). It is thus an implicit function of the design variables. To calculate the gradient of the response, the derivatives of the system eigenproperties with respect to the design variables are required. Solution procedures for derivative calculations of the

general eigenproblem are well established [122]. However, in this study only the sensitivities of the symmetric self-adjoint eigenproblem are considered. For a nonclassically damped case, these can be obtained as [57]:

Derivatives of eigenvectors:

$$\left\{\boldsymbol{\varphi}_j\right\}_{,d} = \sum_{k=1}^{2N} a_{jk}\,\boldsymbol{\varphi}_k \tag{3.63}$$

with

$$a_{jk} = \begin{cases} -\dfrac{1}{2}\left\{\boldsymbol{\varphi}_j\right\}_L^T \mathbf{C}_{,d} \left\{\boldsymbol{\varphi}_j\right\}_L & \text{if } j = k \\ -\dfrac{1}{\left(\mu_k - \mu_j\right)}\left[\left\{\boldsymbol{\varphi}_k\right\}_L^T \left(\mu_j\,\mathbf{C}_{,d}\right)\left\{\boldsymbol{\varphi}_j\right\}_L\right] & \text{if } j \neq k \end{cases} \tag{3.64}$$

and $\left\{\boldsymbol{\varphi}_j\right\}_L$ denotes the lower part of the j^{th} eigenvector.

Derivatives of eigenvalues:

$$\mu_{j,d} = -\left\{\boldsymbol{\varphi}_j\right\}_L^T \left(\mu_j\,\mathbf{C}_{,d}\right)\left\{\boldsymbol{\varphi}_j\right\}_L \tag{3.65}$$

Derivatives of natural frequencies:

$$\omega_{j,d} = \frac{1}{\omega_j}\left\{\mathrm{Re}\left[\mu_j\right]\mathrm{Re}\left[\mu_{j,d}\right] + \mathrm{Im}\left[\mu_j\right]\mathrm{Im}\left[\mu_{j,d}\right]\right\} \tag{3.66}$$

Derivatives of modal damping:

$$\beta_{j,d} = -\frac{1}{\omega_j^2}\left\{\mathrm{Re}\left[\mu_j\right]\,\omega_{j,d} + \omega_j\,\mathrm{Re}\left[\mu_{j,d}\right]\right\} \tag{3.67}$$

The operators Re[] and Im[] denote the real and imaginary parts of the complex number in the square bracket. In terms of these rates of change, the derivative of the i^{th} root mean square response component, $E\left[\mathbf{R}_i(\mathbf{d},t)\right]$, with respect to the d^{th} design variable can be obtained as

$$\left\{E\left[\mathbf{R}_i(\mathbf{d},t)\right]\right\}_{,d} = \frac{\left\{E\left[\mathbf{R}_i^2(\mathbf{d},t)\right]\right\}_{,d}}{2\,E\left[\mathbf{R}_i(\mathbf{d},t)\right]} \tag{3.68}$$

where

$$\left\{E\left[\mathbf{R}_i^2(\mathbf{d},t)\right]\right\}_{,d} = \left(\mathbf{S}_{1i} + \mathbf{S}_{2i} + \mathbf{S}_{3i}\right)_{,d} \tag{3.69}$$

More explicit expressions for the rates of change are provided in Appendix for direct adaptation by a user.

3.6 Sensitivity of Optimum Solution to Problem Parameters

The optimum solutions for the device sizes will depend upon the assumed values of the problem parameters such as the input acceleration intensity parameter and frequency content parameters. It is of practical interest to know how the optimal design is affected when some of these problem parameters are changed. The study of variations in the optimum solutions as some of the problem parameters are changed is known as the post-optimality or sensitivity analysis [164; 188]. The sensitivities of the design variable are defined in terms of their partial derivatives with respect to the problem parameters. In what follows, a procedure is presented to calculate these sensitivities.

Let p be a parameter of interest with respect to which it is desired to determine the sensitivities of the optimally obtained design variables. To obtain these, we differentiate Eqs. (3.12) to (3.15) with respect to the problem parameter p. Assuming that the same set of active constraints still remain active, we obtain the following

$$\sum_{k=1}^{n} \frac{\partial^2 f}{\partial c_d \partial c_k} \frac{\partial c_k}{\partial p} + \frac{\partial^2 f}{\partial p \, \partial c_d} + \sum_{j \in A} \frac{\partial \lambda_j}{\partial p} = 0 \qquad d = 1, \ldots, n_l \tag{3.70}$$

$$\sum_{d=1}^{n_l} \frac{\partial c_d}{\partial p} = 0 \tag{3.71}$$

$$\frac{\partial c_j}{\partial p} = 0, \qquad j \in A \tag{3.72}$$

Eqs. (3.70) to (3.72) provide n_l+q equations to solve for the desired derivatives, where q denotes the number of active constraints. In matrix form these equations can be written as:

$$\begin{bmatrix} \mathbf{H}_{n_l \times n_l} & \mathbf{G}_{n_l \times q} \\ \mathbf{G}^T_{q \times n_l} & \mathbf{0}_{q \times q} \end{bmatrix} \begin{Bmatrix} \mathbf{d}^*_{,p} \\ \boldsymbol{\lambda}^*_{,p} \end{Bmatrix} = - \begin{Bmatrix} \mathbf{p}_{n_l \times 1} \\ \mathbf{0}_{q \times 1} \end{Bmatrix} \tag{3.73}$$

where the elements of the matrices and vectors components in Eq. (3.73) are given by

$$\mathbf{H}_{dk} = \left[f(\mathbf{d}^*) \right]_{,dk} \quad \text{and} \quad \mathbf{p} = \left[f(\mathbf{d}^*) \right]_{,dp} \tag{3.74}$$

$$\mathbf{d}^*_{,p} = \begin{Bmatrix} c_{1,p} \\ \vdots \\ c_{n,p} \end{Bmatrix}, \quad \boldsymbol{\lambda}^*_{,p} = \begin{Bmatrix} \lambda_{1,p} \\ \vdots \\ \lambda_{q,p} \end{Bmatrix} \tag{3.75}$$

Matrix **G** mainly consists of zeroes except for

$$\begin{aligned} G_{i1} &= 1, && i = 1,\ldots,n \\ G_{j(1+i)} &= -1, && j \in A,\ i = 1,\ldots,q-1, \quad \text{if lower bound is active} \\ G_{j(1+i)} &= 1, && j \in A,\ i = 1,\ldots,q-1, \quad \text{if upper bound is active} \end{aligned} \tag{3.76}$$

Here, and in the following, $()_{,p}$ indicates partial differentiation with respect to the problem parameter p, and $()_{,ip}$ denotes the mixed partial derivative with respect to the damping coefficient c_i and the problem parameter p.

The solution of the system of linear equations (3.73) provides a convenient way to calculate these sensitivities. It is relevant to note that to calculate the design sensitivities with respect to different problem parameters, one only needs to change the right hand side of this equation.

Once Eqs. (3.73) are solved for $\mathbf{d}^*_{,p}$ and $\boldsymbol{\lambda}^*_{,p}$, the rate of change of the optimum performance function value with respect to the parameter p can be computed as,

$$\frac{df(\mathbf{d}^*)}{dp} = \left[f(\mathbf{d}^*) \right]_{,p} + \sum_{d=1}^{n_l} \left[f(\mathbf{d}^*) \right]_{,d} c^*_{d,p} \tag{3.77}$$

The changes in the optimum values of c_d and $f(\mathbf{d}^*)$ necessary to satisfy the optimality conditions due to a change Δp in the problem parameter can be estimated as

$$\begin{aligned} \Delta c_d &= c^*_{d,p}\, \Delta p; && d = 1,\ldots,n_l \\ \Delta f(\mathbf{d}) &= \frac{df(\mathbf{d}^*)}{dp}\, \Delta p \end{aligned} \tag{3.78}$$

3.7 Performance Indices

Consistent with the performance-based design of a viscoelastically-damped building structure, an analysis of the structure without any additional devices is made first to assess its design and the improvement it needs. Next, a desired level of response reduction in a quantity of interest is

established. This desired level of response reduction essentially establishes the performance index for the optimal design of the structure. In what follows, the different forms of performance indices considered for the numerical studies of this study are presented.

A non-dimensional form of the performance function could be as follows:

$$f_1\left[R(\mathbf{d},\mathbf{n})\right] = \frac{R(\mathbf{d},\mathbf{n})}{R_o} \tag{3.79}$$

where $R(\mathbf{d},\mathbf{n})$ is the maximum value of the response quantity of interest such as the base shear, over-turning moment, acceleration or drift of a particular floor; and R_o is a normalizing factor that corresponds to the respective response quantity of the original (unmodified) structure. Notice that this performance index measures the reduction in response at a given location. If the goal is to reduce the maximum response value regardless of the place where it occurs, the performance index can be defined as

$$f_2\left[\mathbf{R}(\mathbf{d},\mathbf{n})\right] = \max_i\left[\frac{\mathbf{R}_i(\mathbf{d},\mathbf{n})}{R_o}\right] \tag{3.80}$$

where i represents the location where the maximum response occurs, and R_o is the maximum uncontrolled response. A third possible form of performance function is defined as a norm of a vector of response quantities, such as root mean square values of the story drifts, or acceleration of different floors, etc. This form of the performance function could be expressed in a normalized form as follows:

$$f_3\left[\mathbf{R}(\mathbf{d},\mathbf{n})\right] = \frac{\left\| \mathbf{R}(\mathbf{d},\mathbf{n}) \right\|}{\left\| \mathbf{R}_o \right\|} \tag{3.81}$$

where $\mathbf{R}(\mathbf{d},\mathbf{n})$ and $\mathbf{R}_o$, respectively, are the vectors of the response quantities of interest of the modified and unmodified structures; and $\left\|\mathbf{R}(\mathbf{d},\mathbf{n})\right\| = \sqrt{\mathbf{R}(\mathbf{d},\mathbf{n})\cdot\mathbf{R}(\mathbf{d},\mathbf{n})}$ and $\left\|\mathbf{R}_o\right\| = \sqrt{\mathbf{R}_o\cdot\mathbf{R}_o}$ are the square roots of the second norm response of the modified and original structures, respectively. For mathematical convenience, second norms or quadratic norms are commonly used. To broaden the characteristics of the performance function and to include the representation of more structural response quantities in the optimization process, one could also form a composite performance function that is defined as a weighted contribution of different performance indices, such as:

$$f_c\left[\mathbf{R}(\mathbf{d},\mathbf{n})\right] = \left(w_1 f_2 + w_2 f_3\right)_{drifts} + \left(w_3 f_2 + w_4 f_3\right)_{disp.} + \left(w_5 f_2 + w_6 f_3\right)_{acc.} \quad (3.82)$$

where w_i, i = 1,…,6 are the weights assigned to different drifts, displacements, and acceleration based performance functions.

3.8 Numerical Results

The remainder of this chapter is dedicated to the numerical application of the proposed optimization-based approach for the seismic design of viscoelastically-damped building structures. Both fluid viscous and viscoelastic devices are considered for optimization purposes, as well as different types of building structures.

3.8.1 Fluid Viscous Devices

As the first illustration, viscous dampers are considered as the supplemental devices of choice to reduce the structural response. It is assumed that these devices do not contribute to the overall stiffness of the building. Therefore, their force-deformation is characterized by a viscous dashpot with mathematical model given by Eq. (3.2). Two different buildings are considered for the numerical examples. For each building, the mechanical properties of the devices are optimized using the gradient projection technique and genetic algorithm approach to consider both continuous and discrete design variables representations. Comparisons between the devices distribution are done to check whether the gradient-based procedure converges to a local optimal solution. Conversely, the optimal design solution obtained using the gradient projection technique is used to validate the solution obtained by the genetic algorithm, as no formal proof of the convergence of the genetic approach to a globally optimal solution is available.

Building 1 - Optimization with Genetic Algorithms: The 10-story shear building model, identified as Building 1 in Chapter 2, is considered here for retrofitting purposes. The parameters of the Kanai-Tajimi power spectral density function are taken as: ω_g = 18.85 rad/s, β_g=0.65, and S = 38.3×10^{-4} m^2/s^3/rad. To implement the optimization process, first the mechanical property of a unitary device (e.g., the damper capacity) is selected. The damping coefficient c_d for a damper unit was chosen to be 5.0×10^5 N-s/m. It is desired to reduce the

maximum acceleration by an arbitrarily selected value of 40%. That is, the performance index in Eq. (3.80) is to be minimized to achieve a value of 0.60. The genetic algorithm is used to obtain the least number of dampers and their locations to achieve this design objective. For the numerical calculations of the optimization procedure a population of 40 individuals was considered and the probability of crossover and probability of mutation were taken as p_c = 0.98, p_m = 0.05, respectively. The genetic search indicated that 62 dampers of the chosen unit size are required to achieve this response reduction. To achieve a similar level of reduction if, for example, the dampers were equally distributed among the building stories, one would need 90 such devices. Thus when compared with a uniformly distributed case, searching for optimality does, indeed, reduce the damper requirement by about 30%. The results of this analysis are given in Part A of Table 3.1. Column (2) shows the number of devices in each story, Column (3) the modal frequencies, and Column (4) the modal damping ratios. The damper concentration in the lower stories of the building is noted. Except for mode 7, the frequencies in this table are the absolute values of the complex eigenvalues of the system, as defined by Eq. (3.53). When compared with the corresponding undamped frequencies, they are not changed significantly by the addition of the viscous devices. The damping ratios of several modes, however, are increased significantly; this is the primary reason for the response reduction. The addition of damping devices could increase the level of damping in one or more modes to be higher than critical. Such cases are identified by the eigenvalues with no imaginary part. In Table 3.1, mode 7 is one such mode, and is identified by an asterisk. Although the motion of such modes ceases to be oscillatory, one can define the modal frequency and damping ratio for a pair of real eigenvalues using the following equations that occur in the case of a second order over-damped system:

$$\omega_j = \sqrt{\alpha_j}\ \sqrt{\alpha_{j+1}}\ ; \qquad \beta_j = \frac{\alpha_j + \alpha_{j+1}}{2\,\omega_j} \tag{3.83}$$

where α_j is defined in Eq. (3.51).

Knowing the number of devices and the unit size of devices considered in the genetic search, the total amount of supplemental damping to be added in different stories is easily calculated. Column (5) of Table 3.1 shows the total damping coefficient values of the devices

that are needed in different stories. This value is simply the product of the number of devices and the chosen damping coefficient of a single device.

To achieve a further refinement in this design and in the distribution of dampers, one could start with a large number of smaller devices. To show this, 620 devices are selected that are one-tenth the capacity of the devices initially considered. Since the number of possible combinations has now increased, a larger population need to be considered to improve the convergence. The results for this case are presented in Part B of Table 3.1. These results were obtained for a population of 80 individuals. The final convergence was achieved after 2000 generations. Thus, it required about 16000 design evaluations. Based on the final converged distribution, the total damping coefficient values required in different stories are shown in Column (9) of this table. The fact that these values are quite close to the values in Column (5) lends credence to the convergence of the genetic search procedure. This convergence to the same optimal design values when starting with different unit size of the devices also indicates the robustness of the genetic search.

In Table 3.2 are shown the results for the optimal distribution of the 62 dampers for the drift-based, acceleration-based, and the composite index of Eqs. (3.81) and (3.82). In the composite index, all performance functions were assigned equal weights of 1/6. Notice that for each index, the damper distribution is different, although all these design criteria require a higher concentration of dampers in the lower stories. The response reduction as measured by the three performance indices is now less than 40 percent. The table also shows the modal damping ratios. Figure 3.6 shows the evolution of the optimal design in successive generations and the convergence characteristics of the genetic algorithm used in this study. These results are for 62 dampers. The figure shows the value of the acceleration performance index of Eq. (3.80) for the best, the worst, and the average for the population as the generations evolve. The horizontal line indicates the results for the uniform distribution of devices in various stories. The convergence of the two indices (the average and the best) to each other, and to the final design, is quite evident. In this particular case, the population size was 40 and it took about 200 generations to reach the optimal condition. This shows the efficiency of the genetic search procedure, which required a total of 8000 design evaluations out of 9.54×10^{11} different possible combinations.

Building 1 - Optimization with Gradient Projection Technique: The design of the same 10-story building using the gradient projection technique is considered next. The size of the device to be used in a story is now determined using a continuous description of the mechanical properties c_d. To be able to compare the results obtained using both continuous and discrete variables representation, the same total amount of damping material has to be used. Therefore, the total damping coefficient C_T needed by the constraint Eq. (3.10) is determined by multiplying the number of devices required to achieve a specified level of response reduction by the size of the selected unitary device. For example, it was previously established by the genetic algorithm procedure that 62 unitary devices were required to reduce the maximum acceleration index of Eq. (3.80) by a 40%. Comparable results can thus be obtained if the continuous design problem is solved with the total amount of damping set to $C_T = 62(5.0 \times 10^5$ N-s/m)$= 3.1 \times 10^7$ N-s/m. As an initial guess, this total damping is first distributed uniformly in different stories of the building. The gradient projection algorithm is used to find the sizing of the devices. Column (2) of Table 3.3 shows the optimal distribution of these 62 devices, calculated according to the gradient projection approach. The numbers in this column are not integers. As mentioned before, in this procedure a value is obtained for the device size at each story to provide the desired optimal performance. The number in this column is obtained by dividing this optimal value by the size of the unitary device mentioned earlier. Column 3 of Table 3.3 repeats the distribution of devices previously calculated using genetic algorithms [See Column (2) of Table 3.1]. It can be observed that the distribution calculated by the gradient-based approach is quite close to the discrete numbers calculated by the genetic approach. The next column, Column (4), of this table show the optimal distribution of these devices 62 devices calculated according to the discrete sequential optimization approach of Zhang and Soong [9]. This approach indicates that optimal distribution is 54 in the first story and 8 in the second story. The percent reduction in the index achieved by this particular distribution is, however, only about 35%. This is primarily because the criterion used for the optimal placement of the devices in this approach is merely intuitive. Still, however, this approach provides a quite reasonable optimal solution. The second part of this table [Columns (5), (6), and (7)] provides results similar to those in the first part for the optimal distribution of the 62 devices to maximize the reduction in the normed drift-based index of Eq. (3.81). Again, an excellent comparison of the results in Columns (5) and (6),

pertaining to the gradient projection approach and the genetic approach, respectively, can be noted. The sequential optimization approach values shown in Column (7) again differ from those calculated by the other two approaches.

Building 2 - Optimization with Gradient Projection Technique: In the above example problem of the 10-story uniform building, the majority of the devices were concentrated in the lower stories of the building. However, this may not be the case for other structures. To investigate this, the design of supplemental viscous devices for the 24-story non-uniform Building 2 is considered next. The response reduction target is set to reduce the normed drift response by 40% through optimal distribution of the viscous devices. That is, the performance index in Eq. (3.81) is to be reduced to a value of 0.6. Not knowing a priori the amount of damping required to achieve the desired reduction in the response, an initial choice for the total damping $C_T = 9.0 \times 10^8$ N-s/m is made. As an initial guess, this total damping is first distributed uniformly in different stories of the building. This distribution, however, may not be the best. It is thus refined according to the approach presented earlier to obtain the optimal distribution. This optimal distribution is presented in Column (2) of Table 3.4. For each story, the results for the calculated design variables c_d^* are expressed as percentages of the total damping C_T. The magnitude of the reduction in the performance function achieved by this distribution damping is shown in the last two rows of the table. It is observed that the prescribed reduction level could not be achieved with the chosen amount of damping C_T. Thus, this total amount must be increased. To estimate what additional damping is needed to achieve the desired reduction, we use of the constraint variation sensitivity theorem with Eq. (3.19). Using the Lagrange multiplier value $\lambda_1^* = 1.76 \times 10^{-10}$ at the optimum solution, this additional damping can be calculated from Eq. (3.19) as: $\Delta C_T = (0.6 - 0.6576)/(-1.76 \times 10^{-10}) = 3.27 \times 10^8$ N-s/m. A new optimization problem is solved, with the equality constraint set to the new value $C_T = (9.00 + 3.27) \times 10^8$ N-s/m $= 1.227 \times 10^9$ N-s/m. As shown in Column (3), the level of reduction achieved for this amount of damping is now 39.25 %. There is still a difference of 1.87 % between the predicted and desired values. Although for practical considerations this approximation of the response reduction is quite acceptable, an additional quantity ΔC_T can be determined as a further

refinement by the proposed methodology. Using the new values of the Lagrange multiplier $\lambda_1^* = 1.324 \times 10^{-10}$, further increment in the total damping, again estimated from Eq. (3.19), is $\Delta C_T = (0.6 - 0.6075)/(-1.32 \times 10^{-10}) = 5.68 \times 10^7$ N-s/m. Finally, the optimal design that satisfies the required level of response reduction is shown in Column (4). It is obtained for a total amount of damping $\Delta C_T = (1.227 + 0.057) \times 10^9 = 1.284 \times 10^9$ N-s/m. For this final design, the evolution of the performance function with each iteration is plotted in Figure 3.7. The horizontal line indicates the result for the uniform distribution of devices. About 15% improvement, attributable to the optimization process, is achieved in the response reduction over that of the uniform distribution of damping.

It is quite conceivable that the above design may not be a globally optimal, but it will most likely be an improvement over an arbitrarily selected distribution. If the globally optimal solution is desired, then several randomly selected initial guesses for the distribution may be used to locate such a design.

Column (5) of Table 3.4 shows the damping ratios for different modes calculated for the damping distribution shown in Column (4). It is noted that several modes, shown with damping ratio values more than 100%, are now over-damped. The approach used to calculate the system response, presented earlier in the chapter, is able to include these overdamped modes properly.

It is of interest to know the cross-effectiveness of a design obtained for different performance objectives. For example, it is of interest to know how much reduction in acceleration responses of a structure would be achieved by an optimal design based on an inter-story drift-based performance function, and vice versa. Figure 3.8 shows such a cross comparison of the effectiveness of the two different designs. Design I is based on a 40% reduction in the inter-story drift-based performance function of Eq. (3.81). The optimal distribution for this design is shown in Column (4) of Table 3.4. To obtain Design II, the same total damping obtained in Design I was re-distributed optimally to achieve the best reduction in the floor acceleration-based performance function of Eq. (3.81). In Figure 3.8, we compare the inter-story drift and floor acceleration reductions achieved at different building levels by the two designs. From the figure, we note that both designs achieve about the same reduction in the inter-story drift values at different levels of the building. Of course, the Design I, specifically

made to optimize reduction in the inter-story drifts, provides a superior reduction. The reductions in the accelerations achieved by the two designs have larger differences, especially at the lower levels of building. As one would expect, Design II, specifically made to optimize the floor accelerations, provides a better reduction in the floor accelerations than Design I.

In Figure 3.9 we compare the response reduction effectiveness of the gradient-based optimization scheme used here with the sequential optimization approach. The total amount of damping used for all the results shown in Figure 3.9 is the same. The reductions in the inter-story drifts and floor accelerations achieved under the gradient-based approach proposed here are compared with the reductions obtained under the sequential approach. Since the sequential algorithm is primarily based on reducing the inter-story drifts, it compares reasonably well with the gradient-based approach in its effectiveness for reducing the inter-story drift responses. The comparison is, however, not that good in its effectiveness for reducing the floor accelerations.

Next, we examine the sensitivity of the optimal design with respect to the changes in the ground motion parameters. For the stochastic description of ground motion given by the Kanai-Tajimi power spectra model, the parameters of interest are ω_g and β_g which define the frequency and damping characteristics of the ground motion respectively, and S which defines the intensity of the motion. The sensitivities of the design variable can be evaluated by calculating their rates of change using Eq. (3.73). Similarly, the sensitivity of the performance function can be obtained from Eq. (3.77).

Table 3.5 shows the results for ω_g parameter and Table 3.6 for β_g parameter. Column (2) in the two tables shows the optimal distributions of the damping coefficient for a reduction of 40% in the normed story drift response. Column (3) in the two tables shows the normalized rates of change of these damping values with respect to the parameters. It is noted that the design variable are relatively more sensitive to the parameter β_g than to ω_g parameter. However, these sensitivities are not high. Based on these rates of change, one can estimate the change in the optimum design values of the damping coefficients from Eq. (3.78) if the parameter is changed by a certain amount. This equation is used to estimate the new values given in Columns (4) and (6) of Tables 3.5 and 3.6. The values in Columns (4) and (6), respectively, are for 10% and 50% changes in the parameter values. The values in Columns (5) and (7) indicate the difference between these estimated values and the values calculated by the optimization algorithm. It is

noted that this difference is not very large, even for a 50% change in parameter value (maximum difference is 9.25% for the damping coefficient in the 12^{th} story). Thus, for the problem at hand Eq. (3.73) can be reliably used to estimate the changes in the optimal design variable and performance function values one can expect for a given change in the design parameter. Results similar to those in Table 3.5 and 3.6 were also obtained for the ground motion intensity parameter. However, the design variable values were quite insensitive to this parameter. This, of course, was expected for this linear problem.

Building 2 - Optimization with Genetic Algorithm: The design of viscous dampers for seismic performance enhancement of Building 2 is repeated here using the genetic algorithm approach. As shown before, the normed interstory-drifts response can be reduced 40% by optimally distributing a total damping amount C_T=1.284 $\times$ 10^9 N-s/m. This quantity has to be properly discretized in order to obtain a solution using the genetic algorithm. Therefore, the continuous design problem can be transcribed to a discrete one by considering a total number of devices n_T=100, with identical damping coefficients c_d calculated as c_d=1.284 $\times$ 10^9/100 = 1.284 $\times$ 10^7 N-s/m. Column (3) of Table 3.7 present the damping distribution obtained by genetic algorithm, while Column (2) show the same results as those presented in Column (4) of Table 3.4. These results are expressed as percentages of the total damping amount C_T. Again, both design solution compare quite well, with the response for the proposed discretization scheme reduced by a 39.98%. Of course, the discrete solution can be further refined by considering a larger number of devices with reduced mechanical properties. Column (4) of the same table shows the distribution of damping material determined by the sequential optimization procedure. For this design solution, the response is reduced by a 37.7%.

The design obtained by a performance index of the form of Eq. (3.79) is presented next. A 50% reduction in the shear force at the base of Building 2 is now set as the desired target for the optimization procedure. A damper with a damping coefficient of c_d=1.2 $\times$ 10^7 N-s/m is arbitrarily selected as a unit device. This response reduction level is achieved with 68 optimally placed devices. Columns (2) and (3) of Table 3.8 show the optimal distribution of viscous devices obtained by genetic algorithms and the sequential procedure respectively. For this

amount of damping, a different optimal design is obtained when the performance index is set to reduce the maximum acceleration at any floor. The resulting distribution of the devices and the response reduction for this criterion are compared in Columns (4) and (5). The last row of this table shows the actual percentage reduction achieved by the distribution of devices shown in the column. This number for Column (2) is nearly equal to 50 percent, as desired. It is also noted that percentage reduction in the base shear for the sequential approach is quite low. It is primarily because this particular approach only focuses on the story drift in its algorithm and not on any other response quantity.

Floor acceleration values obtained for the damper distribution shown in Columns (4) and (5) of Table 3.8 are shown in Figure 3.10. The floor accelerations for the original building are also shown. The reduction in the floor accelerations is noted. The damper distribution calculated with sequential approach also reduced the floor accelerations, but the superiority of the genetic optimization approach is quite evident. Figure 3.11 shows the percent reduction in the floor accelerations at various levels for damper distribution shown in Columns (4) and (5) of Table 3.8. Also shown is the response reduction if the dampers were uniformly distributed in different stories. It is interesting to note that the acceleration reduction for the sequential approach is even lower than the reduction due to uniform distribution.

3.8.2 Fluid Viscoelastic Devices

In the previous subsections, the optimal distribution of fluid viscous devices in a plane shear-building model was presented. It was assumed that the devices did not contribute to the lateral stiffness of the building structure, and that the bracing elements and attachments used for their support were rigid. Therefore, the behavior of the dampers was characterized by viscous dashpots, and their mechanical properties were determined considering both continuous and discrete values representations. This representation of the force-displacement response of the damper greatly simplifies the analysis and is sufficient when considering only low frequencies ranges of interest. However, more refined models may be needed to realistically describe the inherent frequency dependence of the fluid viscoelastic devices, or to include the effect of the flexibility of the bracings used for their support. In the next numerical example, the more accurate representation provided by the Maxwell model of Eq. (3.1) is employed to characterize

the mechanical properties of the devices. A unitary device is selected from a catalog of industrial products, and a genetic algorithm procedure is used to find the number of fluid viscoelastic devices and their best placement pattern in a building

Implementation with Genetic Algorithm: As a numerical example, the retrofit of Building 4 with fluid viscoelastic devices is presented next. Figure 2.4 identifies for each story the possible locations in which a device can be placed (1 to 4). Therefore, there are a total of $n_l = 24$ possible places to locate a damper in this particular building. A viscous fluid damper is selected from available commercial products (Taylor devices) with mechanical properties taken from an experimental study as follows [147]: $c_d = 2.02 \times 10^5$ N-sec/m, and $\tau_d = 0.014$ sec. The excitation along the x and y directions are defined by spectral density functions of the Kanai-Tajimi form. The parameters ω_g, β_g and S can be determined from a site-specific ground motion study [100]. It is assumed for the numerical calculations that the maximum capable earthquake for the building site has a Richter magnitude of $M = 5.5$ with a peak ground acceleration of $a_g = 0.26g$. Based on these assumptions, the parameters ω_g, β_g and S are calculated to be 23.75 rad/s, 0.32 and 5.7×10^{-3} $m^2/s^3/rad$ respectively for each earthquake direction. Of course, one could also use the input defined by a set of ground response spectra.

As the first example, the design objective is to reduce the relative displacements between the ends of the columns of the building along both x and y directions. These quantities are often related to the expected damage during earthquakes. To quantify and evaluate the level of reduction achieved by a specific design, a normalized performance index is defined as:

$$f[\mathbf{R}(\mathbf{n},t)] = \sqrt{\frac{\sum_{j=1}^{n_{cl}} \left[\mathbf{R}_{jx}^2(\mathbf{n}) + \mathbf{R}_{jy}^2(\mathbf{n}) \right]}{\sum_{j=1}^{n_{cl}} \left(\mathbf{R}_{jox}^2 + \mathbf{R}_{joy}^2 \right)}} \tag{3.84}$$

where $\mathbf{R}_{jx}(\mathbf{n})$ and $\mathbf{R}_{jy}(\mathbf{n})$ are the maximum relative displacements experienced by the j^{th} column along the x and y axes, respectively; $\mathbf{R}_{jox}$ and $\mathbf{R}_{joy}$ are the respective quantity of the original (uncontrolled) building, and n_{cl} is the total number of columns in the building.

It is desired to reduce the response by an arbitrarily selected value of 50%. That is, the

performance index of Eq. (3.84) has to be minimized to achieve a value of 0.5. The genetic algorithm is used to obtain the least number of dampers and their locations to achieve this design objective. Table 3.9 shows the distribution of devices for different combinations of eccentricities ratios $\varepsilon = e/r$, where r is the radius of gyration of the floor. Column (2) presents the distribution of devices for a 5% eccentricity ratio along the y axis, while Columns (3) and (4) are for eccentricities values of ε_x =-5%, ε_y = 5%, and ε_x = 10%, ε_y = -5%, respectively. The last row of Table 3.9 gives the total number of devices required to achieve the desired 50% response reduction. Figure 3.12 presents a comparison between the inter-story drifts measured at the mass center of gravity of the original building (dashed line) and the building with supplemental devices (solid line) for the same eccentricities ratios as in Table 3.9. The figures at the top and bottom correspond to the drifts responses along the x and y axes, respectively. It is interesting to notice that the range of natural frequencies for the original building is between 1.5 Hz to 18.3 Hz. From Figure 3.2(b) it can be seen that the damping and stiffness properties of the devices are strongly affected within this range of operation. Moreover, the incorporation of viscous fluid devices causes some of the modes to become overdamped.

Different arrangements and number of devices are required to achieve the same level of reduction (50%) in the maximum floor acceleration of the building along both axes. The magnitude of the acceleration of a building story is related to the discomfort experienced by its occupants during earthquakes. For this case, the performance index takes the form:

$$f\left[\mathbf{R}(\mathbf{n})\right] = \max_i \left[\frac{\mathbf{R}_i^x(\mathbf{n})}{R_0}; \frac{\mathbf{R}_i^y(\mathbf{n})}{R_0} \right] \tag{3.85}$$

where $\mathbf{R}_i^x(\mathbf{n})$ and $\mathbf{R}_i^y(\mathbf{n})$ represents the maximum floor acceleration at the i^{th} story along the x and y directions, respectively, and R_0 is the maximum acceleration along both directions of the original building. Table 3.10 shows the distribution of devices for the same combinations of eccentricities ratios as presented in Table 3.9. It is observed that to achieve the desired level of acceleration reduction, the majority of devices are now located in the upper stories of the building. Figure 3.13 shows for each combination of eccentricity ratios, the percentage of response reduction achieved at each story. The solid line corresponds to the x axis results, while

the dashed line is for the *y* axis. It is observed that the largest reduction levels are obtained for the 3^{rd} and 6^{th} stories.

3.9 Chapter Summary

This chapter described the formulation and solution of the optimal design problem of structures incorporating viscous damping devices. The main assumption made here is that the behavior of the added damping devices is linear and that their installation in a building structure permitted the main structural members to remain within their elastic limits during a seismic event. Consequently, the response of the overall structural system was considered as linear.

Commonly used linear force-deformation models of fluid viscoelastic devices were briefly described. A classical Maxwell model, in which dashpot and spring are joined in series, was presented as an adequate model that is able to capture the dependency of the response of the device on its deformation frequency. The simpler viscous dashpot model was used to portray fluid devices that do not develop any significant stiffness during operating conditions.

A generalized modal-based random vibration approach was developed for estimation of the maximum response quantities of the structural system. This analysis tool is able to treat any linear structural system with arbitrary linear damping characteristics as long as it can be expressed as a set of first-order linear differential equations.

Analytical expressions were provided for the evaluation of the gradient information required to determine the search direction in the continuous parameter optimization problem, and for post-optimality analysis. An approach to evaluate the sensitivity of the optimum solution and the performance function with respect to the problem parameters was described.

The concept of performance-based design of viscoelastically-damped structures was introduced in this chapter. This methodology provides a convenient framework for the design of the fluid viscoelastic devices. The method is able to solve the inverse problem of determining the amount of damping material or number of devices needed to obtain a desired level of response reduction. The method is also able to determine the optimal distribution or placement pattern of the required damping material along the building height.

Both the gradient projection technique and genetic algorithm approach were employed to solve the optimal design problem. It was shown that both approaches applied to the same problem produce identical results within the accuracy of the numerical calculations. It was mentioned, however, that the gradient-based approach cannot be successfully applied to all the optimal design problems.

Numerical results were presented to illustrate the applicability of the proposed performance-based design approach. The presented examples considered both continuous and discrete representations of the mechanical properties of the fluid viscoelastic devices, as well as different forms of performance indices and types of building structures.

Table 3.1: Maximum floor acceleration performance index.

Story Mode (1)	Part A				Part B			
	No. FVD (2)	ω_j [rad/s] (3)	β_j [%] (4)	Total c_d [N-s/m $\times 10^5$] (5)	No. FVD (6)	ω_j [rad/s] (7)	β_j [%] (8)	Total c_d [N-s/m $\times 10^5$] (9)
1	31	6.37	6.9	155.0	314	6.37	6.9	157.0
2	28	19.35	12.1	140.0	281	19.37	12.2	140.5
3	3	31.70	13.7	15.0	25	31.70	13.9	12.5
4	0	42.98	12.2	0.0	0	42.84	12.1	0.0
5	0	53.71	9.8	0.0	0	53.65	9.3	0.0
6	0	63.56	7.3	0.0	0	63.68	6.9	0.0
7	0	69.18	111.1*	0.0	0	69.04	111.8*	0.0
8	0	72.20	5.3	0.0	0	72.35	5.1	0.0
9	0	79.02	3.9	0.0	0	79.10	3.8	0.0
10	0	83.36	3.2	0.0	0	83.38	3.2	0.0
$f_2[\mathbf{R}(\mathbf{n}^*)]$	0.6011				0.6010			
Reduction [%]	39.89				39.90			

Note: overdamped case identified by *; FVD = fluid viscous devices

Table 3.2: Optimal distribution of viscous devices according to the normed drift, normed acceleration, and composite performance indices.

Story Mode (1)	Drift Index f_3			Acceleration Index f_3			Composite Index f_c		
	No. FVD (2)	ω_j [rad/s] (3)	β_j [%] (4)	No. FVD (5)	ω_j [rad/sec] (6)	β_j [%] (7)	No. FVD (8)	ω_j [rad/s] (9)	β_j [%] (10)
1	27	6.36	6.9	21	6.35	6.6	26	6.36	6.9
2	21	19.11	11.1	17	18.97	10.7	20	19.08	10.8
3	14	31.72	10.5	19	31.63	9.9	16	31.69	10.1
4	0	45.27	9.0	0	45.07	7.8	0	45.29	8.5
5	0	56.07	44.2	0	53.94	51.3	0	55.32	49.6
6	0	58.75	6.8	0	59.10	10.0	0	58.67	6.4
7	0	69.89	4.8	0	70.34	5.4	0	69.81	4.6
8	0	72.34	89.9	5	76.91	78.7	0	73.76	87.1
9	0	78.10	3.7	0	79.54	5.5	0	78.06	3.6
10	0	83.15	3.2	0	80.08	9.1	0	83.14	3.2
$f[\mathbf{R}(\mathbf{n}^*)]$	0.6589			0.6265			0.6461		
Reduction [%]	34.11			37.35			35.39		

Note: FVD = fluid viscous devices

Table 3.3: Optimal distribution of viscous devices calculated by different approaches.

Story	Acceleration Index f_2			Drift Index f_3		
	Gradient Projection	Genetic Algorithm	Sequential Procedure	Gradient Projection	Genetic Algorithm	Sequential Procedure
(1)	(2)	(3)	(4)	(5)	(6)	(7)
1	31.45	31	54	27.259	27	54
2	28.07	28	8	20.884	20	8
3	2.48	3	0	13.856	14	0
4	0	0	0	0	0	0
5	0	0	0	0	0	0
6	0	0	0	0	0	0
7	0	0	0	0	0	0
8	0	0	0	0	0	0
9	0	0	0	0	0	0
10	0	0	0	0	0	0
$f\left[\mathbf{R}\left(\mathbf{d}^*,\mathbf{n}^*\right)\right]$	0.60104	0.60107	0.64548	0.65886	0.65887	0.67000
Reduction [%]	39.8958	39.8930	35.4517	34.1133	34.1132	32.9992

Table 3.4: Optimal distribution of damping coefficients in different stories for 40% reduction in drift-based performance function $f_3(\mathbf{d})$: viscous dampers.

Story	$C_T = 9.00 \times 10^8$ N-s/m	$C_T = 1.227 \times 10^9$ N-s/m	$C_T = 1.284 \times 10^9$ N-s/m	
Mode	c_d^* [% of C_T]	c_d^* [% of C_T]	c_d^* [% of C_T]	β_i [%]
(1)	(2)	(3)	(4)	(5)
1	0.00	0.00	0.00	6.97
2	0.00	0.00	0.00	20.11
3	0.00	0.00	0.00	100.72
4	0.00	0.00	0.00	21.06
5	0.00	0.00	0.00	100.08
6	0.00	0.00	0.00	26.01
7	0.00	0.00	0.00	76.26
8	0.00	0.00	0.00	15.80
9	1.51	6.18	7.50	19.87
10	0.00	0.00	0.00	100.30
11	0.00	0.00	0.00	17.96
12	0.00	5.61	6.11	89.33
13	0.00	0.00	0.00	5.79
14	9.15	9.81	9.75	4.96
15	17.17	14.45	14.05	6.98
16	8.90	8.12	7.97	73.52
17	4.83	5.50	5.45	59.59
18	18.30	15.02	14.57	3.30
19	11.50	10.37	10.16	106.13
20	11.00	9.50	9.27	3.20
21	9.82	8.25	8.04	3.08
22	3.72	3.82	3.82	3.00
23	4.10	3.37	3.31	103.12
24	0.00	0.00	0.00	100.09
$f(\mathbf{d}^*)$	0.6576	0.6075	0.6000	
Reduction [%]	34.24	39.25	40.00	

Table 3.5: Sensitivity analysis of the optimal design solution with respect to the frequency parameter ω_g of the ground motion.

Story	c_d^*	$c_{d,p}^*$	$\omega_g+0.1\omega_g$		$\omega_g+0.5\omega_g$	
			Estimated c_i	Error	Estimated c_i	Error
	[%]	$[\%] \times 10^{-2}$	[%]	[%]	[%]	[%]
(1)	(2)	(3)	(4)	(5)	(6)	(7)
1	0.00	0.00	0.00	0.00	0.00	0.00
2	0.00	0.00	0.00	0.00	0.00	0.00
3	0.00	0.00	0.00	0.00	0.00	0.00
4	0.00	0.00	0.00	0.00	0.00	0.00
5	0.00	0.00	0.00	0.00	0.00	0.00
6	0.00	0.00	0.00	0.00	0.00	0.00
7	0.00	0.00	0.00	0.00	0.00	0.00
8	0.00	0.00	0.00	0.00	0.00	0.00
9	7.50	-12.06	7.27	0.07	6.36	-3.35
10	0.00	0.00	0.00	0.00	0.00	0.00
11	0.00	0.00	0.00	0.00	0.00	0.00
12	6.11	11.43	6.33	0.43	7.19	9.25
13	0.00	0.00	0.00	0.00	0.00	0.00
14	9.75	-0.19	9.75	0.03	9.73	1.43
15	14.05	2.93	14.11	-0.09	14.33	-0.53
16	7.97	4.21	8.05	-0.15	8.36	-0.55
17	5.45	4.66	5.54	-0.25	5.89	-0.74
18	14.56	-0.35	14.56	-0.02	14.53	-0.18
19	10.16	-2.33	10.12	-0.04	9.94	-0.59
20	9.27	-2.22	9.23	-0.02	9.06	-0.47
21	8.04	-2.36	8.00	-0.03	7.82	-0.85
22	3.82	-3.42	3.75	0.22	3.49	1.93
23	3.31	-0.29	3.31	0.27	3.28	5.31
24	0.00	0.00	0.00	0.00	0.00	0.00
$f(\mathbf{d}^*)$	60.00×10^{-2}	-	60.03×10^{-2}	-0.02	60.16×10^{-2}	-0.21
$\frac{df(\mathbf{d}^*)}{dp}$	1.74×10^{-4}					

Table 3.6: Sensitivity analysis of the optimal design solution with respect to the damping parameter β_g of the ground motion.

Story	c_d^*	$c_{d,p}^*$	$\beta_g+0.1\beta_g$		$\beta_g+0.5\beta_g$	
			Estimated c_i	Error	Estimated c_i	Error
	[%]	[%]	[%]	[%]	[%]	[%]
(1)	(2)	(3)	(4)	(5)	(6)	(7)
1	0.00	0.00	0.00	0.00	0.00	0.00
2	0.00	0.00	0.00	0.00	0.00	0.00
3	0.00	0.00	0.00	0.00	0.00	0.00
4	0.00	0.00	0.00	0.00	0.00	0.00
5	0.00	0.00	0.00	0.00	0.00	0.00
6	0.00	0.00	0.00	0.00	0.00	0.00
7	0.00	0.00	0.00	0.00	0.00	0.00
8	0.00	0.00	0.00	0.00	0.00	0.00
9	7.50	3.54	7.73	0.37	8.65	5.55
10	0.00	0.00	0.00	0.00	0.00	0.00
11	0.00	0.00	0.00	0.00	0.00	0.00
12	6.11	-2.28	5.97	-0.27	5.37	-5.17
13	0.00	0.00	0.00	0.00	0.00	0.00
14	9.75	-0.30	9.73	-0.04	9.66	-0.78
15	14.05	1.58	14.15	0.06	14.57	1.10
16	7.97	1.47	8.06	0.04	8.44	1.20
17	5.45	1.59	5.55	0.08	5.96	2.07
18	14.56	-0.13	14.56	0.00	14.52	-0.05
19	10.16	-0.66	10.12	-0.02	9.94	-0.53
20	9.27	-0.67	9.23	-0.03	9.06	-0.65
21	8.04	-0.43	8.01	-0.02	7.90	-0.47
22	3.82	-2.24	3.67	-0.21	3.09	-5.06
23	3.31	-1.47	3.22	-0.30	2.83	-4.85
24	0.00	0.00	0.00	0.00	0.00	0.00
$f(\mathbf{d}^*)$	60.00×10^{-2}	-	60.16×10^{-2}	0.02	60.80×10^{-2}	0.42
$\frac{df(\mathbf{d}^*)}{dp}$	2.46×10^{-2}					

Table 3.7: Optimal distribution of viscous devices calculated by different approaches.

Story	Drift Index f_3		
	Gradient Projection [% of C_T]	Genetic Algorithm [% of C_T]	Sequential Procedure [% of C_T]
(1)	(2)	(3)	(4)
1	0.00	0	0
2	0.00	0	0
3	0.00	0	0
4	0.00	0	0
5	0.00	0	0
6	0.00	0	0
7	0.00	0	0
8	0.00	0	0
9	7.50	7	0
10	0.00	0	0
11	0.00	0	0
12	6.11	6	0
13	0.00	0	0
14	9.75	10	6
15	14.05	14	28
16	7.97	8	9
17	5.45	6	0
18	14.57	15	25
19	10.16	10	12
20	9.27	9	11
21	8.04	8	9
22	3.82	4	0
23	3.31	3	0
24	0.00	0	0
$f(\mathbf{d}^*,\mathbf{n}^*)$	0.6000	0.6001	0.6202
Reduction [%]	40.00	39.99	37.98

Table 3.8: Optimal distribution of viscous devices calculated by genetic algorithm and sequential optimization approach.

Story	Base Shear f_1		Acceleration f_2	
	Genetic Algorithm	Sequential Procedure	Genetic Algorithm	Sequential Procedure
(1)	(2)	(3)	(4)	(5)
1	0	0	0	0
2	0	0	0	0
3	0	0	0	0
4	0	0	0	0
5	1	0	0	0
6	1	0	0	0
7	0	0	0	0
8	0	0	1	0
9	1	0	0	0
10	2	0	0	0
11	2	0	0	0
12	2	0	0	0
13	2	0	0	0
14	2	0	4	0
15	4	24	6	24
16	5	0	6	0
17	6	0	5	0
18	5	24	6	24
19	6	5	3	5
20	7	8	12	8
21	7	7	9	7
22	7	0	7	0
23	5	0	6	0
24	3	0	3	0
$f(\mathbf{n}^*)$	0.4977	0.9722	0.4536	0.6045
Reduction [%]	50.23	2.78	54.64	39.55

Table 3.9: Distribution of devices for different eccentricities ratios: 50% reduction in normed inter-story drifts measured at column locations.

Story No. (1)	Number of devices at the d^{th} location											
	ε_x = 0 % ε_y = 5 % (2)				ε_x = -5 % ε_y = 5 % (3)				ε_x = 10 % ε_y = -5 % (4)			
	1	2	3	4	1	2	3	4	1	2	3	4
1	3	2	2	2	1	1	1	1	2	1	1	3
2	0	1	0	1	0	0	0	0	0	0	0	0
3	7	4	4	4	8	5	3	2	3	2	8	5
4	2	2	1	2	1	1	1	1	2	1	0	1
5	4	2	3	2	4	3	2	1	2	2	4	2
6	0	0	0	0	0	0	0	0	0	0	0	0
No. of devices	49				36				39			

Table 3.10: Distribution of devices for different eccentricities ratios: 50% reduction in maximum floor accelerations.

Story No. (1)	Number of devices at the d^{th} location											
	ε_x = 0 % ε_y = 5 % (2)				ε_x = -5 % ε_y = 5 % (3)				ε_x = 10 % ε_y = -5 % (4)			
	1	2	3	4	1	2	3	4	1	2	3	4
1	2	1	0	1	0	0	1	1	0	0	0	0
2	0	1	0	1	0	0	0	0	0	0	0	0
3	3	2	0	2	3	3	0	0	1	0	3	2
4	2	1	0	1	1	1	0	0	0	0	0	1
5	3	3	3	3	4	4	1	1	1	0	5	3
6	2	1	1	1	2	2	1	1	1	0	1	1
No. of devices	34				26				19			

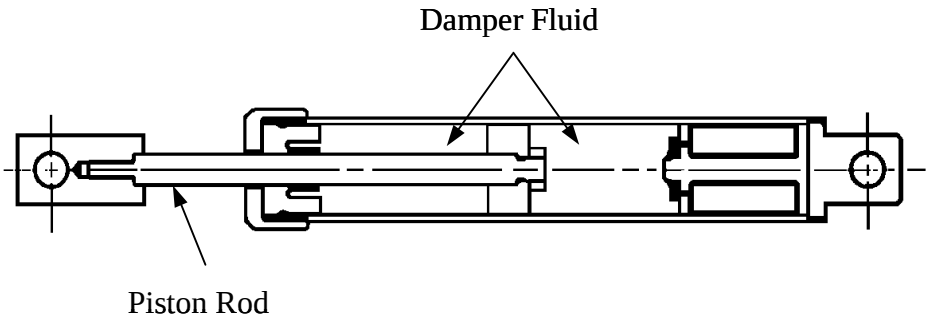

Figure 3.1: Typical fluid viscoelastic device for seismic structural applications.

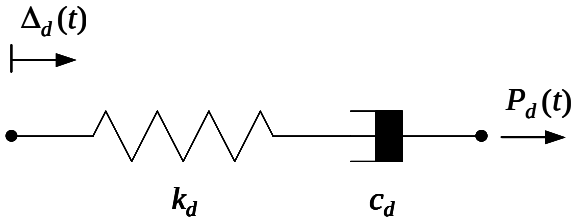

(a)

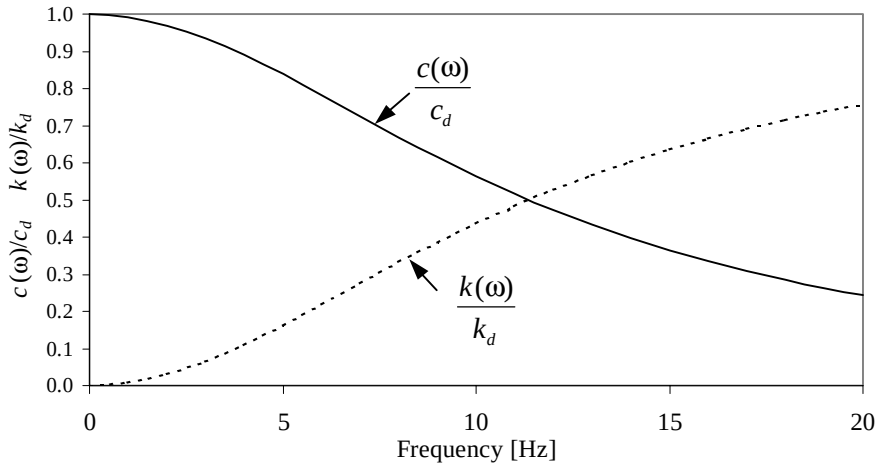

(b)

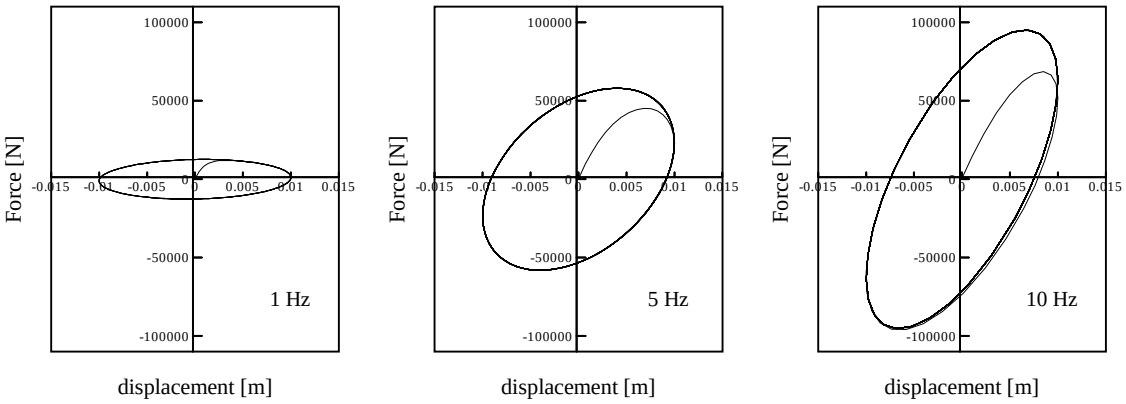

(c)

Figure 3.2: Linear model of fluid viscoelastic devices; (a) Maxwell model, (b) frequency dependency of the stiffness and damping parameters, (c) typical force-deformation responses for different deformations frequencies (1 Hz, 5 Hz, and 10 Hz).

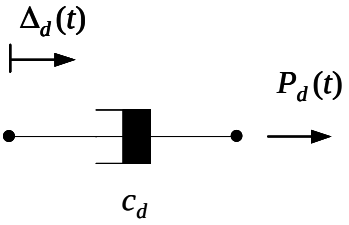

(a)

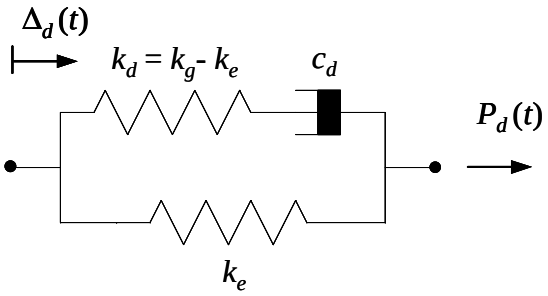

(b)

Figure 3.3: Linear models of fluid viscoelastic devices; (a) viscous dashpot; (b) Wiechert model.

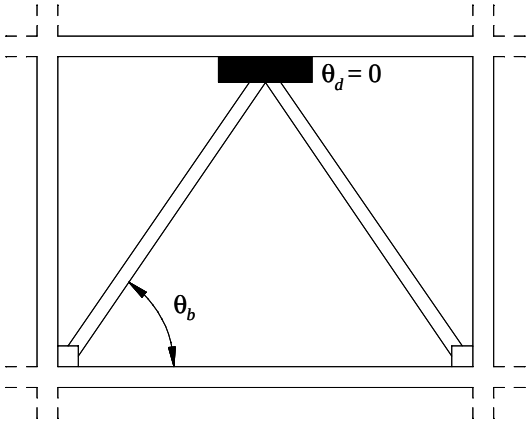

(a)

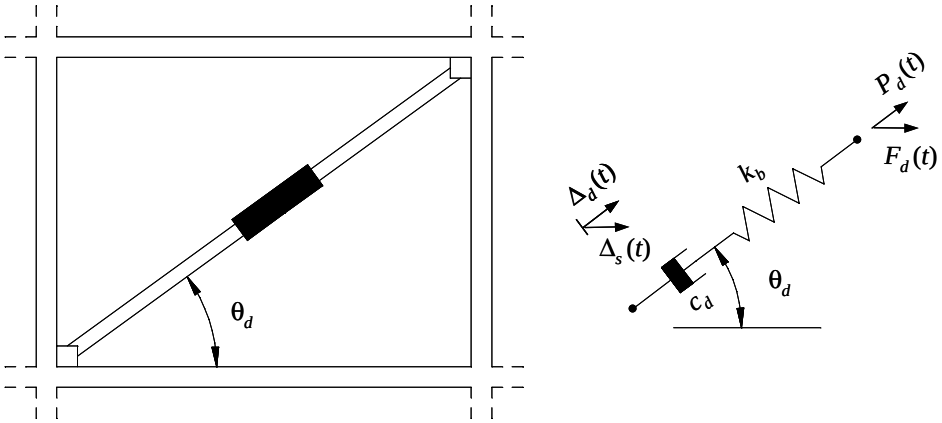

(b)

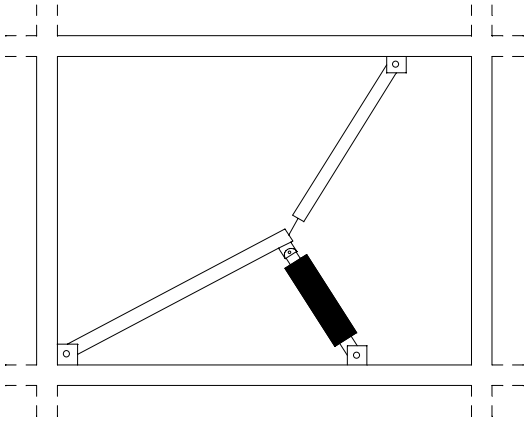

(c)

Figure 3.4: Typical configurations of damping devices and bracings, (a) chevron brace, (b) diagonal bracing, (c) toggle brace-damper system.

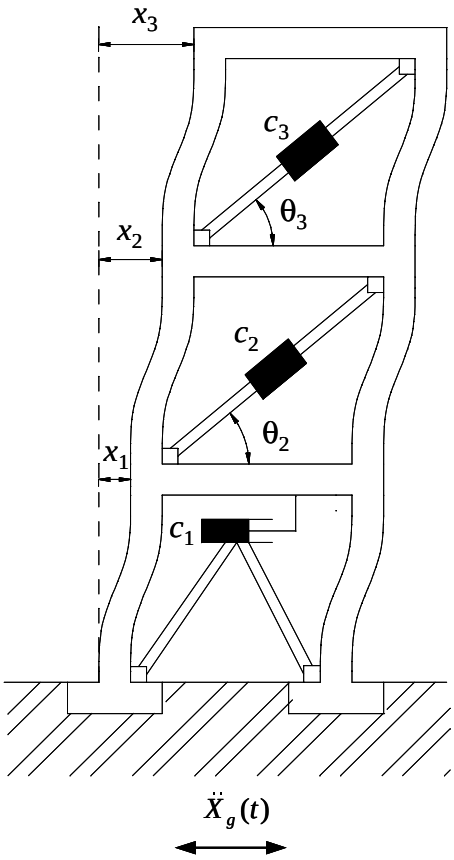

Figure 3.5: Shear model of viscoelastically-damped structure.

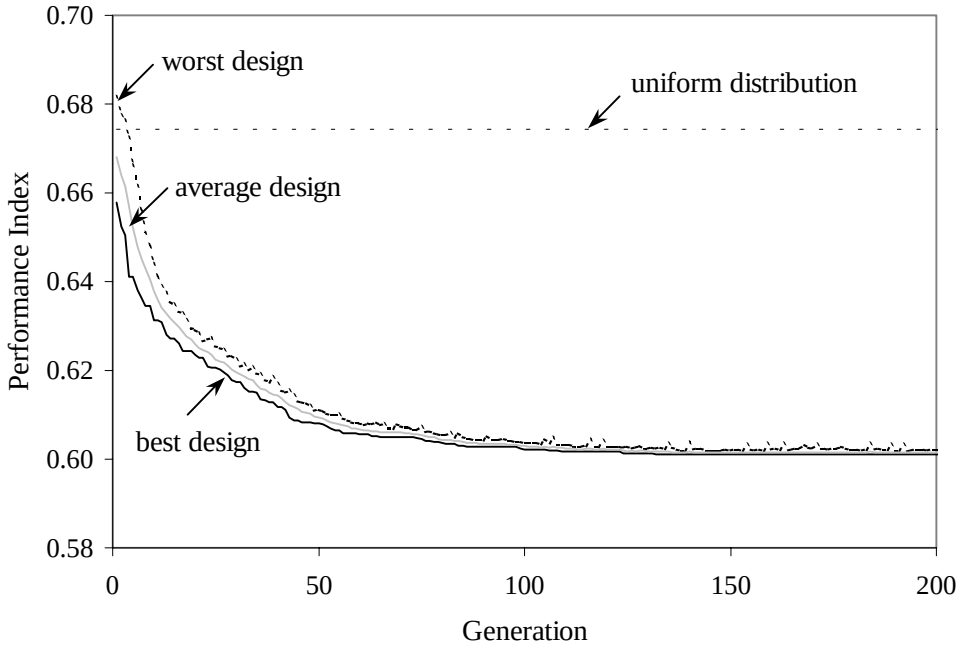

Figure 3.6: Optimization history for acceleration response reduction using genetic algorithm.

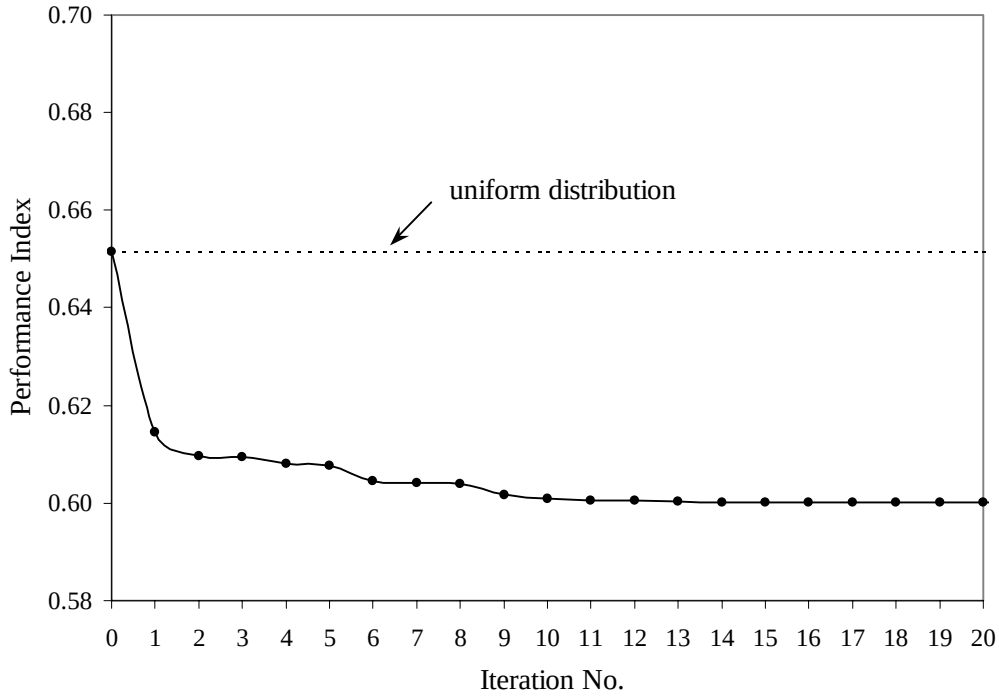

Figure 3.7: Evolution of optimal solution in different iterations for drift-based performance index for viscous dampers using gradient projection method.

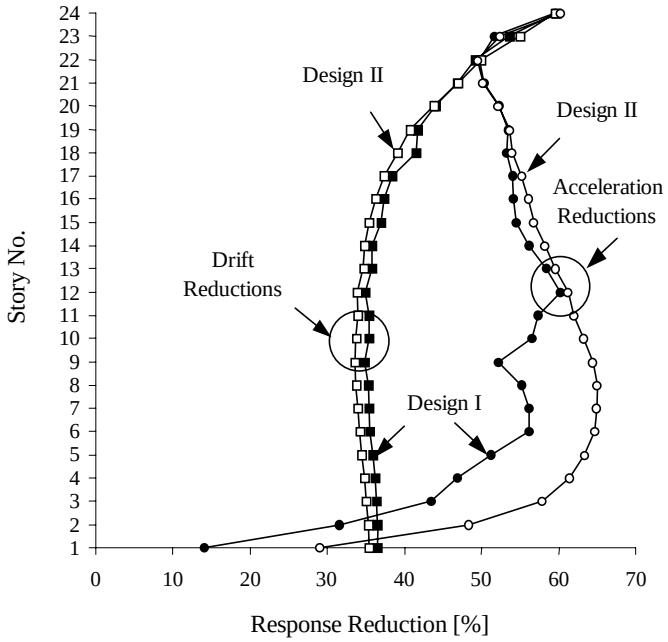

Figure 3.8: Comparison of cross-effectiveness of two designs developed for drift-based and acceleration-based performance functions.

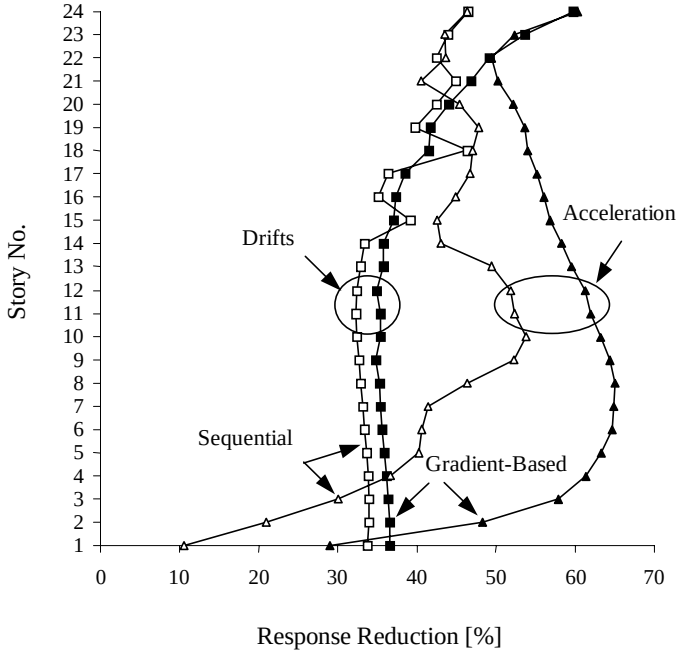

Figure 3.9: Comparison of response reductions achieved in the gradient-based optimal designs and the sequential optimization-based design.

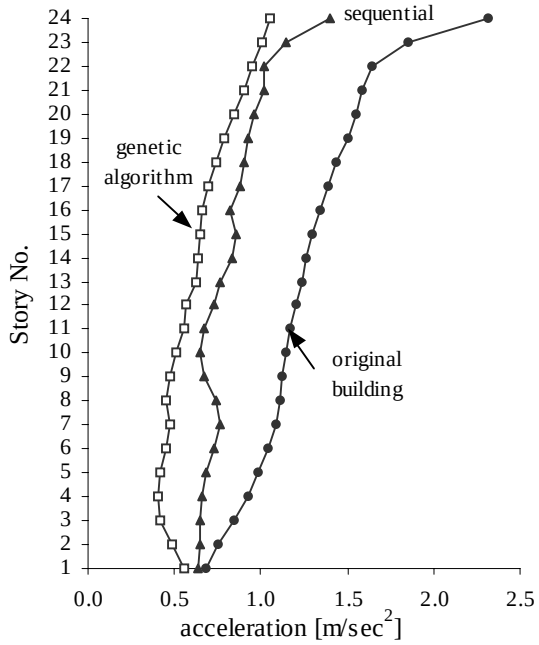

Figure 3.10: Comparison of acceleration responses for damper distributions obtained by different approaches.

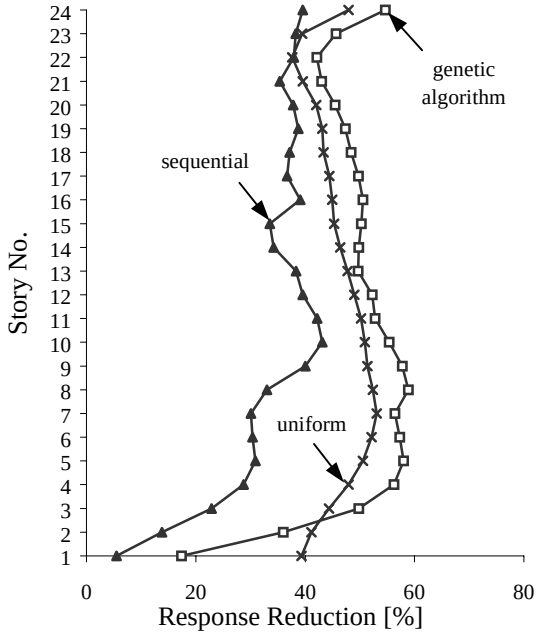

Figure 3.11: Comparisons of acceleration response reductions caused by different damper distributions.

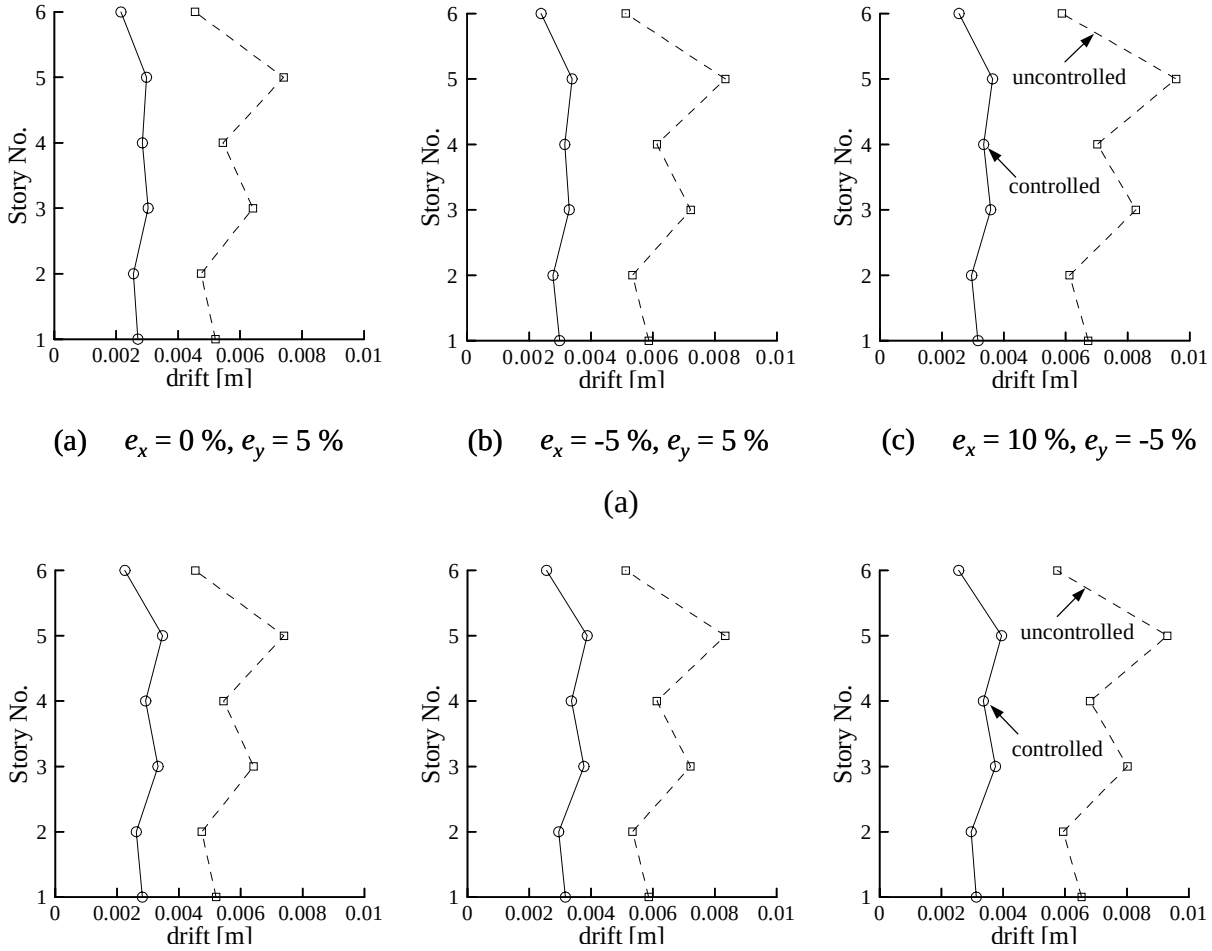

Figure 3.12: Comparisons of controlled and uncontrolled inter-story drifts responses for different combinations of eccentricities, (a) along *x*-direction, (b) along *y*-direction.

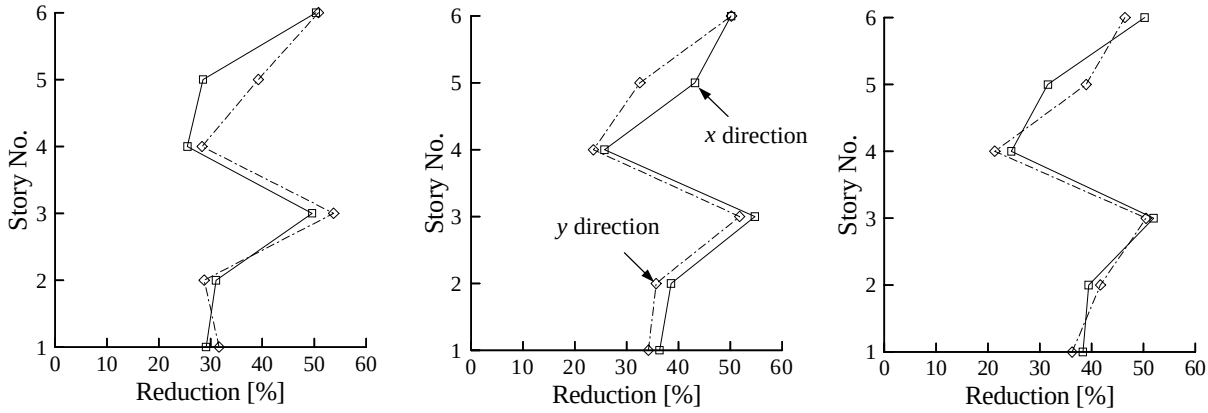

Figure 3.13: Percentage of reduction in floor accelerations along *x*-axis and *y*-axis for different eccentricities combinations.

Chapter 4

Solid Viscoelastic Devices

4.1 Introduction

The previous chapter presented a methodology for the design of fluid viscoelastic devices. The behavior of these devices was assumed to be linear. Their force-deformation relationships were characterized by mechanical models consisting of various arrangements of springs and viscous dashpots. This chapter will study the optimal design problem of solid viscoelastic devices for seismic applications. Solid viscoelastic devices rely on the shear deformation mechanism of a polymeric material to dissipate the input earthquake energy. These devices add stiffness as well as damping to the structure. Figure 4.1 shows a typical solid viscoelastic device employed for seismic rehabilitation of building structures.

Although fluid and solid viscoelastic devices differ on the materials employed to dissipate the input earthquake energy, their cyclic responses share similar characteristics. The force-deformation responses are dependent on the relative velocity between each end of the device, the frequency and amplitude of the motion, and the operating temperature conditions including temperature rise in the viscoelastic material due to the heat generated during the loading cycles. However, for design purposes of solid viscoelastic devices it is usually assumed that if the variation on the operation temperature of the device is small and the device is subjected to moderate strain levels, the force-deformation characteristic can be expressed by means of linear relations. Under this linear behavior assumption, the design of an elastic building structure with supplemental solid viscoelastic devices can also be formulated using the

performance-based design approach presented in Chapter 3. Therefore, this chapter essentially follows the same approach previously established for the design of fluid viscoelastic devices. A level of structural response reduction is first decided and the number of devices and their best locations are then determined by solving the corresponding optimization problem. Section 4.2 briefly describes the mechanical models used in the design practice to characterize the force-deformation of solid viscoelastic devices. The equations of motion of the overall structural system have to be modified to account for both the added damping and stiffness contributions. This is described in Section 4.3 where the approach for response and performance indices calculations is also presented. The rates of change of the eigenproperties of the system are also affected by the stiffness added by the solid viscoelastic devices. Therefore, the necessary modifications on the gradients expressions are provided in Section 4.4. The remainder of the chapter is dedicated to the numerical applications of the proposed design procedure.

4.2 Analytical Modeling of Solid Viscoelastic Devices

As suggested in the FEMA-273 Guidelines [43], solid viscoelastic devices may be modeled using a classical Kelvin model in which a linear spring is placed in parallel with a viscous dashpot, as shown in Figure 4.2(a). Besides adding supplementary energy dissipation capabilities to the structure due to the incorporated damping, the devices also contribute to the overall lateral stiffness of the building. For this model, the general relation for the resistance force $P_d(t)$ in the d^{th} damping element [Eq. (2.2)] takes the form

$$P_d(t) = k_d(\omega)\,\Delta_d(t) + c_d(\omega)\,\dot{\Delta}_d(t) \tag{4.1}$$

where $k_d(\omega)$ and $c_d(\omega)$ denote, respectively, the frequency dependent stiffness and damping coefficient values for the device. For a viscoelastic damper with total shear area A and total thickness h, the following relations apply:

$$k_d(\omega) = \frac{AG'(\omega)}{h}, \qquad c_d(\omega) = \frac{AG''(\omega)}{\omega h}, \qquad \eta(\omega) = \frac{G''(\omega)}{G'(\omega)} \tag{4.2}$$

where $G'(\omega)$ and $G''(\omega)$ are defined, respectively, as the shear storage modulus and shear loss modulus of the viscoelastic material, $\eta(\omega)$ is the loss factor that provides a measure of the energy dissipation capability of the viscoelastic material, and ω corresponds to the frequency at which

these properties are determined. From Eq. (4.2), the relationship between the damping and stiffness added by a solid viscoelastic device can be determined as:

$$k_d = \frac{G'(\omega)}{G''(\omega)}\omega c_d = \frac{\omega}{\eta(\omega)} c_d \tag{4.3}$$

Although the mechanical properties k_d and c_d are dependent on the deformation frequency ω, in practice these quantities are considered as nearly constants within a narrow frequency band and operating temperature. Of course, the frequency dependency of the material properties of the device can be more accurately represented by the Maxwell model described in Chapter 3.

The flexibility of the supporting bracings may also be incorporated in the analysis. This can be accomplished by combining the damper and brace in series, as shown in Figure 4.2(b). The mathematical model that describes the force $F_d(t)$ applied to the structure by the damping component can be obtained by considering a procedure similar to the one presented in Section 3.2. It is straightforward to show that this relationship is of the form:

$$F_d(t) + \frac{c_d}{k_b + k_d}\dot{F}_d(t) = k_{bd}\left[\Delta_s(t) + \frac{c_d}{k_d}\dot{\Delta}_s(t)\right] \tag{4.4}$$

In this expression, k_{bd} represents the overall stiffness of the damper-brace assembly. It is obtained as a function of the stiffness of the bracing k_b, and the stiffness added by the viscoelastic material k_d, as

$$k_{bd} = \frac{1}{\frac{1}{k_b} + \frac{1}{k_d}} = \frac{k_d\, k_b}{k_b + k_d} \tag{4.5}$$

It is clear that if the brace is considered as rigid, the deformation experienced by the damper is the same as the one in the structure. In this case, $k_b = \infty$, and $k_{bd} = k_d$, and Eq. (4.4) reduces to Eq. (4.1).

4.3 Response Calculations

In Chapter 3, the equations of motion for an N-degree of freedom shear building model with supplementary viscoelastic devices subjected to a ground motion disturbance at its base were presented. They are rewritten here for convenience as:

$$\mathbf{M}\,\ddot{\mathbf{x}}(t)+\mathbf{C}_s\,\dot{\mathbf{x}}(t)+\mathbf{K}_s\,\mathbf{x}(t)+\sum_{d=1}^{n_l}\mathbf{r}_d\,n_d P_d(t)=-\mathbf{M}\,\mathbf{E}\,\ddot{X}_g(t) \tag{4.6}$$

If the force exerted by the d^{th} solid viscoelastic device is characterized by the Kelvin model of Eq. (4.1), in which a linear spring is placed in parallel with a viscous dashpot, the following relations can be established between the local deformations at the damper element and those of the main structural members:

$$\left.\begin{aligned} P_d(t) &= k_d\,\Delta_d(t)+c_d\,\dot{\Delta}_d(t)\\ \Delta_d(t) &= \mathbf{r}_d^T\,\mathbf{x}(t)\\ \dot{\Delta}_d(t) &= \mathbf{r}_d^T\,\dot{\mathbf{x}}(t) \end{aligned}\right\} \quad P_d(t)=k_d\,\mathbf{r}_d^T\,\mathbf{x}(t)+c_d\,\mathbf{r}_d^T\,\dot{\mathbf{x}}(t) \tag{4.7}$$

Substitution of Eq. (3.23) in Eqs. (3.22) leads to,

$$\mathbf{M}\,\ddot{\mathbf{x}}(t)+\left(\mathbf{C}_s+\sum_{d=1}^{n_l}\mathbf{r}_d\,n_d\,c_d\,\mathbf{r}_d^T\right)\dot{\mathbf{x}}(t)+\left(\mathbf{K}_s+\sum_{d=1}^{n_l}\mathbf{r}_d\,n_d\,k_d\,\mathbf{r}_d^T\right)\mathbf{x}(t)=-\mathbf{M}\,\mathbf{E}\,\ddot{X}_g(t) \tag{4.8}$$

Therefore, the damping and stiffness matrices of the overall structural system, defined respectively as **C** and **K**, are obtained by adding to the original structural matrices $\mathbf{C}_s$ and $\mathbf{K}_s$ the contribution in damping and stiffness from the devices. That is,

$$\mathbf{C}=\mathbf{C}_s+\sum_{d=1}^{n_l}\mathbf{r}_d\,n_d\,c_d\,\mathbf{r}_d^T; \qquad \mathbf{K}=\mathbf{K}_s+\sum_{d=1}^{n_l}\mathbf{r}_d\,n_d\,k_d\,\mathbf{r}_d^T \tag{4.9}$$

Similar to the situation encountered when fluid viscoelastic devices were incorporated at different locations of a structure, the resultant modified structure can become a non-classically damped system. This non-classically damped system can also be overdamped in certain modes, depending upon the amount of supplemental damping introduced.

The analysis of the resulting non-classically damped linear system can be done using the general formulation developed in Chapter 3. Since the force-deformation characterization of the solid viscoelastic device is given by an algebraic relation, the maximum structural responses can be conveniently estimated through the eigensolution of the self-adjoint eigenvalue problem,

$$-\mu_j\,\mathbf{A}_s\,\boldsymbol{\varphi}_j=\mathbf{B}_s\,\boldsymbol{\varphi}_j; \qquad j=1,\ldots,2N \tag{4.10}$$

The symmetric $2N\times 2N$ matrices $\mathbf{A}_s$ and $\mathbf{B}_s$, defined as:

$$\mathbf{A}_s=\begin{bmatrix}\mathbf{0} & \mathbf{M}\\ \mathbf{M} & \mathbf{C}\end{bmatrix}; \qquad \mathbf{B}_s=\begin{bmatrix}-\mathbf{M} & \mathbf{0}\\ \mathbf{0} & \mathbf{K}\end{bmatrix} \tag{4.11}$$

are obtained by transcribing the equations of motions (4.8) into a set of first-order differential equations.

The influence of the flexibility of the bracings in the response and design of solid viscoelastic devices can be determined if the model of Eq. (4.4) is used instead of the one provided by Eq. (4.1). In this case, the behavior of the damper-brace assembly is expressed by a first-order differential equation. Therefore, the dynamic properties of the system are described in terms of a single non-symmetric matrix, and the structural analysis has to be done using the generalized approach of Section 3.3.

4.4 Gradients Calculations

The expressions for the gradients calculations with respect to the damping parameters were provided in Chapter 3. As shown there, the rates of change of eigenvalues and eigenvectors can be obtained in terms of the derivatives of the overall damping matrix **C** with respect to the d^{th} damping coefficients c_d, that is, $\mathbf{C}_{,d}$. Since the solid viscoelastic devices also contribute to the structural stiffness of the system, it can be shown that the expressions for the rates of changes have to include the derivatives $\mathbf{K}_{,d}$ as follows:

Derivatives of eigenvectors:

$$\left\{\boldsymbol{\varphi}_j\right\}_{,d} = \sum_{k=1}^{2N} a_{jk}\,\boldsymbol{\varphi}_k \tag{4.12}$$

with

$$a_{jk} = \begin{cases} -\dfrac{1}{2}\left\{\boldsymbol{\varphi}_j\right\}_L^T \mathbf{C}_{,d} \left\{\boldsymbol{\varphi}_j\right\}_L & \text{if } j = k \\ -\dfrac{1}{\left(\mu_k - \mu_j\right)}\left[\left\{\boldsymbol{\varphi}_k\right\}_L^T \left(\mu_j \mathbf{C}_{,d} + \mathbf{K}_{,d}\right)\left\{\boldsymbol{\varphi}_j\right\}_L\right] & \text{if } j \neq k \end{cases} \tag{4.13}$$

Derivatives of eigenvalues:

$$\mu_{j,d} = -\left\{\boldsymbol{\varphi}_j\right\}_L^T \left(\mu_j \mathbf{C}_{,d} + \mathbf{K}_{,d}\right)\left\{\boldsymbol{\varphi}_j\right\}_L \tag{4.14}$$

The expressions for the sensitivities of natural frequencies, modal damping ratios and mean square response values are similar to those presented in Section 3.5.

4.5 Numerical Results

The application of the proposed performance-based approach for the design of solid viscoelastic devices is demonstrated next. For the numerical studies of this section, it is assumed that the bracings used to support the devices are rigid. Two different buildings are considered for the numerical examples. For each building, the mechanical properties of the devices are optimized using the gradient projection technique and genetic algorithm approach to consider both continuous and discrete design variables representations. Comparisons between the devices distribution are done to check whether the gradient-based procedure converges to a local optimal solution. Conversely, the optimal design solution obtained using the gradient projection technique is used to validate the solution obtained by the genetic algorithm.

The performance indices used to measure the improvement achieved with a given installation of solid viscoelastic devices are similar to those presented in Chapter 4. They are repeated here for convenience.

$$f_1\left[R(\mathbf{d},\mathbf{n},t)\right]=\frac{R(\mathbf{d},\mathbf{n})}{R_o} \tag{4.15}$$

$R(\mathbf{d},\mathbf{n})$ is the maximum value of the response quantity of interest such as the base shear, over-turning moment, acceleration or drift of a particular floor; and R_o is a normalizing factor that corresponds to the respective response quantity of the original (unmodified) structure.

$$f_2\left[\mathbf{R}(\mathbf{d},\mathbf{n},t)\right]=\max_i\left[\frac{\mathbf{R}_i(\mathbf{d},\mathbf{n})}{R_o}\right] \tag{4.16}$$

where i represents the location where the maximum response occurs, and R_o is the maximum uncontrolled response.

$$f_3\left[\mathbf{R}(\mathbf{d},\mathbf{n},t)\right]=\frac{\|\,\mathbf{R}(\mathbf{d},\mathbf{n})\,\|}{\|\,\mathbf{R}_o\,\|} \tag{4.17}$$

$\mathbf{R}(\mathbf{d},\mathbf{n})$ and $\mathbf{R}_o$ are, respectively, the vectors of the response quantities of interest of the modified and unmodified structures; and $\|\mathbf{R}(\mathbf{d},\mathbf{n})\|=\sqrt{\mathbf{R}(\mathbf{d},\mathbf{n})\cdot\mathbf{R}(\mathbf{d},\mathbf{n})}$ and $\|\mathbf{R}_o\|=\sqrt{\mathbf{R}_o\cdot\mathbf{R}_o}$ are the square roots of the second norm response of the modified and original structures, respectively.

$$f_c\left[\mathbf{R}(\mathbf{d},\mathbf{n},t)\right]=\left(w_1f_2+w_2f_3\right)_{drifts}+\left(w_3f_2+w_4f_3\right)_{disp.}+\left(w_5f_2+w_6f_3\right)_{acc.} \tag{4.18}$$

where w_i, i = 1,…,6 are the weights assigned to different drifts, displacements, and acceleration based performance functions.

Building 1 - Optimization with Genetic Algorithm: As application of the genetic search procedure, the optimal distribution of the solid viscoelastic damping devices to reduce the structural response of Building 1 is considered next. For illustration purposes, the mechanical properties of the unitary viscoelastic damper are taken from the Zhang and Soong study [200] as follows: $G' = 286.6 \times 10^4$ N/m^2, $G'' = 430.3 \times 10^4$ N/m^2, with the shear area of the viscoelastic material A=0.011 m^2, and thickness h=0.015 m. Therefore, the equivalent stiffness and damping coefficient values for the unit device are calculated from Eqs. (4.2) to be $k_d = 2.10 \times 10^6$ N/m and $c_d = 5.0 \times 10^5$ N-s/m, respectively. The parameters of the Kanai-Tajimi power spectral density function are taken as: ω_g = 18.85 rad/s, β_g = 0.65, and $S = 38.3 \times 10^{-4}$ m^2/s^3/rad.

Following the performance-based design guidelines, a 40% reduction in the maximum inter-story drift response defined according to Eq. (3.80) was set as the desired level of response reduction. The genetic algorithm determined that 67 devices were necessary to achieve this objective. The optimal placement of the devices is shown in Part A of Table 4.1. To achieve a similar level of reduction in the response if the devices were to be uniformly distributed along the height, one would require 130 devices. Thus, the optimization has reduced the number of the devices required by 49%. It can be noticed that the devices are concentrated in the lower stories [See Column (2)]. The modal frequencies and damping ratios are shown in Columns (3) and (4) of this table. A small increase in the frequencies due to added stiffness, and a significant increase in the modal damping ratios, is noted. As with viscous dampers, a further refinement in the design can be achieved by considering more devices of a smaller size. Part B of Table 4.1 shows results for devices that are one-tenth of the size considered in Part A of the table. Comparison of the results shown in Parts A and B of Table 4.1 shows that there is some refinement in the numbers of devices and total damping coefficient needed in various stories, with some slight improvement in the level of response reduction as well. The convergence characteristics of the optimal algorithm for the solid viscoelastic dampers, as shown in Figure 4.3, were qualitatively similar to those depicted in Figure 3.6 for the fluid viscous dampers.

Table 4.2 shows the optimal placement of 67 devices for the drift-based, acceleration-based and the composite indices of Eqs. (3.81) and (3.82), respectively. In the composite index, all performance functions were assigned equal weights of 1/6. The table also shows the damping ratios in Columns (4), (7) and (10), and the level of response reduction achieved in each case in the bottom row of the table. The distribution of devices for different indices is different, but again the majority of them are concentrated in the lower stories. The enhancement of the acceleration related performance now calls for placement of some more devices in the higher stories as well [See Column (5) of Table 4.2].

The final step in the design procedure involves the sizing of the devices. Based on the optimal distribution of the 67 devices, the stiffness and damping quantities required for each floor are easily determined. For example, based on the drift reduction criteria, 30 devices are needed in the first story [See Column (2) of Table 4.1]. Therefore, the total stiffness to be provided by the viscoelastic devices is $k_{desired} = 30(2.1 \times 10^6) = 63.0 \times 10^6$ N/m. The desired area of a single viscoelastic damper which will provide this stiffness can be calculated from Eq. (4.2) as $A = k_{desired}\, h/G'$.

Building 1 - Optimization with Gradient Projection Technique: The design of the same 10-story building using the gradient projection technique is considered next. The size of the device to be used in a story is now determined using a continuous description of the mechanical properties c_d. The equivalent stiffness for a device at a given story is obtained from Eq. (4.3), where ω is the fundamental natural frequency of the building. Following the procedure described in Chapter 3, the total amount of damping material required to achieve a 40% reduction in the normed acceleration index of Eq. (4.17) is $C_T = 4.35 \times 10^7$ N-s/m. This amount has to be properly discretized in order to permit a comparison of both solutions obtained by the gradient projection technique and genetic algorithm. Therefore, 87 devices with damping coefficient $c_d = 5.0 \times 10^5$ N-s/m provide the required amount of damping material. The numerical results are presented in Table 4.3. Column (3) of this table shows the total number of solid viscoelastic devices and their optimal distribution in various stories, calculated according to the genetic algorithm approach. Column (2) of the same table presents the optimal distribution

of the 87 devices calculated according to the gradient projection technique. The numbers in this column are not integers. They are obtained by dividing the optimal value obtained for a given locations by the size of the selected unitary device mentioned earlier. An excellent comparison of distribution of the devices in various stories, calculated by the genetic approach as well as by the gradient based approach is noted. The same trend can be observed when comparing Columns (5) and (6) of Table 4.3. These columns provide results for the optimal distributions of the same amount of damping material C_T, but now considering the maximum inter-story drifts performance function of Eq. (4.16). Columns (4) and (7) present the results obtained with the discrete sequential optimization procedure. It is observed that for the drift performance index, this approach provides a good estimate of the optimal solution. However, quite different results are obtained when the solution provided by the sequential procedure is used for acceleration reduction purposes.

Building 2 - Optimization with Gradient Projection Technique: The procedure described above was also implemented for the determination of the amount of viscoelastic material and its distribution along the height of Building 2. For illustration purposes, the loss factor for the viscoelastic dampers is now taken to be $\eta = 1.35$. As before, the equivalent stiffness for a device at a given story can be obtained from Eq. (4.3).

Figures 4.4 shows the distribution of the coefficient C_T, representing the total damping coefficient to be provided by the solid viscoelastic devices in the different stories of the building. Figure 4.4(a) is for 40% reduction in the floor acceleration-based performance function $f_3(\mathbf{R})$ of Eq. (4.17) and Figure 4.4(b) for 40% reduction in the base shear-based performance function $f_1(\mathbf{R})$ of Eq. (4.15). The two distributions are similar, with more damping material required near the top stories. Figures 4.5(a) and 4.5(b), respectively, compare the reduced floor accelerations and story shear values with the corresponding quantities of the unmodified structure for the two designs shown in Figures 4.4(a) and 4.4(b).

Building 2 - Optimization with Genetic Algorithms: The design of the solid viscoelastic devices to achieve the same levels of response reduction for Building 2 is now considered

assuming a discretized description of the mechanical properties of the devices. For the numerical implementation with genetic algorithms, one hundred devices are used with mechanical properties determined as $C_T/100$ and proportional stiffness. Columns (2) to (4) of Table 4.4 compare the results obtained by three different optimization procedures for the normed acceleration performance index. Column (2) present the distribution of damping material previously calculated by the gradient projection technique and depicted in Figure 4.4(a). The results obtained using the genetic algorithm, expressed as integer numbers in Column (3), closely match the ones obtained using the continuous description of the design variables. Although the sequential optimization procedure, as shown by the results provided in Column (3), also locates the majority of the devices along the top stories of the building, only achieves a 32% reduction in the acceleration response.

Similar conclusions can be stated when comparing the distributions of damping material obtained to reduce the shear at the base of the Building 2. The design solutions provided the gradient and genetic search procedures, as shown respectively in Columns (5) and (6), are quite comparable producing the desired 40% reduction in the base shear response. However, the last row of Column (7) shows that this response is only reduced by a 22% when considering the distribution of viscoelastic material according to the sequential procedure.

4.6 Chapter Summary

This chapter considered the design of solid viscoelastic devices for seismic applications. The behavior of a device is characterized by a linear Kelvin model consisting of a linear spring and a viscous dashpot placed in parallel. The determination of the mechanical properties of the devices and their required quantities along the building height were determined within the context of the performance-based design approach presented in Chapter 3.

Along with damping, the solid viscoelastic also contributed to the lateral stiffness of the main structure. Correspondingly, the equations of motions and expressions for gradients calculations were modified to incorporate this effect.

Numerical results were presented to demonstrate the applicability and effectiveness of the proposed performance-based design procedure to two different buildings. The design problem

was solved using both continuous and discrete design variables representations. The results were compared to evaluate the convergence characteristics of the proposed optimization procedures.

Table 4.1: Optimal distribution of solid viscoelastic devices for 40% reduction in the maximum inter-story drifts.

Story Mode (1)	Part A				Part B			
	No. SVD (2)	ω_j [rad/s] (3)	β_j [%] (4)	Total c_d [N-s/m $\times 10^{5}$] (5)	No. SVD (6)	ω_j [rad/s] (7)	β_j [%] (8)	Total c_d [N-s/m $\times 10^{5}$] (9)
1	30	6.53	6.6	150.0	302	6.53	6.6	151.0
2	24	19.51	11.0	120.0	236	19.51	11.0	118.0
3	13	32.06	10.9	65.0	128	32.09	11.0	64.0
4	0	45.30	9.3	0.0	4	45.31	9.6	2.0
5	0	58.72	7.1	0.0	0	58.66	7.6	0.0
6	0	58.73	40.7	0.0	0	59.03	40.1	0.0
7	0	69.91	5.0	0.0	0	69.82	5.3	0.0
8	0	75.59	95.6	0.0	0	75.39	94.7	0.0
9	0	78.12	3.8	0.0	0	78.04	3.9	0.0
10	0	83.15	3.2	0.0	0	83.12	3.2	0.0
$f_1[\mathbf{R}(\mathbf{n}^*)]$	0.5986				0.5978			
Reduction [%]	40.14				40.22			

Note: SVD = solid viscoelastic devices

Table 4.2: Optimal distribution of solid viscoelastic devices according to the normed drift, normed acceleration, and composite performance indices.

Story	Drift Index f_2			Acceleration Index f_3			Composite Index f_c		
Mode	No. SVD	ω_j [rad/s]	β_j [%]	No. SVD	ω_j [rad/s]	β_j [%]	No. SVD	ω_j [rad/s]	β_j [%]
(1)	(2)	(3)	(4)	(5)	(6)	(7)	(8)	(9)	(10)
1	23	6.52	6.7	19	6.49	6.2	26	6.52	6.6
2	20	19.31	9.8	15	19.29	10.9	19	19.38	10.2
3	17	32.21	10.6	18	31.71	10.8	17	32.05	11.1
4	7	45.80	14.1	0	45.12	10.7	3	45.13	10.4
5	0	55.97	14.1	2	56.35	44.9	2	58.66	8.6
6	0	62.88	48.6	4	59.28	13.8	0	58.83	50.2
7	0	66.80	7.5	3	71.31	9.4	0	70.25	8.8
8	0	76.55	4.5	5	77.34	12.5	0	76.62	7.2
9	0	79.29	81.6	1	80.10	6.9	0	78.34	81.2
10	0	82.74	3.3	0	83.03	17.8	0	82.47	3.8
$f_1[\mathbf{R}(\mathbf{n}^*)]$	0.6456			64.14			0.6391		
Reduction [%]	35.44			35.86			36.09		

Note: SVD = solid viscoelastic devices

Table 4.3: Optimal distribution of solid viscoelastic devices calculated by different approaches: Building 1.

Story	Acceleration Index f_3			Drift Index f_2		
	Gradient Projection	Genetic Algorithm	Sequential Procedure	Gradient Projection	Genetic Algorithm	Sequential Procedure
(1)	(2)	(3)	(4)	(5)	(6)	(7)
1	19.40	19	35	35.39	35	35
2	16.73	17	31	30.66	30	31
3	19.51	20	19	18.81	18	19
4	3.28	3	2	2.13	4	2
5	5.42	5	0	0	0	0
6	6.73	7	0	0	0	0
7	6.22	6	0	0	0	0
8	7.45	8	0	0	0	0
9	2.23	2	0	0	0	0
10	0	0	0	0	0	0
$f[\mathbf{R}(\mathbf{d}^*,\mathbf{n}^*)]$	0.60	0.6010	0.6285	0.5507	0.5511	0.5511
Reduction [%]	40.00	39.8986	37.1457	44.9267	44.8906	44.8892

Table 4.4: Optimal distribution of solid viscoelastic devices calculated by different approaches: Building 3.

Story	Normed Acceleration f_3			Base Shear f_1		
	Gradient Projection [% of C_T]	Genetic Algorithm [% of C_T]	Sequential Procedure [% of C_T]	Gradient Projection [% of C_T]	Genetic Algorithm [% of C_T]	Sequential Procedure [% of C_T]
(1)	(2)	(3)	(4)	(5)	(6)	(7)
1	0.00	0	0	0.00	0	0
2	0.00	0	0	0.00	0	0
3	0.00	0	0	0.00	0	0
4	0.00	0	0	0.00	0	0
5	0.00	0	0	0.00	0	0
6	0.00	0	0	0.00	1	0
7	0.00	0	0	0.05	1	0
8	0.05	0	0	0.62	1	0
9	0.19	1	0	0.85	1	0
10	0.91	2	0	1.69	1	0
11	0.09	2	0	1.96	1	0
12	1.36	2	0	2.13	2	0
13	1.34	1	0	2.39	3	0
14	1.68	1	7	2.04	2	5
15	4.87	4	25	4.22	4	26
16	9.56	6	7	8.00	7	6
17	5.19	4	0	6.06	5	0
18	8.19	6	30	8.52	7	31
19	9.30	11	10	10.00	10	10
20	12.27	11	10	9.68	11	11
21	15.43	18	11	12.81	13	11
22	12.38	14	0	12.80	14	0
23	11.19	11	0	9.71	10	0
24	6.00	6	0	6.48	6	0
$f(\mathbf{d}^*,\mathbf{n}^*)$	0.600	0.6002	0.6775	0.600	0.5990	0.7847
Reduction [%]	40.00	39.98	32.25	40.00	40.10	21.53

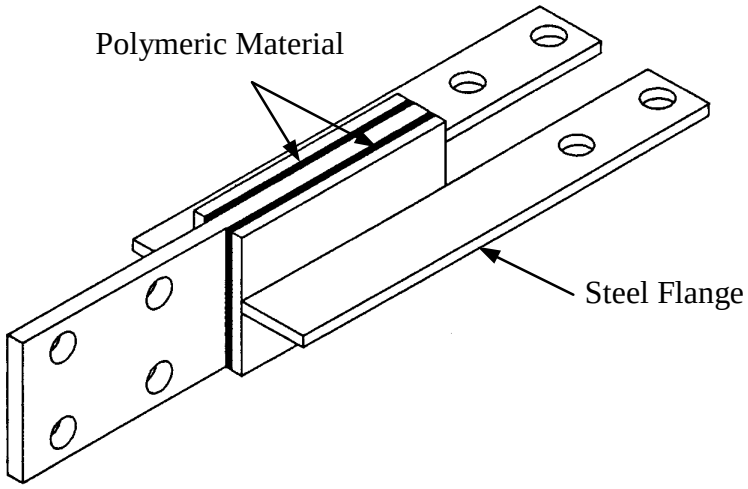

Figure 4.1: Typical solid viscoelastic device for seismic structural applications.

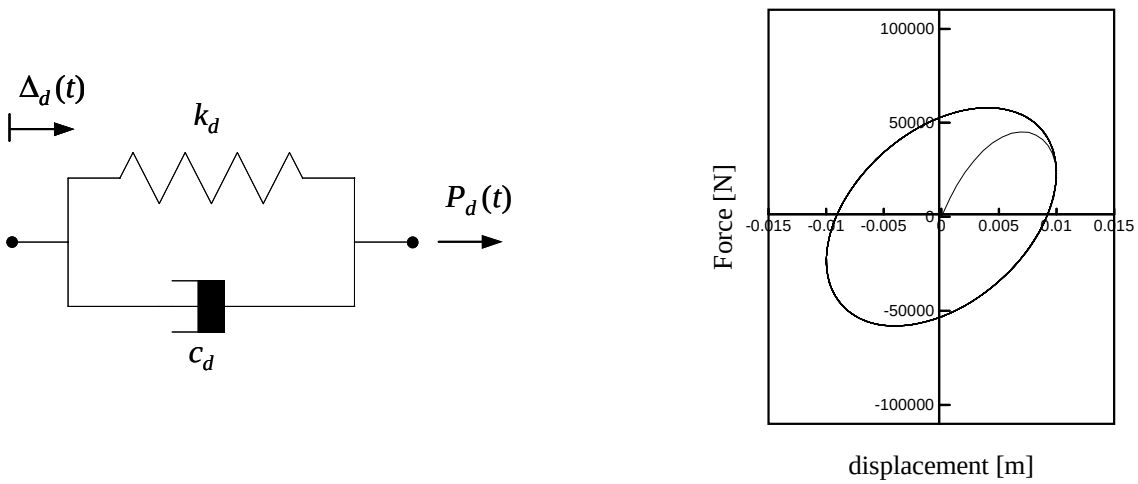

(a)

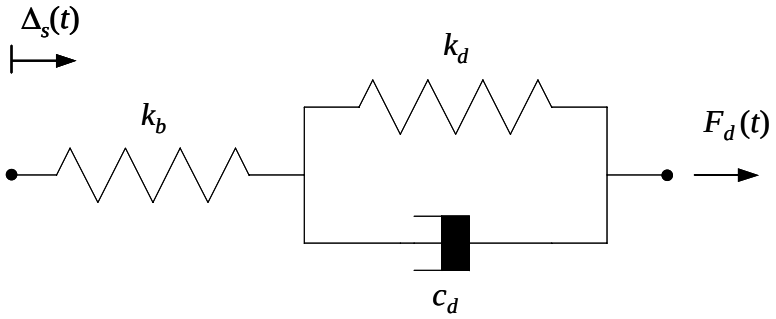

(b)

Figure 4.2: Linear models of viscoelastic devices, (a) Kelvin model and corresponding force-deformation response, (b) damper-brace assembly model.

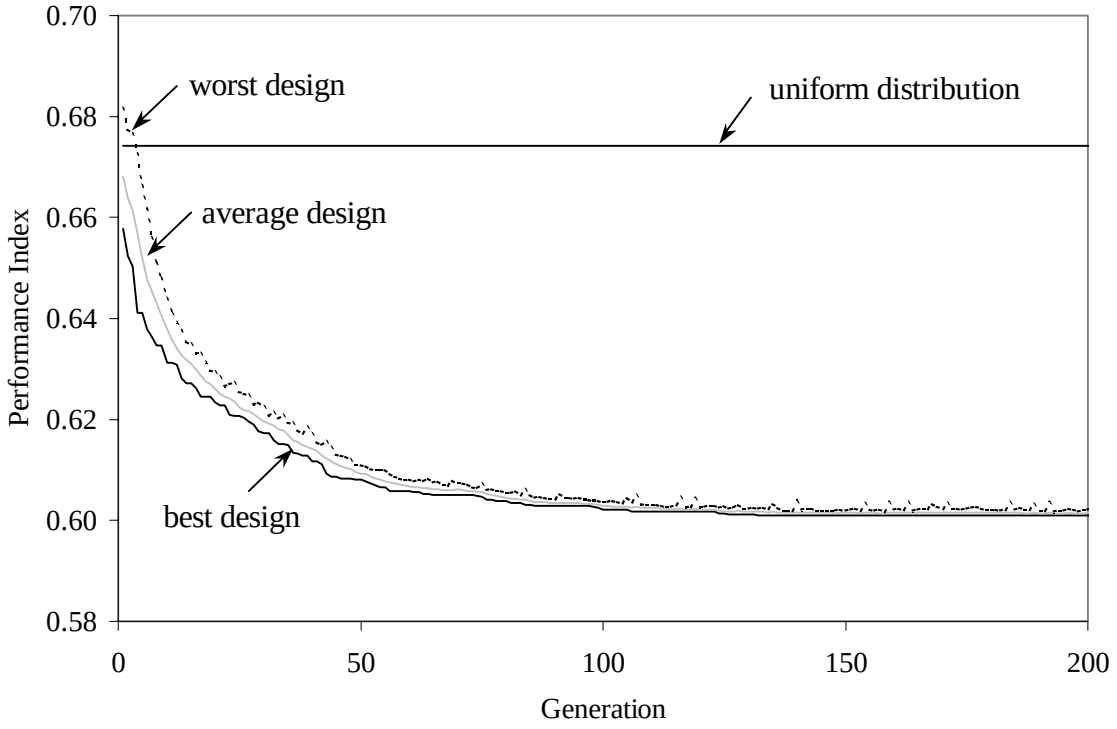

Figure 4.3: Optimization history for maximum inter-story drifts response reduction.

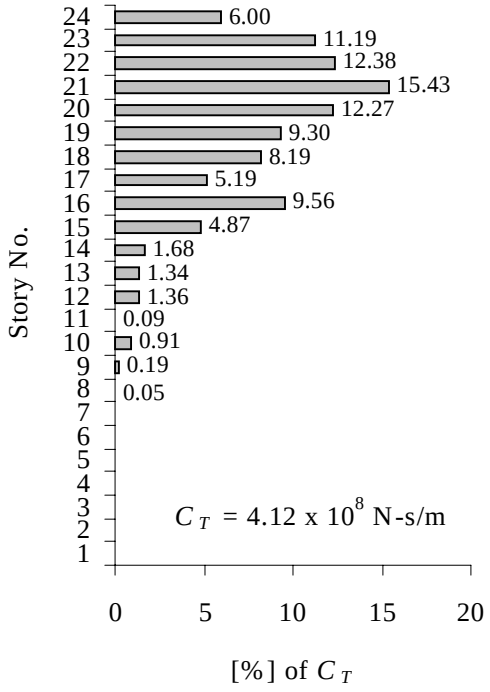

(a)

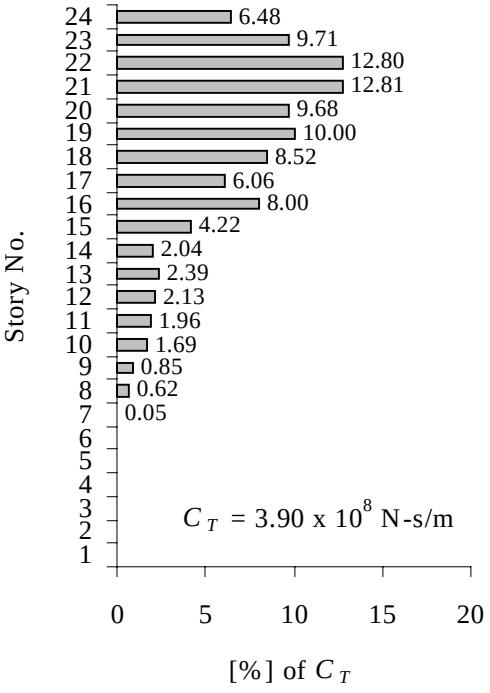

(b)

Figure 4.4: Optimal distribution of total damping in different stories for solid viscoelastic dampers for 40% response reduction, (a) normed floor accelerations, (b) base shear.

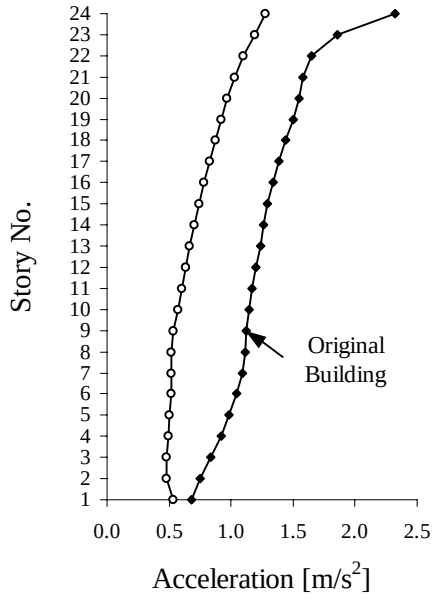

(a)

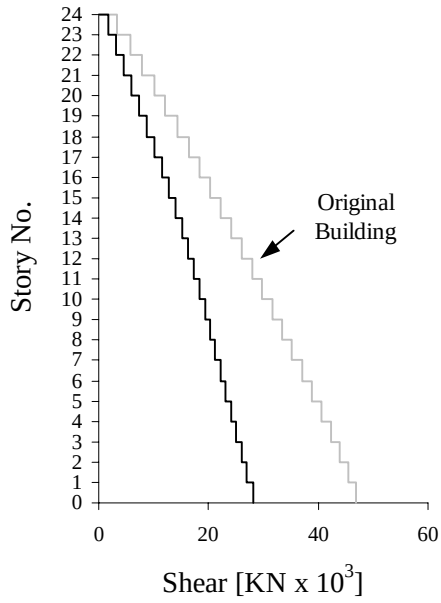

(b)

Figure 4.5: Comparison of controlled and uncontrolled responses quantities, (a) floor accelerations corresponding to the design of Figure 4.4(a), (b) shear forces corresponding to the design of Figure 4.4(b).

Chapter 5

Yielding Metallic Devices

5.1 Introduction

The previous two chapters focused on the design of viscoelastically-damped structures. The evaluation of performance indices and gradient information required by the optimization procedures was benefited from the assumed linear behavior of the building structure and installed damping devices. The maximum seismic responses were estimated considering a statistical characterization of the earthquake ground motion and the random vibration analysis of the structural system. A gradient projection methodology and a genetic algorithm approach were then used to determine the required amount of damping material and its optimal distribution within a building structure to achieve a desired performance criterion.

In this chapter, the attention is shifted to the design of yielding metallic devices. Although a number of devices have been proposed in the literature, the Bechtel's Added Damping and Stiffness (ADAS) and Triangular-plate Added Damping and Stiffness (TADAS) dampers have been found particularly suitable for the retrofit of existing structures as well as the construction of new ones. Figure 5.1 depicts the typical configuration of these devices. The ADAS devices, schematically represented in Figure 5.1(a), are made of X-shaped mild steel plates to deform in double curvature. TADAS is a variation of ADAS consisting of triangular plate elements that are made to deform as cantilever beams, as shown in Figure 5.1(b). Because of their shapes, the metal plates in these devices experience uniform flexural strains along their length. Thus when the strain reaches the yield level, yielding occurs over their entire volume.

During cyclic deformations, the metal plates are subjected to hysteretic mechanism and the plastification of these plates consumes a substantial portion of the structural vibration energy. Moreover, the additional stiffness introduced by the metallic elements increase the lateral strength of the building, with the consequent reduction in deformations and damage in the main structural members. In this chapter, an approach is formulated to design these devices in an optimal fashion. That is, the design parameters of these devices are obtained such that a pre-selected performance index is optimized.

It is noted that in contrast to the viscoelastic devices considered in the previous chapters, the cyclic response of yielding metallic devices is strongly nonlinear accompanied of abrupt changes in element stiffness due to the loading, unloading and reloading of yielded elements. The introduction of these devices in a structure will render it to behave nonlinearly, even if the other structural elements are designed to remain linear. Here in this study, it is assumed that the structural elements and the braces that support these devices remain linear when they are subjected to the design level earthquake.

There are two special issues that must be considered in the optimal design of structures installed with yielding metallic devices. First is that because of the highly nonlinear characteristics of these devices, accurate system dynamic analysis has to be done by a step-by-step time history analysis approach. This requires that the seismic design motion be defined by recorded or synthetic created ground motion accelerograms. One can still use the ground motion response spectra or spectral density function inputs in the analyses by adopting equivalent linear or equivalent nonlinear approaches. However, it is noted that such methodologies are necessarily approximate. In this study, the step-by-step time history analysis approach has been used to compute the structural response and performance indices required for optimization studies. More details of the time history analysis approach are provided in Section 5.3.

The second special consideration for optimal design of yielding metallic devices is the selection of the optimization algorithm. This is especially relevant here because the solution of the optimization problem is to be done by time history analyses, and the performance indices are usually defined in terms of the maximum values of different response quantities. The difficulty is related with the character of the earthquake excitation and the resulting structural response [97]. To better explain this concept, consider the typical situation encountered when designing

an elastic building structure subjected to an earthquake disturbance at its base. A single degree of freedom system is used here to characterize a hypothetical building structure, and for fixed values of mass and damping, the goal is to determine the stiffness of the system such that its maximum response is minimized when subjected to a given seismic excitation. Due to the simplicity of the model under consideration, the stiffness of the system can be varied within a specified design range and a series of time history analyses can be performed to determine the corresponding maximum responses. A plot of the peak values as a function of the stiffness of the system reveals those values that minimize the maximum response for the given earthquake excitation. In particular, a plot of the maximum responses as a function the natural vibration period of the system is nothing but the response spectrum, commonly used by the earthquake engineering community. Figures 5.2 (a) and (b) show, respectively, the deformation and acceleration response spectra for the 1971 San Fernando earthquake. From these response spectra, one can easily select the stiffness parameter that minimizes the peak value of deformation or acceleration and satisfies all the problem constraints. Of course, this solution has been obtained at the expense of an exhaustive analysis in which the response of the system has been examined for a sequence of stiffnesses values. The same design problem could also be solved using, for example, a gradient-based optimization technique. However, due to the jaggedness characteristics of the response spectra with the alternate presence of peaks and valleys, the search procedure will likely be trapped near the local optimum closer to the initial design guess. If the globally optimal solution is desired, then several randomly selected initial guesses must be used to locate such design.

Although the design problem discussed above was simple in nature, it revealed some of the difficulties encountered in the solution of optimal design problems by a gradient-based approach involving time history analyses of earthquakes disturbances. Not only the presence of numerous local minima have to be addressed by the optimization procedure, but also the cumbersome calculation of sensitivities derivatives of performance functions and constraints. This did not pose a special problem in the previous two chapters when the performance functions were continuously defined and the seismic input motion was defined in terms of response spectral density functions. However, in the optimization problem with metallic dampers, the determination of these quantities can be cumbersome. Also, the force-deformation relationships

of these devices may introduce discontinuities in the gradient functions depending on the model used to characterize their hysteretic cyclic behavior [146].

In this chapter, therefore, a genetic algorithm is used to cope with the aforementioned difficulties. This optimization scheme reduces the chance of converging to local optima by considering simultaneously many design points in the search space. Furthermore, genetic algorithm only requires the values of the performance function to guide its search for the best solution. Details of the implementation of this search procedure are presented in Section 5.5, as well as numerical results.

In the sequel, a brief description of the mechanical model employed in this study to characterize the behavior of yielding metallic devices is presented.

5.2 Analytical Modeling of Yielding Metallic Devices

The force-deformation response under arbitrary cyclic loading of the yielding metallic devices has often been approximated by discrete multi-linear models, such as the elasto-perfectly-plastic model and the bilinear model. A simple bilinear hysteretic forcing model is used next to identify the parameters involved in the design of a typical metallic element. Figure 5.3(a) represents a structural frame bay with an added hysteretic damper. Herein, the combination of a yielding metallic element and the bracing members that support the device is called as the device-brace assembly. The combined lateral stiffness of this assembly is schematically shown in Figure 5.3(b). This combined stiffness, denoted as k_{bd}, can be obtained by considering the contribution in stiffness k_d due to the metallic device and the stiffness k_b added by the bracing. Since these stiffnesses are connected in series, as shown in Figure 5.3(c), it follows that

$$k_{bd} = \frac{1}{\frac{1}{k_b} + \frac{1}{k_d}} = \frac{k_d}{1 + \frac{1}{\mathrm{B/D}}} \tag{5.1}$$

where B/D is the ratio between the bracing and device stiffness.

$$\mathrm{B/D} = \frac{k_b}{k_d} \tag{5.2}$$

Another quantity of interest is the stiffness ratio *SR* defined as the ratio of assembly stiffness to the stiffness of the story k_s as,

$$SR = \frac{k_{bd}}{k_s} \tag{5.3}$$

In this study, it is assumed that the bracing members as well as the main structural members are designed to remain elastic during an earthquake and that the stiffnesses and ratios previously defined correspond only to the initial elastic values of the yielding elements. The yield force of the yielding element, denoted by P_y, is related to the yield displacement of the device Δ_{yd}, and also to the yield displacement experienced by the device-brace assembly Δ_y as:

$$P_y = k_d \, \Delta_{yd} = k_{bd} \Delta_y \tag{5.4}$$

For design purposes, this equation can be expressed in terms of the parameters *SR* and B/D by considering Eqs. (5.1) and (5.3) in Eq. (5.4) as:

$$P_y = SR \; k_s \left(1 + \frac{1}{\text{B/D}} \right) \Delta_{y_d} \tag{5.5}$$

Equation (5.5) is the basic expression that establishes the relationship between the parameters of the assumed bilinear model. From this equation, it can be observed that in a given structure (i.e. k_s known) the behavior of a metallic yielding element is governed by four key parameters. They are: the yielding load P_y, the yield displacement of the metallic device Δ_{yd}, and the stiffness ratios *SR* and B/D. However, only three of these variables are independent since the fourth one can be determined from Eq. (5.5).

A bilinear model has been considered in the above discussion to represent the hysteretic behavior of the metallic yielding element. Because of its mathematical simplicity, it provided a convenient tool to establish the relationship between the model parameters. However, numerical complications may arise when performing time history analyses of a structural system incorporating this model due to the sharp transitions from the inelastic to elastic states during the loading and reloading cycles. The presence of such abrupt changes in stiffness call for numerical procedures having the capacity to locate these transition points in order to avoid erroneous results. As the number of devices installed in a building structure increases and the different phase or stiffness transitions conditions for each device have to be taken into account in the numerical calculations, the bilinear representation of the devices becomes computationally inefficient. In any case, the assumed bilinear behavior of a device is an idealization and not the

true representation. In this study, therefore, a continuous Bouc-Wen's model is used to characterize the hysteretic force-deformation characteristic of the yielding metallic element [190].

A particularly attractive feature of the Bouc-Wen's model is that the same equation governs the different stages of the inelastic cyclic response of the device. Moreover, since this model is in the form of a differential equation, it can be conveniently coupled with the equations that describe the motion of the building structure. The restoring force $P(t)$ developed in the device-brace assembly can be expressed by the following equation:

$$P(t) = k_0 \left[\alpha \Delta(t) + (1-\alpha) \Delta_y \, h(t) \right] \tag{5.6}$$

$$\Delta_y \, \dot{h}(t) - H \, \dot{\Delta}(t) + \gamma \left| \dot{\Delta}(t) \right| h(t) \left| h(t) \right|^{\eta-1} + \beta \, \dot{\Delta}(t) \left| h(t) \right|^{\eta} = 0 \tag{5.7}$$

where $h(t)$ is a dimensionless auxiliary variable that has hysteretic characteristics; and k_0, α, Δ_y, H, γ, β and η are the model parameters. These values must be chosen to calibrate the predicted response of the metallic element with the one obtained experimentally. In particular, the parameters H, γ, β and η control the shape of the hysteretic curves. It can be shown that by choosing $H = 1$, the value of k_0 defines the initial stiffness of the metallic device-brace assembly, and α represents the post-yielding or strain-hardening ratio. For given values of the parameters γ and β, the exponent η control the sharpness of transition from the elastic to the inelastic region. As the value of $\eta \to \infty$, the model approaches the bilinear model. Figure 5.4 shows the hysteresis loops generated by the Bouc-Wen's model for exponent values of η = 1, 5 and 25 when subjected to a sinusoidal excitation. The values of $H = 1$, $\alpha = 0.02$, $\eta = 25$, $\beta = 0.1$, and $\gamma = 0.9$ have been selected in this chapter to characterize the hysteretic behavior of the metallic device-brace assembly. The remaining parameters of the model can be selected to closely match the hysteretic force-deformation characteristic of the metallic element. From the above discussion, and considering the relationships given by Eqs. (5.3) and (5.5), it follows that

$$k_0 = SR \, k_s; \qquad \Delta_y = \left(1 + \frac{1}{\text{B/D}} \right) \Delta_{yd} \tag{5.8}$$

Therefore, the yield displacement of the metallic device Δ_{yd}, and the ratios SR and B/D can be selected as the mechanical variables governing the behavior of the device-brace assembly. Once

the values of these parameters are selected, the Bouc-Wen's hysteretic model is completely determined.

5.3 Response Calculations

In the previous chapters, the structural response of the assumed linear viscoelastically-damped structure was estimated using a modal-based random vibration technique. This approach permitted the efficient calculations of performance indices and gradient information required by the optimization procedures. Moreover, this methodology was able to include in a single analysis the inherent random characteristics of earthquake ground motions. The modal superposition principle, essential to the development of the cited analysis technique, is not longer valid for nonlinear system. Therefore, the responses and performance indices have to be determined by performing time history analysis. The random variability in the seismic motion at a site can be included by considering several records of actual or simulated ground motions.

The equations of motion (3.22) for a plane shear building, as presented in Chapter 3, are slightly modified here to include a single device installed at each story. In this case, they can be written as:

$$\mathbf{M}\,\ddot{\mathbf{x}}(t)+\mathbf{C}_s\,\dot{\mathbf{x}}(t)+\mathbf{K}_s\,\mathbf{x}(t)+\sum_{d=1}^{n_l}\mathbf{r}_d\,P_d(t)=-\mathbf{M}\,\mathbf{E}\,\ddot{X}_g(t) \tag{5.9}$$

If the force $P_d(t)$ exerted by the d^{th} damper element on the structure is characterized by a continuous hysteretic Bouc-Wen' s model, it can be expressed as:

$$P_d(t)=SR_d\,k_s^d\left[\alpha\,\Delta_d(t)+(1-\alpha)\,\Delta_y^d\,h_d(t)\right] \tag{5.10}$$

$$\Delta_y^d\,\dot{h}_d(t)-\dot{\Delta}_d(t)+\gamma\left|\dot{\Delta}_d\right|h_d(t)\left|h_d(t)\right|^{\eta-1}+\beta\,\dot{\Delta}_d\left|h_d(t)\right|^{\eta}=0 \tag{5.11}$$

where Δ_y^d is the yielding displacement of the d^{th} device-brace assembly and k_s^d denotes the stiffness of the story in which the element is located. Combining the expressions (5.10) and (5.11) for the element forces with the equations of motion (5.9), the complete set of equations of motion of the resulting structural system takes the form:

$$\mathbf{M}\,\ddot{\mathbf{x}}(t)+\mathbf{C}_s\,\dot{\mathbf{x}}(t)+\left(\mathbf{K}_s+\alpha\sum_{d=1}^{n_l}\mathbf{r}_d\,SR_d\,k_s^d\,\mathbf{r}_d^T\right)\mathbf{x}(t)+(1-\alpha)\sum_{d=1}^{n_l}\mathbf{r}_d\,SR_d\,k_s^d\Delta_y^d\,h_d(t)=-\mathbf{M}\,\mathbf{E}\,\ddot{X}_g(t)$$
$$\Delta_y^d\,\dot{h}_d(t)-\mathbf{r}_d^T\dot{\mathbf{x}}(t)+\gamma\left|\mathbf{r}_d^T\dot{\mathbf{x}}(t)\right|h_d(t)\left|h_d(t)\right|^{\eta-1}+\beta\,\mathbf{r}_d^T\dot{\mathbf{x}}(t)\left|h_d(t)\right|^{\eta}=0;\qquad d=1,\ldots,n_l \tag{5.12}$$

The different response quantities required for the evaluation of the optimization performance indices can be calculated by solving the system of equations (5.12). The numerical integration of these equations can be done using a state-space formulation. In this approach, the governing equations (5.12) have to be rewritten as a set of first-order differential equations. Once in this form, the system of equations can be conveniently integrated using several accurate and efficient solvers [80].

For the system of equations (5.12), the state of the dynamic system is expressed in terms of the displacement, velocity and hysteretic variables vectors, as:

$$\mathbf{z}(t)=\begin{Bmatrix}\dot{\mathbf{x}}(t)\\ \mathbf{x}(t)\\ \mathbf{h}(t)\end{Bmatrix} \tag{5.13}$$

The first-order differential equation of the system then can be written as:

$$\begin{Bmatrix}\ddot{\mathbf{x}}(t)\\ \dot{\mathbf{x}}(t)\\ \dot{\mathbf{h}}(t)\end{Bmatrix}=g\left[\mathbf{x}(t),\dot{\mathbf{x}}(t),\mathbf{h}(t),\ddot{X}_g(t),t\right] \tag{5.14}$$

Using Eqs. (5.12), this first-order differential representation of the system can be explicitly defined as:

$$\ddot{\mathbf{x}}(t)=-\mathbf{M}^{-1}\left[\mathbf{C}_s\,\dot{\mathbf{x}}(t)+\left(\mathbf{K}_s+\alpha\sum_{d=1}^{n_l}\mathbf{r}_d\,SR_d\,k_s^d\,\mathbf{r}_d^T\right)\mathbf{x}(t)+\left(1-\alpha\right)\sum_{d=1}^{n_l}\mathbf{r}_d\,SR_d\,k_s^d\Delta_y^d\,h_d(t)\right]-\mathbf{E}\,\ddot{X}_g(t)$$
$$\dot{\mathbf{x}}(t)=\dot{\mathbf{x}}(t)$$
$$\dot{h}_d(t)=\frac{1}{\Delta_y^d}\left[\,\mathbf{r}_d^T\dot{\mathbf{x}}(t)-\gamma\left|\mathbf{r}_d^T\dot{\mathbf{x}}(t)\right|h_d(t)\left|h_d(t)\right|^{\eta-1}-\beta\,\mathbf{r}_d^T\dot{\mathbf{x}}(t)\left|h_d(t)\right|^{\eta}\right];\qquad d=1,\ldots,n_l \tag{5.15}$$

For a given installation of devices, any response quantity can be obtained as a linear combination of the states of the system as:

$$\mathbf{R}(\mathbf{d},\mathbf{n},t)=\mathbf{T}\,\mathbf{z}(t) \tag{5.16}$$

where **T** is a transformation matrix of appropriate dimensions.

The differential equations (5.15) constitute a set of coupled nonlinear differential

equations. These equations can be solved using different integration schemes. For this study, the solver LSODA from the ODEPACK package [75; 139] is implemented for the numerical integration of Eqs. (5.15). It uses Adams methods (predictor-corrector) if the differential equations are nonstiff, and automatically switches to a Backward Differentiation Formula (BDF) method if the problem is regarded as stiff.

5.4 Performance Indices

Depending on the performance desired different design solutions could be obtained by the search procedure. In this section, a description of the performance indices considered in this study is presented. The improvement in the seismic performance of a building structure obtained with the incorporation of the protective devices can be measured by a number of alternative indices. In previous chapters, several forms of performance indices were presented, and different responses quantities were used in their evaluation. In particular, inter-story drifts were used as a measure of the deformations and possible damage of structural members and non-structural components. The floor accelerations were alternatively employed to assess the discomfort experienced by the building occupants, as well as a measure of the shear forces and stresses developed in the main structural members. In this regard, it is interesting to examine the effectiveness of the yielding metallic devices in reducing these response quantities.

Consider a simple structure characterized by its mass m and stiffness k_s, as schematized in Figure 5.5, in which a yielding metallic device has been installed. For illustration purposes, a natural period of T_s = 1.0 s, and an inherent damping ratio of 0.03 of the critical value has been assigned to the structure. The device-brace assembly hysteretic behavior is characterized using the previously presented Bouc-Wen's model, with a yielding displacement Δ_y = 0.005 m and a stiffness ratio B/D = 2. The structure is subjected to the 1971 San Fernando earthquake and its maximum displacement and acceleration response values are computed as the stiffness ratio SR of the metallic element is increased. The ratios between the peak response values of the controlled and original structure are plotted against the elastic period of the modified structure T_m, as shown in Figure 5.6, where

$$T_m = \frac{T_s}{(1+SR)^{1/2}} \tag{5.17}$$

From Figure 5.6(a) it can be observed that as the stiffness of the device is increased, with the consequent decrease in the elastic period of vibration of the structure, the maximum displacement response is always reduced. However, Figure 5.6(b) reveals that the acceleration response does not follow the same pattern. For a stiffness ratio *SR* below 5.25 (T_m = 0.4 s), the structural system is benefited from the added stiffness and the maximum acceleration response is reduced. However, as the stiffness of the metallic element is further increased and the structure becomes more rigid, the peak acceleration values are amplified.

From the preceding discussion, it is clear that a trade off has to be made between these response quantities. Therefore, a performance index that considers simultaneously the reductions in the maximum inter-story drift and maximum story acceleration is defined in this study. This index can be expressed as:

$$f\left[\mathbf{R}(\mathbf{d},t)\right] = \frac{1}{2}\left\{\frac{\max_i \Delta_i(t)}{\max_i \Delta_{i(o)}(t)} + \frac{\max_i \left[\ddot{x}_i(t) + \ddot{X}_g(t)\right]}{\max_i \left[\ddot{x}_{i(o)} + \ddot{X}_g(t)\right]}\right\} \tag{5.18}$$

where the deformation experienced at the i^{th} story, denoted as Δ_i, and absolute floor acceleration are normalized with respect to the corresponding values of the original building. It is noted that this index gives equal weights to the deformation and acceleration related responses. If desired, different weights can also be assigned.

Thus far, the improvement in the seismic performance of a building structure with supplemental passive energy dissipation devices has been measured in terms of the reduction achieved in different response quantities, such as floor accelerations and inter-story drifts. Alternatively, a performance index can be defined to measure the ability of a damper to dissipate the energy input into the building structure by the seismic disturbance. Since the main assumptions in this study has been that the mechanism of energy dissipation is entrusted entirely to the passive devices to keep the main structure undamaged, it seems appropriate to design the devices in order to maximize their energy dissipation capabilities. A review of the formulation required for the definition of an energy-based design criterion is presented next.

The energy equations for a multi-degree of freedom elastic structural system subjected to a seismic ground motion can be obtained by integrating the individual force terms in the equations of motion (5.9) over the entire relative displacement history. That is,

$$\int \left\{ \left[\ddot{\mathbf{x}}(t) + \mathbf{E}\, \ddot{X}_g(t) \right]^T \mathbf{M} + \dot{\mathbf{x}}(t)^T \mathbf{C}_s + \mathbf{x}(t)^T \mathbf{K}_s + \sum_{d=1}^{n_l} \mathbf{r}_d^T P_d(t) \right\} d\mathbf{x} = 0 \tag{5.19}$$

The first term of Eq. (5.19) can be expressed in terms of the absolute acceleration vector, $\ddot{\mathbf{x}}_{abs}(t)$, and absolute displacement vector, $\mathbf{x}_{abs}(t)$, as

$$\begin{aligned} \int \ddot{\mathbf{x}}_{abs}^T \mathbf{M}\, d\mathbf{x} &= \int \ddot{\mathbf{x}}_{abs}^T \mathbf{M} \left(d\mathbf{x}_{abs} - \mathbf{E}\, dX_g \right) = \int \ddot{\mathbf{x}}_{abs}^T \mathbf{M}\, d\mathbf{x}_{abs} - \int \ddot{\mathbf{x}}_{abs}^T \mathbf{M}\mathbf{E}\, dX_g \\ &= \frac{1}{2} \dot{\mathbf{x}}_{abs}^T \mathbf{M}\, \dot{\mathbf{x}}_{abs} - \int \ddot{\mathbf{x}}_{abs}^T \mathbf{M}\mathbf{E}\, \dot{X}_g\, dt \end{aligned} \tag{5.20}$$

Substituting Eq. (5.20) in Eq. (5.19) yields

$$\frac{1}{2} \dot{\mathbf{x}}_{abs}^T \mathbf{M}\, \dot{\mathbf{x}}_{abs} + \int \dot{\mathbf{x}}^T \mathbf{C}_s\, d\mathbf{x} + \int \mathbf{x}^T \mathbf{K}_s\, d\mathbf{x} + \int \sum_{d=1}^{n_l} \mathbf{r}_d^T P_d\, d\mathbf{x} = \int \ddot{\mathbf{x}}_{abs}^T \mathbf{M}\mathbf{E}\, \dot{X}_g\, dt \tag{5.21}$$

The right hand side term of Eq. (5.21) is the absolute earthquake input energy E_I,

$$E_I = \int \ddot{\mathbf{x}}_{abs}^T \mathbf{M}\mathbf{E}\, \dot{X}_g\, dt \tag{5.22}$$

The absolute kinetic energy E_K, elastic strain energy E_S, and inherent viscous damped energy E_D of the structural system are defined as:

$$E_K = \frac{1}{2} \dot{\mathbf{x}}_{abs}^T \mathbf{M}\, \dot{\mathbf{x}}_{abs}; \qquad E_S = \frac{1}{2} \mathbf{x}^T \mathbf{K}_s\, \mathbf{x}; \qquad E_D = \int \dot{\mathbf{x}}^T \mathbf{C}_s\, \dot{\mathbf{x}}\, dt \tag{5.23}$$

The remaining term corresponds to the energy associated with the passive energy dissipation devices. This energy quantity, denoted E_P, can be further subdivided in terms of the energy dissipated in the hysteretic devices, E_{PH}, and the recoverable elastic strain energy, E_{PS}, stored by the device-brace assemblages during the excitation. That is,

$$E_P = \int \sum_d \mathbf{r}_d^T P_d(t)\, d\mathbf{x} = E_{PH} + E_{PS} \tag{5.24}$$

The resulting scalar energy balance equation can then be expressed as follows [187]:

$$E_K + E_D + E_S + E_P = E_I \tag{5.25}$$

It is clear from the energy balance equation (5.25), that to achieve an efficient aseismic design it is necessary to control or reduce the input earthquake energy, as well as to increase the energy dissipation capabilities of the structure by the incorporation of the passive devices.

Therefore, it seems adequate to use a performance index that relates these energy quantities. In this study, the maximization of the ratio between the hysteretic energy dissipated in the devices and the input earthquake energy has been considered for optimization purposes. It can be expressed as:

$$f\left[\mathbf{R}(\mathbf{d},t)\right]=\frac{E_{PH}}{E_I} \tag{5.26}$$

The energy dissipated though the devices, E_{PH}, can be evaluated from Eq. (5.24) as the difference between the work done by the metallic devices and the instantaneous strain energy of the device-brace assemblages,

$$E_{PH}=\int \sum_d \mathbf{r}_d^T P_d(t)\,\dot{\mathbf{x}}(t)\,dt-\sum_d \frac{\left[P_d(t)\right]^2}{2\,k_{bd}} \tag{5.27}$$

It is clear that the maximization of the performance index of Eq. (5.26) attempts not only to maximize the dissipation of energy through the metallic yielding devices, but also tries to minimize the input earthquake energy attracted by the building structure.

5.5 Numerical Results

This section illustrates the application of the genetic algorithm approach to the design of the yielding metallic dampers for seismic protection of building structures. The ten-story Building 2 is considered in this section for retrofitting purposes. For the numerical calculations, it is assumed that a single metallic element is installed at each story, with mechanical properties to be determined by the optimization procedure. In Section 5.2, the different parameters governing the behavior of the metallic yielding elements were identified. For optimization purposes, the stiffness ratios *SR* and B/D, and the device yield displacement Δ_{yd} are considered here. Since the genetic algorithms operate in a discrete design space, the design variables have to be properly discretized.

To define the ground motion characteristics, the 1971 San Fernando earthquake, N21E component, with peak ground acceleration of 0.315*g* is used as the design earthquake. For numerical calculations, a set of four artificially generated accelerograms is used. These synthetic earthquakes are compatible with the Kanai-Tajimi power spectral density function of the actual

San Fernando ground motion. The parameters ω_g, β_g and S for this seismic event were determined to be 23.96 rad/s, 0.32 and 19.86×10^{-3} m^2/s^3, respectively [100].

First, it is assumed that all the devices yield at the same displacement $\Delta_{yd} = 0.005$ m, and that the metallic elements are designed using a stiffness ratio B/D = 2. Under these circumstances, the only independent design variable is the stiffness ratio SR_d for each story. For discretization purposes, this variable is considered to take on integer values between zero and ten, with zero representing the case of no device or unbraced story. This discretization scheme, as shown in Figure 5.7(a), leads to eleven possible values of stiffness ratio SR_d for each floor, and for this particular building, the design space encompass a total of 11^{10} possible combinations. Figure 5.8(a) illustrates some of the possible combinations for the stiffness ratios SR_d, under the assumption of uniform distribution of yield displacements Δ_{yd} and stiffness ratio B/D along the building height. The design problem is solved using the genetic algorithm employing a population of 20 individuals evolving through 400 generations. Three different performance indices are used to quantify the reduction in response. Column (4) of Table 5.1 shows the distribution along the building height of the stiffness ratio SR_d averaged over the four earthquakes calculated according to the performance index of Eq. (5.18). The corresponding yield load values P_y^d, presented in Column (5), have been calculated using Eq. (5.5) and are expressed as percentages of the total building weight W. The last row presents the value of the performance index achieved by the corresponding design solution. Table 5.1 also presents the results obtained when the performance index is defined in terms of the maximum inter-story drifts alone [See Columns (6) and (7)], and for the case in which only the maximum acceleration values are used to evaluate the improvement in the seismic response of the building [See Columns (8) and (9)].

Next, the device yield displacement Δ_{yd}, previously considered as fixed throughout the building height, is added to the set of design variables. Based on observations of experimental studies and suggested design guidelines [195; 196], the admissible values of Δ_{yd} have been considered to range between 0.005 m and 0.008 m. This interval is divided in ten equal parts for discretization purposes leading to eleven possible values of yield displacement for each device. Since the number of possible combinations has been increased with the inclusion of the new

design variable, as shown in Figure 5.7(b), a larger population of 30 individuals undergoing 800 generations is considered for the numerical studies. Figure 5.8(b) depicts some of the possible combinations of stiffness values and yielding displacements for metallic devices located at different stories in the building. The results obtained for the performance index of Eq. (5.18) are presented in Columns (4) to (6) of Table 5.2. Columns (2) and (3) of this table replicate the solution presented in Columns (4) and (5) of Table 5.1 when the only independent variable was the stiffness ratio SR_d. It can be noticed by comparing the indices values of both solutions that the response is further reduced by a 9%. This further reduction in the performance index value can be attributed to the increased flexibility introduced in the design by the addition of a second variable per device.

Previous studies suggest that the ratio between the stiffness of the damper element and supporting bracing, B/D, has little influence on the response of the structural system [195; 196]. To examine this statement, the stiffness ratio B/D is also included to the set of design variables. This variable is considered to vary between one and ten. As before, due to the increased size of the design space with the addition of the new variable, a larger population of 40 individuals is selected for the search procedure. Figure 5.7(c) presents one of the potential design solutions. Columns (7) to (10) of Table 5.2 present the results obtained for this case. As before, the performance index is reduced by another 8%. For this final design, the evolution of the performance function with each generation is plotted in Figure 5.9. Figure 5.10(a) presents the corresponding hysteresis loops for devices located at different building stories.

Next, the design of the yielding metallic elements is repeated considering the energy performance index of Eq. (5.26). As in the previous design example, it is assumed first that all the devices yield at the same displacement $\Delta_{yd} = 0.005$ m, and that the metallic elements are designed using a stiffness ratio B/D = 2. Columns (2) and (3) of Table 5.3 present the results for this case in which the only design variable is stiffness ratio SR_d at each story. The last row shows that a 79.1% of the input energy is dissipated through the metallic yielding elements for this distribution of stiffness. As shown in Columns (4) to (6) of the same table, the dissipation of energy is slightly improved when considering the inclusion of the device yield displacement Δ_{yd} as second design variable per device. The stiffness ratio B/D is then included to the set of design variables. For this case, Columns (7) to (10) of Table 5.3 show the optimal distribution of the

mechanical properties of the devices. The force-deformation responses corresponding to this final design are presented in Figure 5.10(b) for metallic devices installed at different stories.

Figure 5.11 provides a comparison of the maximum inter-story drifts, maximum displacements and absolute accelerations for the original (uncontrolled) building and the retrofitted structure designed according to the results presented in Columns (7) to (10) of Tables 5.2 and 5.3, respectively. It is observed that both designs achieve comparable reductions in the inter-story drifts and displacement values at different levels of the building. The reductions in the maximum acceleration, however, have large differences. As expected, the design obtained using the response performance index of Eq. (5.18), specially made to reduce both the interstory-drifts and floor accelerations, provides a better reduction in the floor accelerations than the design based on the energy index of Eq. (5.26).

5.6 Chapter Summary

This chapter examined the design of yielding metallic devices for seismic protection of building structures. These devices dissipate a large amount of the input earthquake energy through the inelastic deformation of metallic plates.

The parameters governing the force-deformation characteristics of a metallic devices were identified to be: the yield displacement of the device, the ratio of bracing stiffness to device stiffness, the ratio of brace-device assemblage stiffness to device stiffness, and the ratio of the assemblage stiffness to stiffness of corresponding structural story. The hysteretic behavior of the devices and supporting bracings was described using a continuous Bouc-Wen's model. Although it has been assumed that the main structure remained linear during a seismic event, the inelastic energy dissipation mechanism of the devices introduced localized nonlinearities. Consequently, the seismic structural response was obtained by performing time history analyses of actual and simulated ground motions. The equations of motion of the combined structural system were obtained using a state space representation for its convenient numerical solution. For optimization purposes, the presence of several local minima combined with the cumbersome calculation of gradient information motivated the implementation of a genetic algorithm search procedure. Numerical results were presented to illustrate the application of this optimization

approach. The versatility of this technique was further evidenced when considering distinct forms of performance indices requiring the evaluation of maximum response quantities and energy integrals.

Several optimal designs with different possible variations of the design parameters of the devices were considered. It was observed that for a chosen index, the structural performance could be further improved by considering the inclusion of more design parameters. This added more flexibility, and thus the possibility of obtaining a more efficient design.

Table 5.1: Comparison of design solutions obtained using different performance indices.

Story	Δ_{yd} [m]	B/D	$f_1[\mathbf{R}(\mathbf{d},t)]$		$f_2[\mathbf{R}(\mathbf{d},t)]$		$f_3[\mathbf{R}(\mathbf{d},t)]$	
			SR_d	P_y^d [%W]	SR_d	P_y^d [%W]	SR_d	P_y^d [%W]
(1)	(2)	(3)	(4)	(5)	(6)	(7)	(8)	(9)
1	0.005	2	1.50	4.2	6.00	17.0	1.00	2.8
2	0.005	2	2.75	7.2	4.50	11.8	7.50	19.7
3	0.005	2	8.50	20.5	3.75	9.0	8.00	19.3
4	0.005	2	3.00	6.6	5.75	12.7	2.25	5.0
5	0.005	2	2.25	4.5	5.50	11.0	6.00	12.0
6	0.005	2	4.50	8.0	7.00	12.5	7.00	12.5
7	0.005	2	2.50	3.9	5.25	8.3	4.25	6.7
8	0.005	2	4.75	6.5	9.50	12.9	6.75	9.2
9	0.005	2	5.50	6.3	6.75	7.8	5.25	6.1
10	0.005	2	1.66	1.6	5.84	5.5	1.17	1.1
$f[\mathbf{R}(\mathbf{d}^*,t)]$	-		0.68		0.38		0.74	

Note:

$$f_1\left[\mathbf{R}\left(\mathbf{d},t\right)\right]=\frac{1}{2}\left\{\frac{\max_i \Delta_i(t)}{\max_i \Delta_{i(o)}(t)}+\frac{\max_i\left[\ddot{x}_i(t)+\ddot{X}_g(t)\right]}{\max_i\left[\ddot{x}_{i(o)}(t)+\ddot{X}_g(t)\right]}\right\}$$

$$f_2\left[\mathbf{R}\left(\mathbf{d},t\right)\right]=\frac{\max_i \Delta_i(t)}{\max_i \Delta_{i(o)}(t)}$$

$$f_3\left[\mathbf{R}\left(\mathbf{d},t\right)\right]=\frac{\max_i\left[\ddot{x}_i(t)+\ddot{X}_g(t)\right]}{\max_i\left[\ddot{x}_{i(o)}(t)+\ddot{X}_g(t)\right]}$$

Table 5.2: Design of yielding metallic devices according to the response performance index of Eq. (5.18).

Story	*SR*		*SR* and Δ_{yd}			*SR*, Δ_{yd} and B/D			
	SR_d	P_y^d [%*W*]	Δ_{yd} [m]	SR_d	P_y^d [%*W*]	Δ_{yd} [m]	SR_d	B/D$_d$	P_y^d [%*W*]
(1)	(2)	(3)	(4)	(5)	(6)	(7)	(8)	(9)	(10)
1	1.50	4.2	0.00575	1.50	4.9	0.00695	2.00	8.25	5.9
2	2.75	7.2	0.00605	3.50	11.1	0.00575	4.50	5.00	10.9
3	8.50	20.5	0.00507	5.50	13.5	0.00605	7.00	6.50	15.7
4	3.00	6.6	0.00537	7.00	16.6	0.00545	4.75	5.75	8.9
5	2.25	4.5	0.00560	3.75	8.4	0.00537	4.25	9.75	6.7
6	4.50	8.0	0.00582	3.75	7.8	0.00515	3.50	8.50	4.8
7	2.50	3.9	0.00552	5.00	8.7	0.00500	3.00	4.25	3.9
8	4.75	6.5	0.00507	6.75	9.3	0.00537	4.25	6.50	4.8
9	5.50	6.3	0.00537	6.50	8.1	0.00545	4.50	5.75	4.4
10	1.66	1.6	0.00522	3.40	3.3	0.00590	5.38	3.25	5.2
$f[\mathbf{R}(\mathbf{d}^*,t)]$	0.68		0.62			0.57			

Table 5.3: Design of yielding metallic devices according to the energy performance index of Eq. (5.24)

Story	*SR*		*SR* and Δ_{yd}			*SR*, Δ_{yd} and B/D			
	SR_d	P_y^d [%*W*]	Δ_{yd} [m]	SR_d	P_y^d [%*W*]	Δ_{yd} [m]	SR_d	B/D_d	P_y^d [%*W*]
(1)	(2)	(3)	(4)	(5)	(6)	(7)	(8)	(9)	(10)
1	6.00	17.00	0.00665	6.75	25.4	0.00545	8.50	4.75	0.212
2	10.00	26.22	0.00560	10.00	29.4	0.00585	8.75	9.25	0.198
3	10.00	24.12	0.00605	9.75	28.5	0.00572	10.00	5.75	0.216
4	8.00	17.62	0.00582	9.75	25.0	0.00537	7.75	4.50	0.149
5	6.75	13.45	0.00560	6.25	13.9	0.00507	6.00	6.50	0.093
6	6.25	11.14	0.00507	6.25	11.3	0.00530	4.50	4.75	0.069
7	7.00	11.01	0.00530	4.50	7.5	0.00612	7.25	6.00	0.109
8	7.75	10.56	0.00560	8.00	12.2	0.00605	9.75	8.50	0.120
9	7.25	8.36	0.00567	7.00	9.2	0.00545	5.00	6.25	0.049
10	5.70	5.37	0.00567	5.45	5.8	0.00595	5.46	3.00	0.054
$f[\mathbf{R}(\mathbf{d}^*,t)]$	0.791		0.801			0.833			

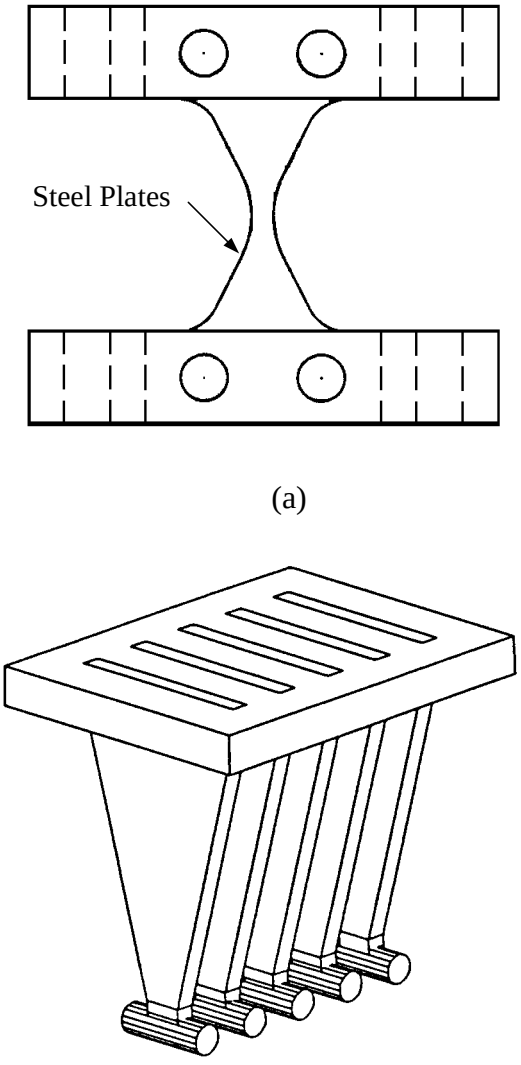

Figure 5.1: Typical yielding metallic devices for seismic structural applications, (a) ADAS device, (b) TADAS device [128].

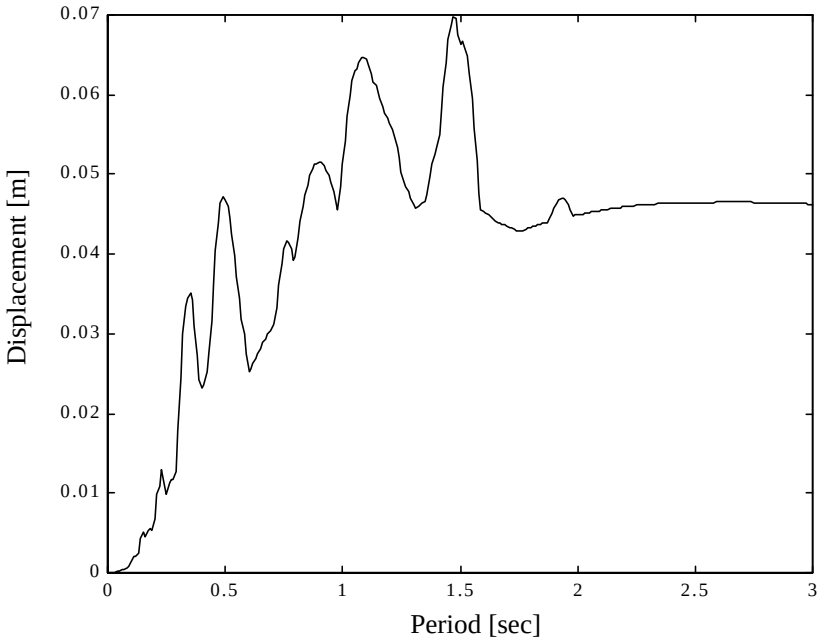

(a)

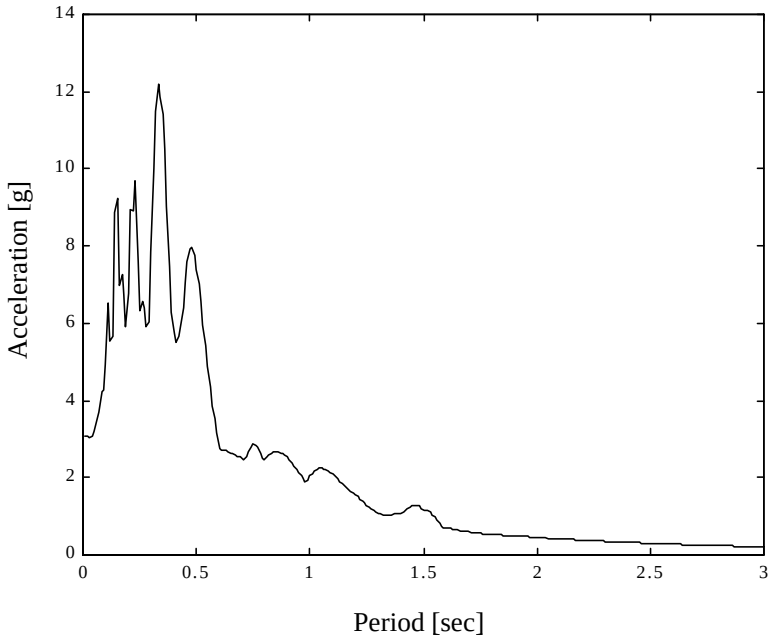

(b)

Figure 5.2: San Fernando earthquake response spectra for 3% damping; (a) relative displacement response spectra, (b) acceleration response spectra.

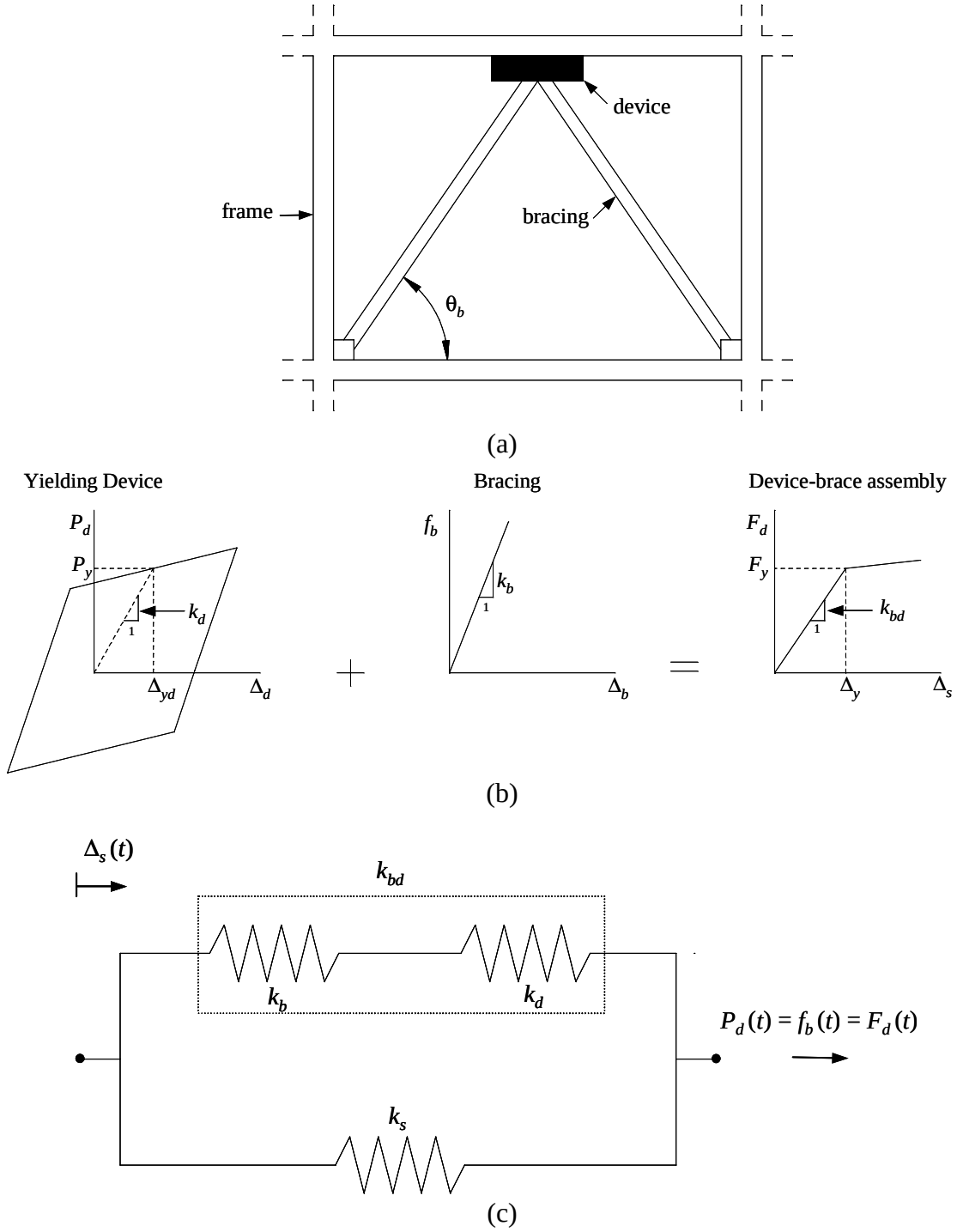

Figure 5.3: Yielding metallic damper, (a) typical configuration, (b) yielding metallic device, bracing and yielding element parameters, (c) stiffness properties of device-bracing assembly.

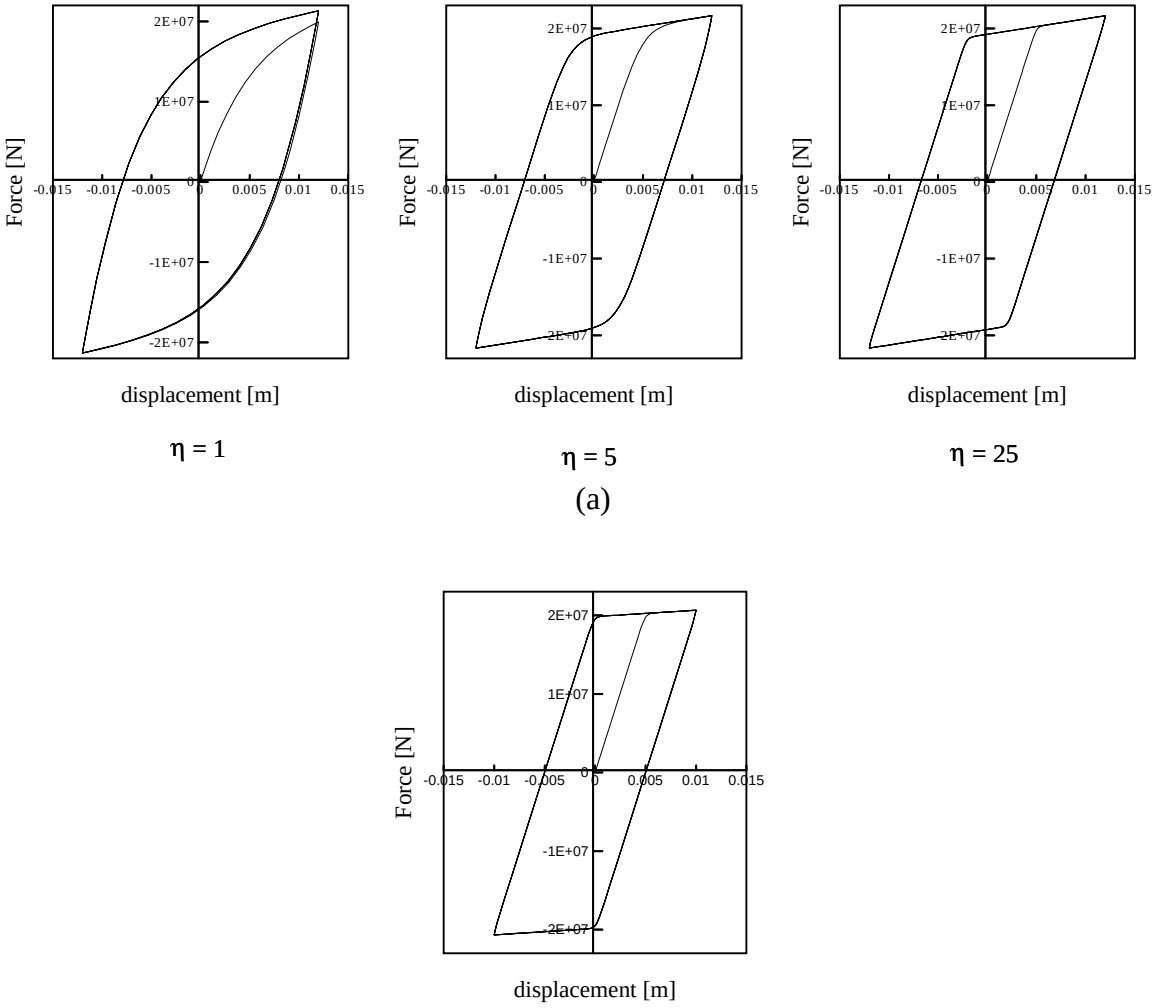

Figure 5.4: Hysteresis loops generated by the Bouc-Wen's model under sinusoidal excitation, (a) exponent values $\eta = 1$, 5 and 25 ($\gamma = 0.9$, $\beta = 0.1$, $\alpha = 0.05$, $H = 1$, $\Delta_y = 0.005$m), (b) hysteretic model used in this study ($\eta = 25$, $\gamma = 0.9$, $\beta = 0.1$, $\alpha = 0.02$, $H = 1$).

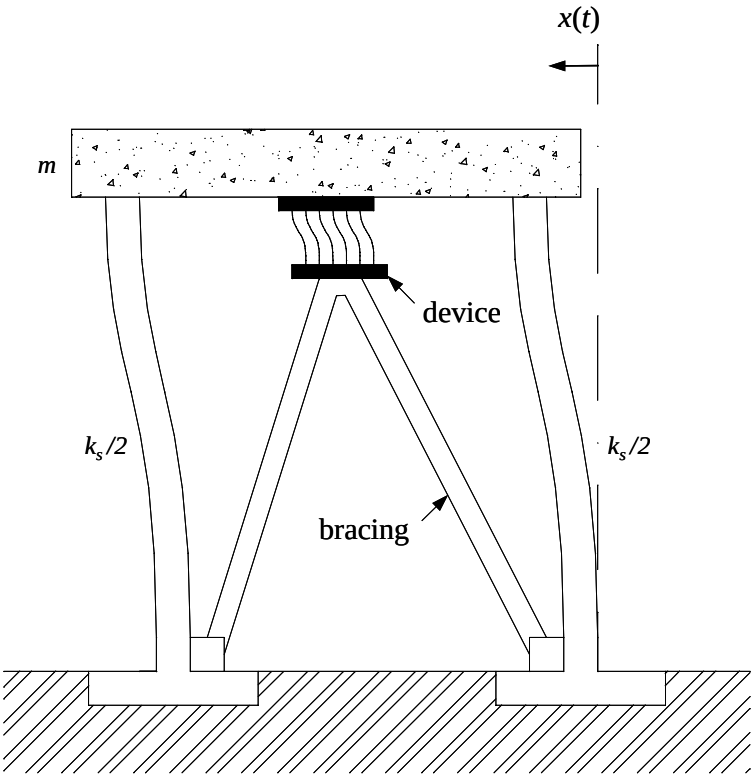

Figure 5.5: Idealized building structure with supplemental yielding metallic element.

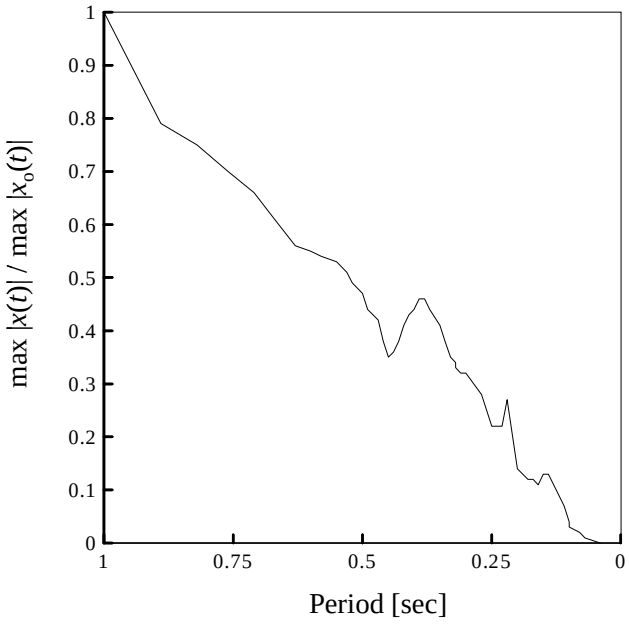

(a)

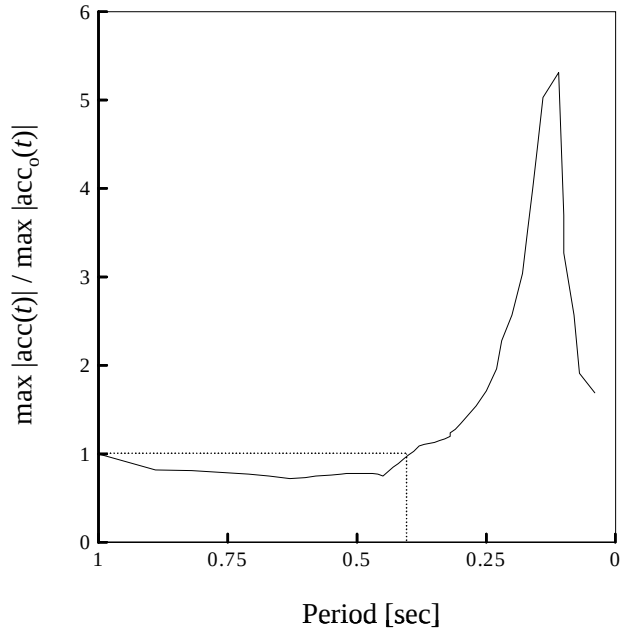

(b)

Figure 5.6: Peak response ratios obtained as a function of the period for a SDOF building model with a yielding metallic element when subjected to the San Fernando earthquake, (a) maximum displacement ratio, (b) maximum absolute acceleration ratio.

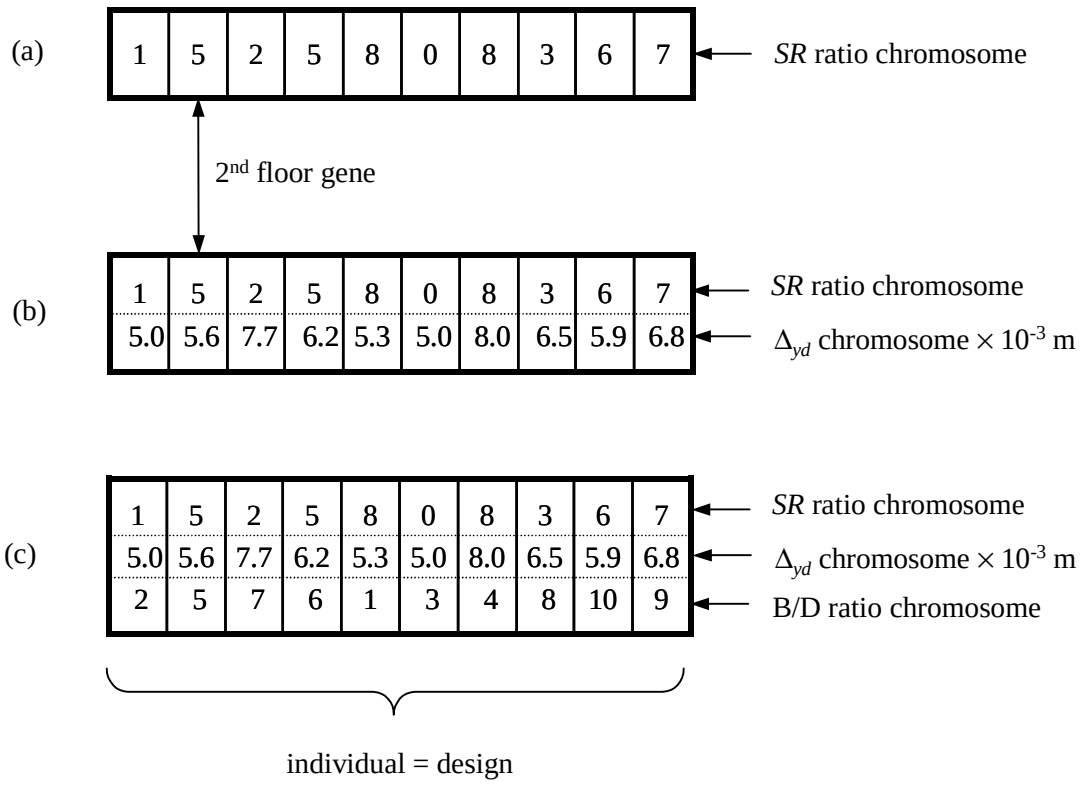

Figure 5.7: Discrete representation of design variables used in this study, (a) *SR* stiffness ratio chromosome, (b) *SR* stiffness ratio and device yield displacement Δ_{yd} chromosomes, (c) *SR* stiffness ratio, device yield displacement Δ_{yd} and B/D stiffness ratio chromosomes.

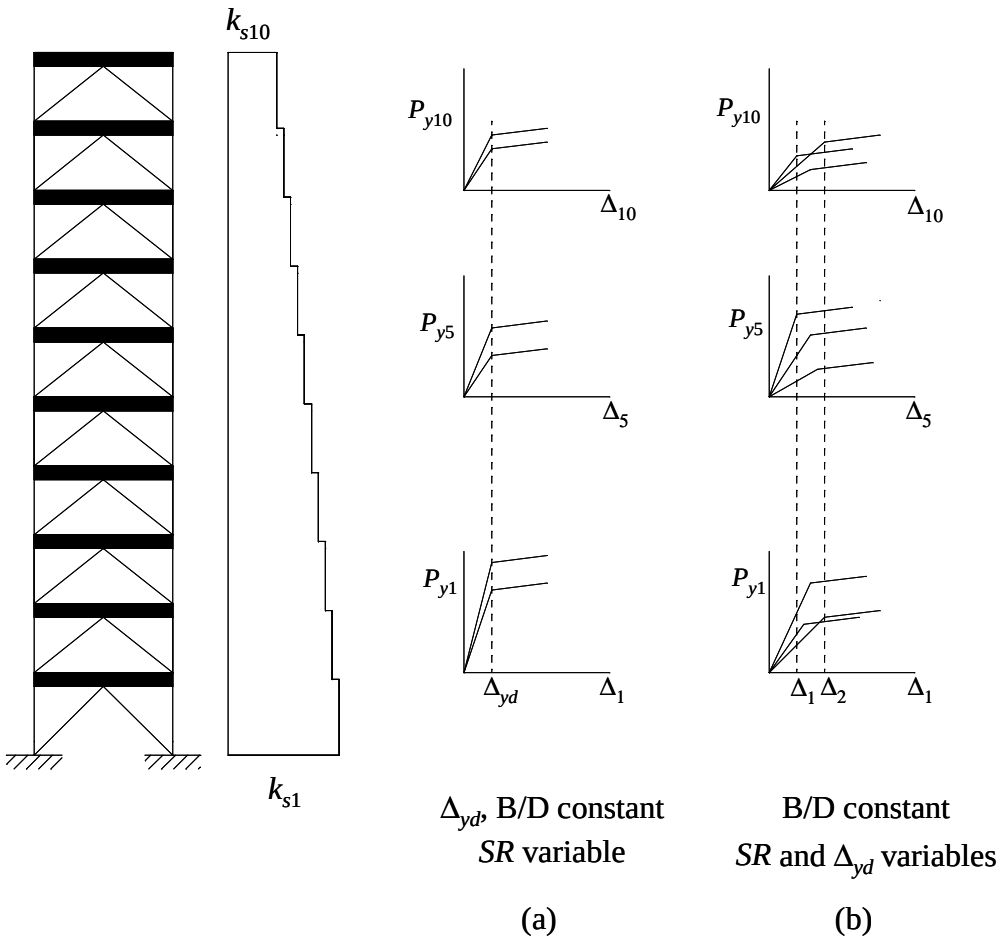

Figure 5.8: Possible combinations of the design variables of yielding metallic elements at different stories, (a) constant yield displacement of the device Δ_{yd} and constant stiffness ratio B/D, (b) constant stiffness ratio B/D.

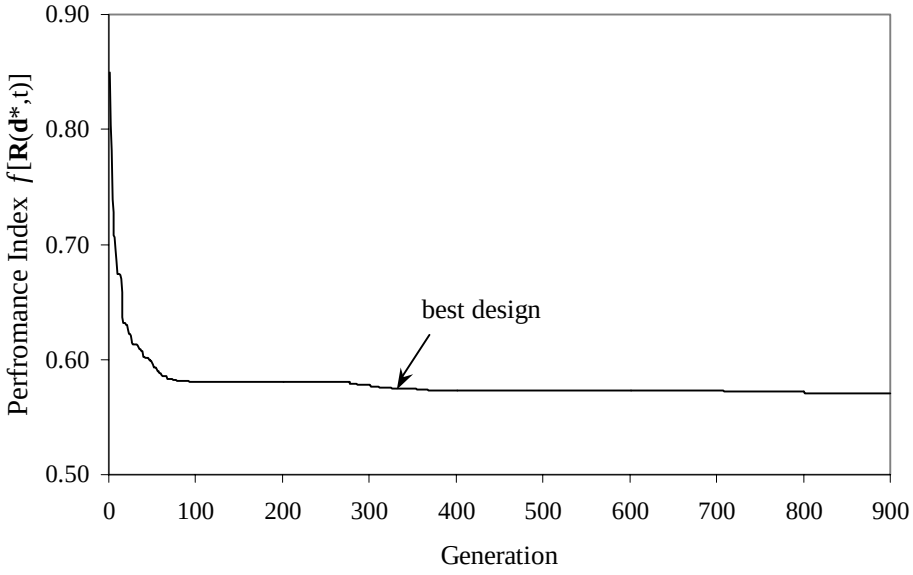

Figure 5.9: Optimization history for performance index of Eq. (5.18) using genetic algorithm.

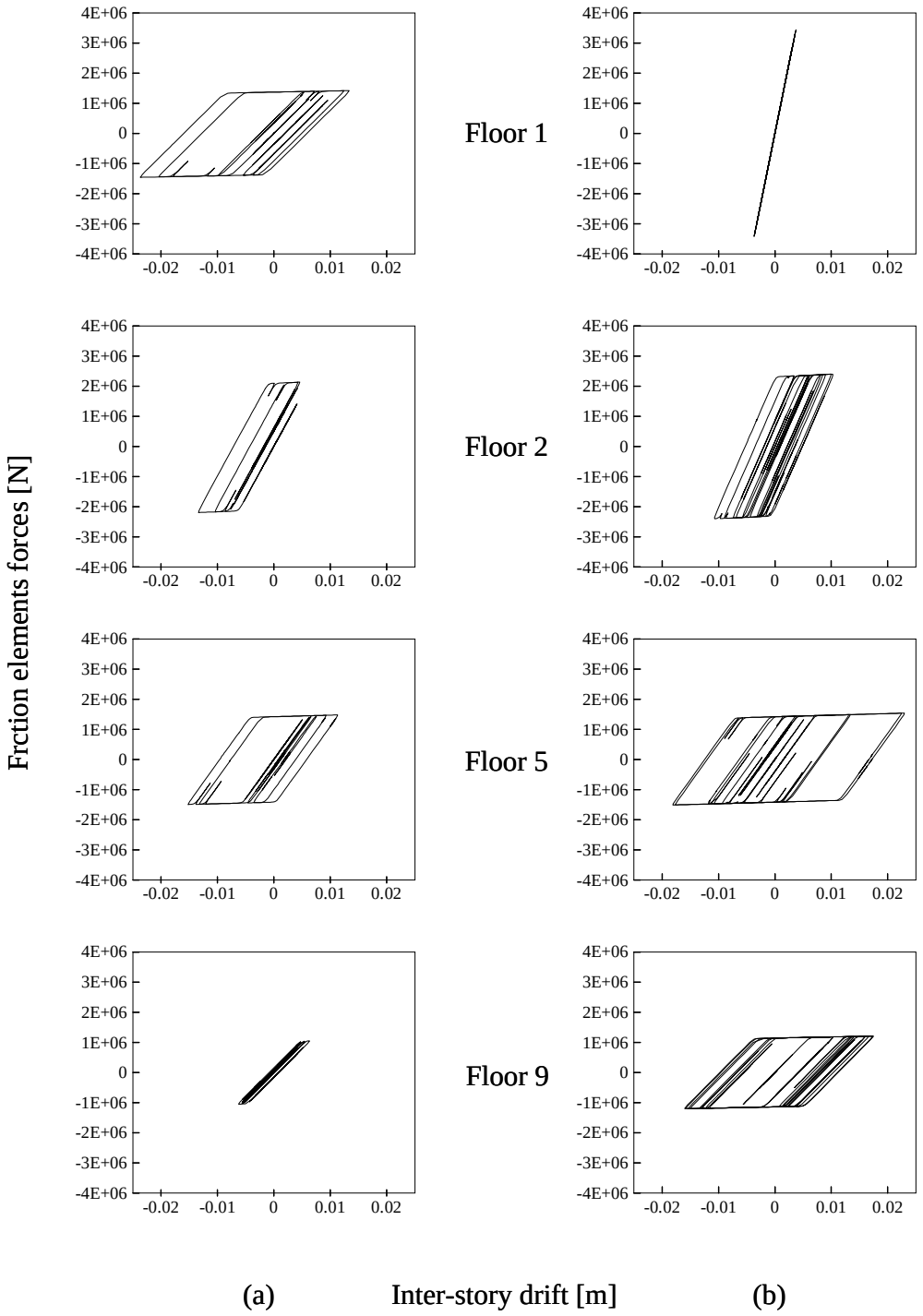

Figure 5.10: Comparison of force-deformation responses for metallic elements, (a) response performance index of Eq. (5.18) [Columns (7) to (10) of Table 5.2], (b) energy performance index of Eq. (5.26) [Columns (7) to (10) of Table 5.3].

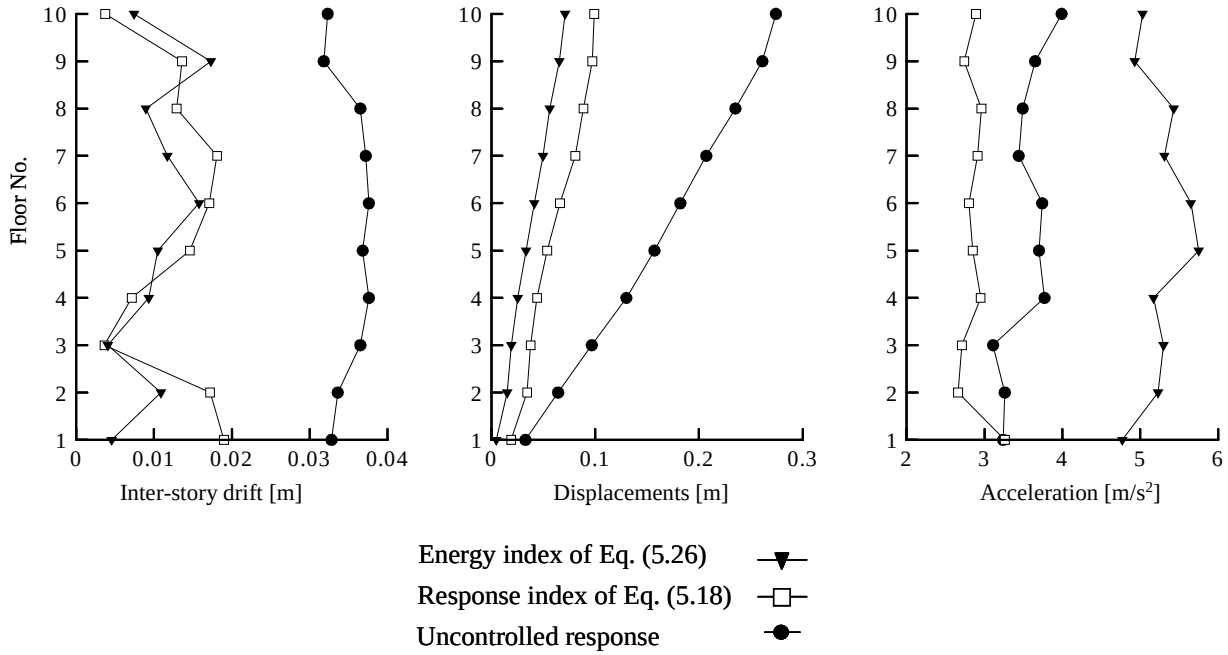

Figure 5.11: Comparison of maximum response quantities along the building height averaged over the four artificially generated accelerations records for distributions of damper parameters obtained according to different performance indices.

Chapter 6

Friction Devices

6.1 Introduction

Chapters 3 and 4 presented the optimal design of fluid and solid viscoelastic devices for seismic protection of building structures. Their cyclic response was characterized by linear velocity dependent mechanical models. Chapter 5, on the other hand, considered the design of metallic devices with highly nonlinear displacement dependent force-deformation response. Friction devices, the subject of study of this chapter, exhibit a hysteretic behavior similar to the one displayed by the metallic devices. These devices rely on the resistance developed between moving solid interfaces to dissipate a substantial amount of the input energy in the form of heat. During severe seismic excitations, the friction device slips at a predetermined load, providing the desired energy dissipation by friction while at the same time shifting the structural fundamental mode away from the earthquake resonant frequencies. Friction dampers are not susceptible to thermal effects, have a reliable performance and posses a stable hysteretic behavior. Figure 6.1 shows a schematic representation of typical friction devices for seismic structural applications.

Regardless of the fact that metallic yielding elements and friction devices differ in the principles used to extract vibration energy from a structure, they share similar design characteristics. The maximum force developed in the friction and yielding damper is controlled respectively by the design slip-load and yield load plus strain hardening. Virtually any desired combination of limiting loads and maximum displacements is feasible. However, by considering high limiting loads the energy dissipated (area under the force-deformation curve) will be

minimal since there will be no incursion of the devices into their slippage or inelastic ranges. In this case, the structure will behave as a braced frame. If the limiting loads are low, large incursion in the inelastic and slippage phases will be expected but again the amount of energy will be negligible.

From the above discussion, it is clear that the optimal design of friction devices poses challenges similar to the ones encountered in the design of yielding metallic elements. Therefore, the design of friction devices is done in this study following the same design procedure presented in the previous chapter. In Section 6.2, the mechanical properties governing the behavior of friction devices are identified. A continuous Bouc-Wen's model is then used to estimate the cyclic response of the friction element. After a hysteretic model is validated, it is incorporated for the numerical analysis of the overall structural system. Section 6.3 presents the details of such implementation. Finally, the optimal design of friction-damped structures is considered in Section 6.4. The seismic structural performance enhancement achieved with the incorporation of friction devices is measured using different performance indices. A genetic algorithm optimization procedure is then employed for the determination of the design parameters of the devices.

6.2 Analytical Modeling of Friction Devices

The cyclic force-deformation response of friction devices is characterized by rectangular hysteresis loops. This behavior has been represented in practice by rigid-perfectly-plastic models, as shown in Figure 6.2(a). The threshold force at which the device starts to deform continuously is called the slip-load. The value of this parameter, denoted here as P_s, provides a complete definition of the idealized model of the device.

The above description is sufficient to portray the behavior of a friction damper in which the elements used to support and connect the device to the main structural members are considered as rigid. The flexibility of the bracings can also be introduced in the analysis. In the previous chapter, this was accomplished by considering the *SR* ratio between the stiffness k_{bd} of the device-brace assembly and the structural stiffness k_s. These relationships are rewritten here for convenience as:

$$SR = \frac{k_{bd}}{k_s}; \qquad k_{bd} = \frac{1}{\frac{1}{k_d} + \frac{1}{k_b}} \tag{6.1}$$

In the case of a friction element, the stiffness k_d of the device can be considered as infinitely large, i.e., $k_d \approx \infty$ [See Figure 6.2(a)], and the stiffness k_{bd} of the friction assemblage becomes the same as the stiffness k_b of the supporting bracing. That is,

$$k_{bd} = k_b; \qquad SR = \frac{k_b}{k_s} \tag{6.2}$$

As shown in Figure 6.2(b), the slip-load can then be related to the deformation Δ_y experienced by the device-brace assembly as

$$P_s = k_{bd}\, \Delta_y = k_b\, \Delta_y \tag{6.3}$$

For design purposes, this equation can be expressed in terms of the stiffness parameter *SR*. Consideration of Eq. (6.2) in Eq. (6.3) leads to:

$$P_s = SR\, k_s\, \Delta_y \tag{6.4}$$

Equation (6.4) is the basic expression relating the mechanical parameters of a friction element. From this equation, it can be observed that the behavior of a friction element is governed by the slip load P_s, the stiffness ratio *SR*, and the displacement of the bracing Δ_y at which the device starts to slip. However, only two of these variables are independent since the third one can be determined from Eq. (6.4).

The hysteretic behavior of the friction element can also be characterized using a continuous Bouc-Wen's model. Recognizing the absence of any post-yielding or strain-hardening effect, the force $P(t)$ developed in a friction element can be obtained as [See Eqs. (5.6) and (5.7)]:

$$P(t) = k_0\, \Delta_y\, h(t) \tag{6.5}$$

$$\Delta_y\, \dot{h}(t) - H\, \dot{\Delta}(t) + \gamma \left|\dot{\Delta}(t)\right| h(t) \left|h(t)\right|^{\eta-1} + \beta\, \dot{\Delta}(t) \left|h(t)\right|^{\eta} = 0 \tag{6.6}$$

The model parameters H, γ, β and η are adjusted to approximate the shape of the hysteresis loops. A value of $\eta = 2$, with $H = 1$ and $\gamma + \beta = 1$ ($\beta = 0.1$, $\gamma = 0.9$) have been proposed in the literature to produce loops of frictional forces versus sliding displacements that are in good

agreement with experimental results [31; 147]. For these parameters values, Figure 6.3(a) shows the hysteresis loop generated by the Bouc-Wen's model for different combinations of excitation frequencies and amplitudes. If the flexibility of the bracing is included in the analysis, the hysteretic loop of the friction assemblage is better approximated by using an exponent coefficient $\eta = 25$, as shown in Figure 6.3(b). The remaining model parameters, k_0 and Δ_y, can be related to the mechanical properties of the friction element. This can be done by considering that at the slipping condition, the hysteretic variable $h(t)$ takes values of ±1, and the friction element force $P(t)$ is equal to the slip-load P_s. Thus, by considering Eq. (6.3) and (6.5) it can be easily shown that

$$k_0 = SR\,k_s; \qquad \Delta_y = \frac{P_s}{SR\,k_s} \tag{6.7}$$

6.3 Response Calculations

The equations of motion for a plane shear building presented in the previous chapter with a single device per story, are rewritten here for convenience as,

$$\mathbf{M}\,\ddot{\mathbf{x}}(t) + \mathbf{C}_s\,\dot{\mathbf{x}}(t) + \mathbf{K}_s\,\mathbf{x}(t) + \sum_{d=1}^{n_l} \mathbf{r}_d\,P_d(t) = -\mathbf{M}\,\mathbf{E}\,\ddot{X}_g(t) \tag{6.8}$$

If the force $P_d(t)$ exerted by the d^{th} damper element on the structure is characterized by a continuous hysteretic Bouc-Wen' s model, it can be expressed as:

$$P_d(t) = SR_d\,k_s^d\,\Delta_y^d\,h_d(t) \tag{6.9}$$

$$\Delta_y^d\,\dot{h}_d(t) - \dot{\Delta}_d(t) + \gamma\left|\dot{\Delta}_d\right| h_d(t)\left|h_d(t)\right|^{\eta-1} + \beta\,\dot{\Delta}_d\left|h_d(t)\right|^{\eta} = 0 \tag{6.10}$$

where Δ_y^d is the displacement at which slipping begins in the d^{th} device-brace assembly, and k_s^d denotes the stiffness of the story in which the element is located. In designing friction elements, it may be more convenient to express Eqs. (6.9) and (6.10) in terms of the slip-load $P_s^{\,d}$. Thus, these equations can be rewritten by considering the relations given in Eqs. (6.7), as:

$$P_d(t) = P_s^d\,h_d(t) \tag{6.11}$$

$$P_s^d\,\dot{h}_d(t) - SR_d\,k_s^d\left[\,\dot{\Delta}_d(t) - \gamma\left|\dot{\Delta}_d\right| h_d(t)\left|h_d(t)\right|^{\eta-1} - \beta\,\dot{\Delta}_d\left|h_d(t)\right|^{\eta}\right] = 0 \tag{6.12}$$

Combining the expressions (5.10) and (5.11) for the element forces with the equations of motion

(5.9), the complete set of equations of motion of the resulting structural system takes the form:

$$\begin{aligned} &\mathbf{M}\,\ddot{\mathbf{x}}(t)+\mathbf{C}_s\,\dot{\mathbf{x}}(t)+\mathbf{K}_s\mathbf{x}(t)+\sum_{d=1}^{n_l}\mathbf{r}_d\,P_s^d\,h_d(t)=-\mathbf{M}\,\mathbf{E}\,\ddot{X}_g(t) \\ &P_s^d\,\dot{h}_d(t)-SR_d\,k_s^d\left[\mathbf{r}_d^T\dot{\mathbf{x}}(t)-\gamma\left|\mathbf{r}_d^T\dot{\mathbf{x}}(t)\right|h_d(t)\left|h_d(t)\right|^{\eta-1}-\beta\,\mathbf{r}_d^T\dot{\mathbf{x}}(t)\left|h_d(t)\right|^{\eta}\right]=0; \qquad d=1,\ldots,n_l \end{aligned} \tag{6.13}$$

The numerical integration of these equations can be conveniently done, as before, using a state-space formulation. The first-order differential equation of the system takes the form:

$$\begin{aligned} \ddot{\mathbf{x}}(t) &= -\mathbf{M}^{-1}\left[\mathbf{C}_s\,\dot{\mathbf{x}}(t)+\mathbf{K}_s\,\mathbf{x}(t)+\sum_{d=1}^{n_l}\mathbf{r}_d\,P_s^d\,h_d(t)\right]-\mathbf{E}\,\ddot{X}_g(t) \\ \dot{\mathbf{x}}(t) &= \dot{\mathbf{x}}(t) \\ \dot{h}_d(t) &= \frac{SR_d\,k_s^d}{P_s^d}\left[\mathbf{r}_d^T\dot{\mathbf{x}}(t)-\gamma\left|\mathbf{r}_d^T\dot{\mathbf{x}}(t)\right|h_d(t)\left|h_d(t)\right|^{\eta-1}-\beta\,\mathbf{r}_d^T\dot{\mathbf{x}}(t)\left|h_d(t)\right|^{\eta}\right]; \qquad d=1,\ldots,n_l \end{aligned} \tag{6.14}$$

As in Chapter 5, the solver LSODA from the ODEPACK package is implemented for the numerical integration of Eqs. (6.14). This solver has the capability to automatically choose the appropriate method of integration depending on the characteristic of the differential equations.

6.4 Numerical Results

As mentioned at the beginning of this chapter, the design of friction devices can be done following a procedure similar to the one previously presented for the design of yielding metallic devices. It is assumed that a single device is placed at each location. The mechanical properties of the friction elements are then determined using a genetic algorithm optimization procedure according to a specified performance index.

For illustration purposes, the seismic rehabilitation of the ten-story shear Building 2 is considered next. The seismic motions used in Chapter 5 have also been used in this chapter.

In Section 6.2, the parameters governing the behavior of the friction dampers were identified to be: the slip-loads P_s^d and stiffness ratios SR_d. A number of simplified procedures and design guidelines have been proposed in the literature for the determination of these parameters. In general, these design methodologies are based on the results of extensive parametric analysis [28; 51; 136]. In one of these studies, Filiatrault and Cherry [49] assumed that all the friction devices placed at different building locations were designed to slip at the same threshold load $P_s^d = P_s$. Also in their study, the same diagonal braces were used in each

story to support the devices. Under these assumptions, schematically represented in Figure 6.4(a), the design problem reduced to the determination of a single parameter, the slip-load P_s. A series of time-history analyses were then carried out for different levels of slip-load, and the optimum value of P_s was selected as the one that minimized a relative performance index *RPI* index, defined as:

$$RPI = \frac{1}{2}\left(\frac{SEA}{SEA_{(o)}} + \frac{U_{\max}}{U_{\max(o)}} \right) \tag{6.15}$$

where *SEA* and $U_{\max}$ are, respectively, the area under the elastic strain-energy time history and the maximum strain energy for a friction-damped structure; $SEA_{(o)}$ and $U_{\max(o)}$ are the respective quantities of the original uncontrolled structure. The selection of this performance index was motivated by the direct relation that exists between the amount of elastic strain energy imparted into a building and the resulting structural response.

In the design methodology presented above, the number of design variables has been reduced under the assumption of uniform distribution of slip-loads and bracing elements over the height of the structure, and the optimal slip-load is then determined by direct enumeration analyses. These assumptions have been motivated by the "very little benefit obtained from the use of other possible optimum solutions when compared with the use of the simpler uniform slip-load distribution" [49]. Herein, the validity of this statement is investigated next.

In what follows, the friction devices are designed with the same assumptions as made by Filiatrault and Cherry. The stiffnesses of the supporting bracings are assumed proportional to those of the main structural frame and a value of $SR_d = 2$ is adopted for the numerical calculations. The friction-damped structure is then subjected to the set of four artificially generated earthquakes compatible with the power spectral density function of the 1971 San Fernando earthquake. For each earthquake, the value of the slip-load P_s is varied using increments of $P_s/W = 0.005$, where W is the total building weight. The *RPI* index of Eq. (6.15) is then evaluated for each nonlinear time history response analysis. The value of slip-load P_s that minimizes this *RPI* index, averaged over the four earthquakes, is presented in Column (2) of Table 6.1. These results are expressed as percentages of the total building weight. Figure 6.5

presents the results of the uniform slip-load optimization study, in which a total of 25 load increments have been used. The same final result is obtained by the genetic algorithm.

Next, the same design problem is solved considering the slip-load at each d^{th} location as an independent variable, denoted here as P_s^d. Therefore, the assumption of uniform slip-load distribution is removed, and the genetic algorithm is used to find the optimal design solution. For a proper implementation of this search procedure, the slip-load design space has to be discretized. In this regard, the same load interval and load increment used in the previous design example are adapted for the numerical calculations. That is, the slip-load ratio P_s^d/W can take on any multiple value of 0.005 between 0.0 and 0.125W, with zero corresponding to the situation of no device. This discretization scheme leads to twenty-six possible values of slip-load for each floor, and a total of 26^{10} possible combinations for the devices loads P_s^d. To make the solutions obtained by the simplified approach and the genetic algorithm comparable, a constraint is added to the optimization problem such that the same total friction load is distributed in both cases along the building height. The improvement in the seismic structural performance is measured, as before, by the minimization of the *RPI* index. Column (3) of Table 6.1 presents the slip-load distribution obtained using the genetic algorithm approach averaged over the four earthquakes. These results have been obtained for a population of 20 individuals after 500 generations. The additional input parameter for the optimization runs are as follows: probability of crossover p_c = 0.9, and probability of slip-load mutation = 0.03. It can be noticed from the last row of Table 6.1 that for the same amount of total friction force, the slip-load distribution obtained using the genetic algorithm further reduces the *RPI* index value by an almost 13%.

The design of the previous friction-damped structure is repeated here adding a second variable per device. In this case, the parameter SR_d is set free and able to take on any integer value ranging from 1 to 10. The genetic algorithm is then used to search for the best design solution. Since the number of possible combinations has increased, a larger population of 30 individuals has been considered for the numerical calculations. The parameters of the optimization algorithm have been taken as follows: probability of crossover p_c = 0.9, probability of slip-load mutation p_{mPs} = 0.15, and probability of *SR* ratio mutation p_{mSR} = 015. Columns (4) and (5) of Table 6.1 show, respectively, the values of the slip-loads P_s^d and stiffness ratios SR_d

for each story. These results have been obtained after 700 generations. Although the same total friction load is used, the *RPI* index is further reduced by a 60%. Such dramatic improvement in the seismic performance of the structural system can be attributed to the additional stiffness contributed by the friction elements, and to a better utilization of their energy dissipation capabilities. Figure 6.6 compares the force-deformation responses of the friction elements located at different building stories when the structure is subjected to the San Fernando earthquake. For the uniform slip-load distribution solution, shown in Figure 6.6(a), the devices located at the upper stories are not slipping and consequently do not extract any energy from the system. On the other hand, Figure 6.6(b) presents the friction hysteresis loops corresponding to the design solution of Columns (4) and (5) of Table 6.1 obtained using the genetic algorithm optimization procedure. It can be observed that for this distribution, all the friction elements are actively engaged in the energy dissipation mechanism.

Figure 6.7 investigates the reduction achieved in the maximum inter-story drifts, displacements and absolute accelerations for the original building and the friction-damped structure designed using the uniform slip-load distribution and the design solution obtained by the genetic algorithm. These quantities have been obtained by averaging the responses obtained for the simulated acceleration records. Figure 6.8(a) shows the time histories of the top floor displacement for the controlled and uncontrolled cases for the actual San Fernando earthquake, whereas Figure 6.8(b) presents a similar comparison for the drift experienced at the first story. As evidenced from the design solutions presented above, the friction dampers reduce the structural response through a combination of improved energy dissipation capabilities and increased lateral stiffness of the building. However, as mentioned in the previous chapter, the presence of additional stiffness may also induce larger floor accelerations and structural members stresses. Therefore, it may be convenient to design the friction-damped building structure according to the performance index of Eq. (5.18) defined in Chapter 5. This index is intended to reduce both the maximum floor accelerations and inter-story drifts. It has been expressed as:

$$f\left[\mathbf{R}(\mathbf{d},t)\right]=\frac{1}{2}\left\{\frac{\max_i \Delta_i(t)}{\max_i \Delta_{i(o)}(t)}+\frac{\max_i\left[\ddot{x}_i(t)+\ddot{X}_g(t)\right]}{\max_i\left[\ddot{x}_{i(o)}+\ddot{X}_g(t)\right]}\right\} \tag{6.16}$$

The design of the friction-damped Building 2 is now repeated. The goal is to determine the slip-load and stiffness ratio distribution required to minimize the index of Eq. (6.16). As before, the slip-load P_s^d is considered first as the only design parameter per device. The bracings are designed proportional to the stiffness of the building stories in which the device is placed, and a value of $SR = 2$ is adopted for the numerical calculations. Columns (2) and (3) of Table 6.2 presents the results obtained under these conditions by the genetic algorithm optimization procedure. Columns (4) and (5) of the same table show the design solution obtained when the stiffness ratio of each device, SR_d, is included to the set of design variables. For this design solution, Figure 6.9 compares the maximum inter-story drifts, maximum displacements and maximum absolute accelerations obtained at different stories of the original and friction-damped structures. These responses have been averaged over the four simulated earthquakes. This figure also shows the corresponding maximum responses obtained for the structure designed using the slip-load distribution that minimized the *RPI* index. These responses quantities were previously presented in Figure 6.7. It can be observed from Figures 6.7 and 6.9 that the design solution obtained by minimizing the performance index of Eq. (6.16) provides comparable reductions in the maximum inter-story drifts and displacements, while reducing substantially the maximum accelerations at all building levels. Figure 6.10 shows the evolution of the best design in successive generations and the convergence characteristics of the genetic algorithm used in this study.

6.5 Chapter Summary

In this chapter, the design of a friction-damped structure subjected to seismic disturbances has been accomplished within the context of a structural optimization problem. For design purposes, the parameters governing the hysteretic behavior of the friction dampers were first identified. A continuous Bouc-Wen's model was then used to characterize the hysteretic behavior of the friction dampers. The convenience of this model is evidenced when the equations of motion of the overall structural system are cast as a set of first-order nonlinear differential for their efficient and accurate numerical integration. The characteristic presence of alternate peaks and valleys in the maximum earthquake response of the system called for an optimization procedure capable of

selecting the best design solution from a number of possible sub-optimal alternatives. A genetic algorithm was iemployed to cope with the aforementioned difficulty, as well as the avoidance of cumbersome gradients calculations. Numerical results were presented to illustrate the application of the proposed optimization methodology. Comparisons of the design solutions obtained by the genetic algorithm and a simplified design approach were also provided.

Table 6.1: Comparison of design solutions for friction devices obtained using a simplified design approach and a genetic algorithm optimization approach.

Story	Uniform Slip-Load P_s [%W]	Variable Slip-Load P_s^d [%W]	Slip-Load P_s^d and SR_d ratios	
			P_s^d [%W]	SR_d
(1)	(2)	(3)	(4)	(5)
1	3.25	5.30	5.9	9.75
2	3.25	4.50	4.9	9.25
3	3.25	3.80	4.6	8.75
4	3.25	3.60	3.8	7.25
5	3.25	3.00	3.4	9.50
6	3.25	2.40	2.9	9.25
7	3.25	2.40	2.5	9.50
8	3.25	2.10	2.1	9.00
9	3.25	2.10	1.5	9.00
10	3.25	3.40	1.0	8.00
Total load	32.5	32.5	32.5	
RPI	0.2681	0.2347	0.1060	

Note: the results of Columns (2) and (3) have been obtained for a stiffness ratio $SR = 2$.

Table 6.2: Optimal design of friction devices according to the performance index of Eq. (6.16).

Story	Slip-Load P_s^d		Slip-Load P_s^d and SR_d	
	SR_d	P_s^d [%W]	SR_d	P_s^d [%W]
(1)	(2)	(3)	(4)	(5)
1	2.0	1.6	5.50	3.5
2	2.0	3.6	3.00	3.8
3	2.0	3.1	7.25	4.3
4	2.0	2.6	7.25	4.5
5	2.0	2.1	7.50	2.5
6	2.0	2.0	6.25	2.5
7	2.0	2.4	6.00	3.5
8	2.0	2.1	4.75	3.8
9	2.0	1.1	7.75	2.8
10	2.0	0.8	5.50	2.5
$f[\mathbf{R}(\mathbf{d}^*,t)]$	0.5226		0.4617	

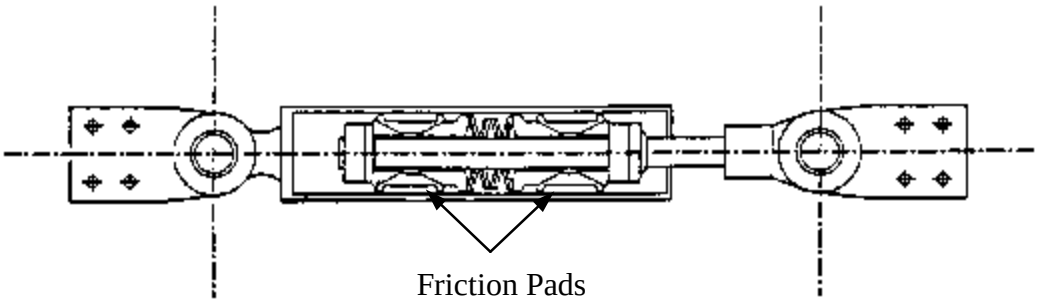

(a)

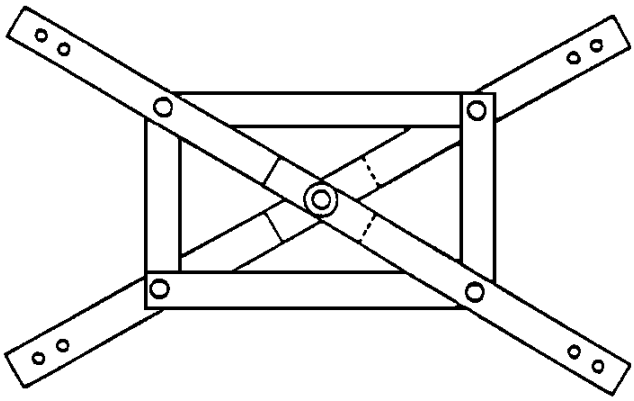

(b)

Figure 6.1: Typical friction devices for seismic structural applications, (a) Sumitomo friction damper, (b) Pall friction device.

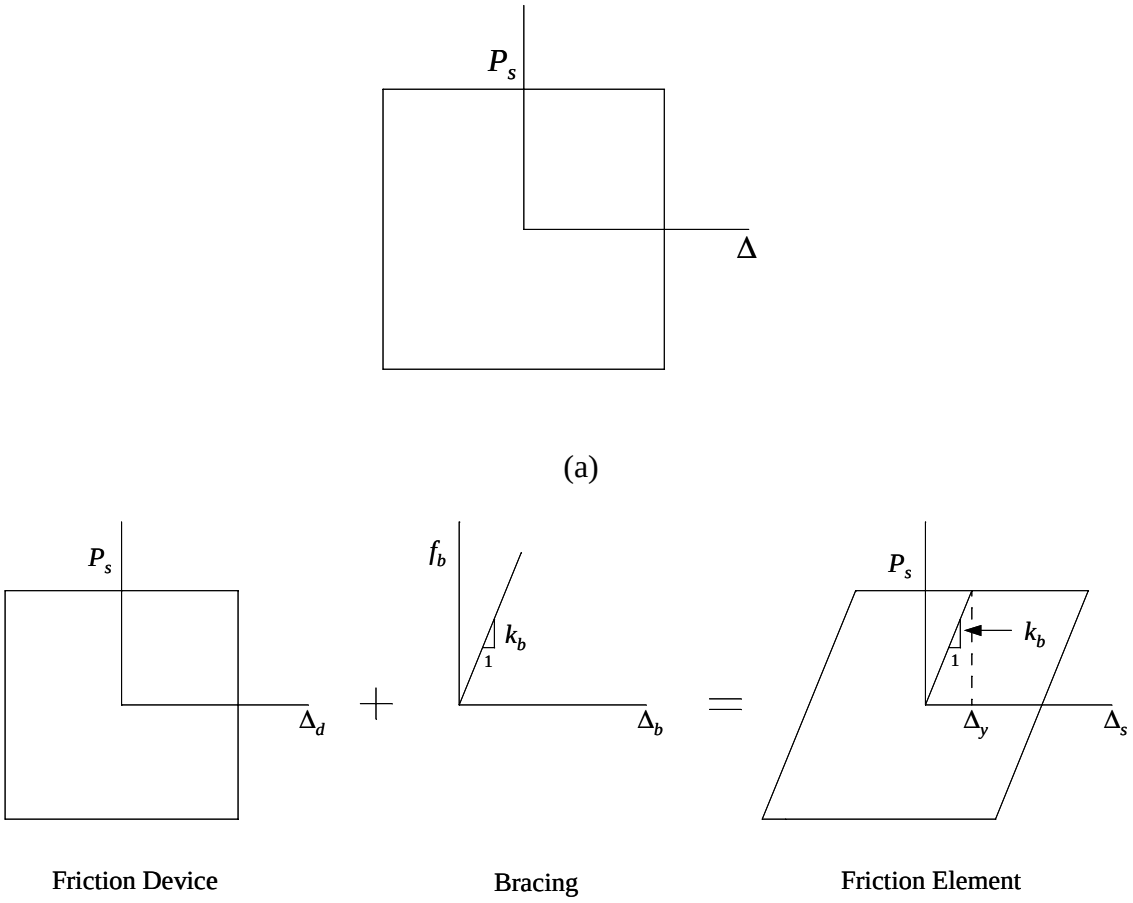

Figure 6.2: Idealized hysteretic behavior of friction dampers, (a) friction device on rigid bracing, (b) friction device mounted on flexible support.

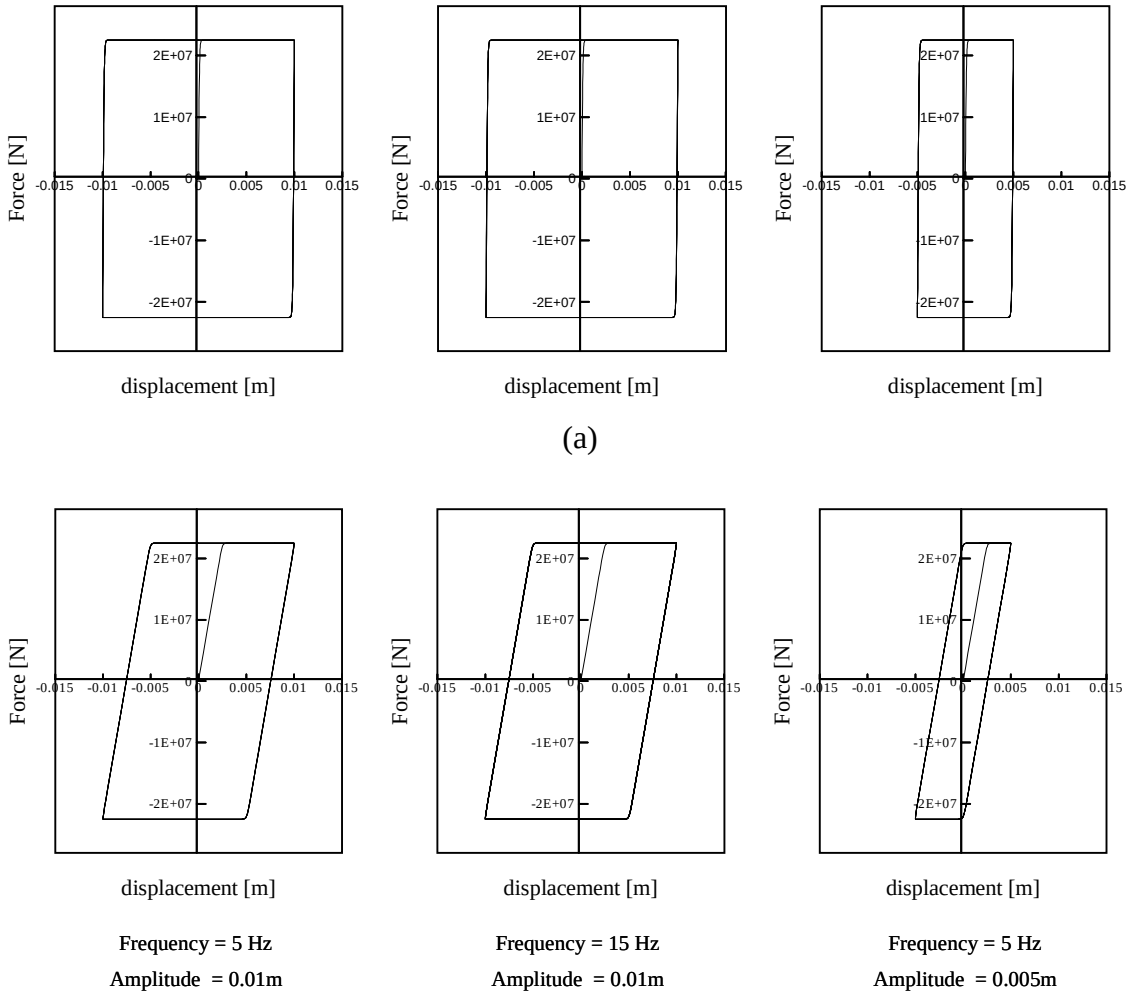

Figure 6.3: Hysteresis loops generated by the Bouc-Wen's model under sinusoidal excitation for different values of frequency excitation and deformation amplitudes, (a) rigid bracings, (γ=0.9, β=0.1, η=2, H=1), (b) flexible bracings (γ=0.9, β=0.1, η=25, H=1).

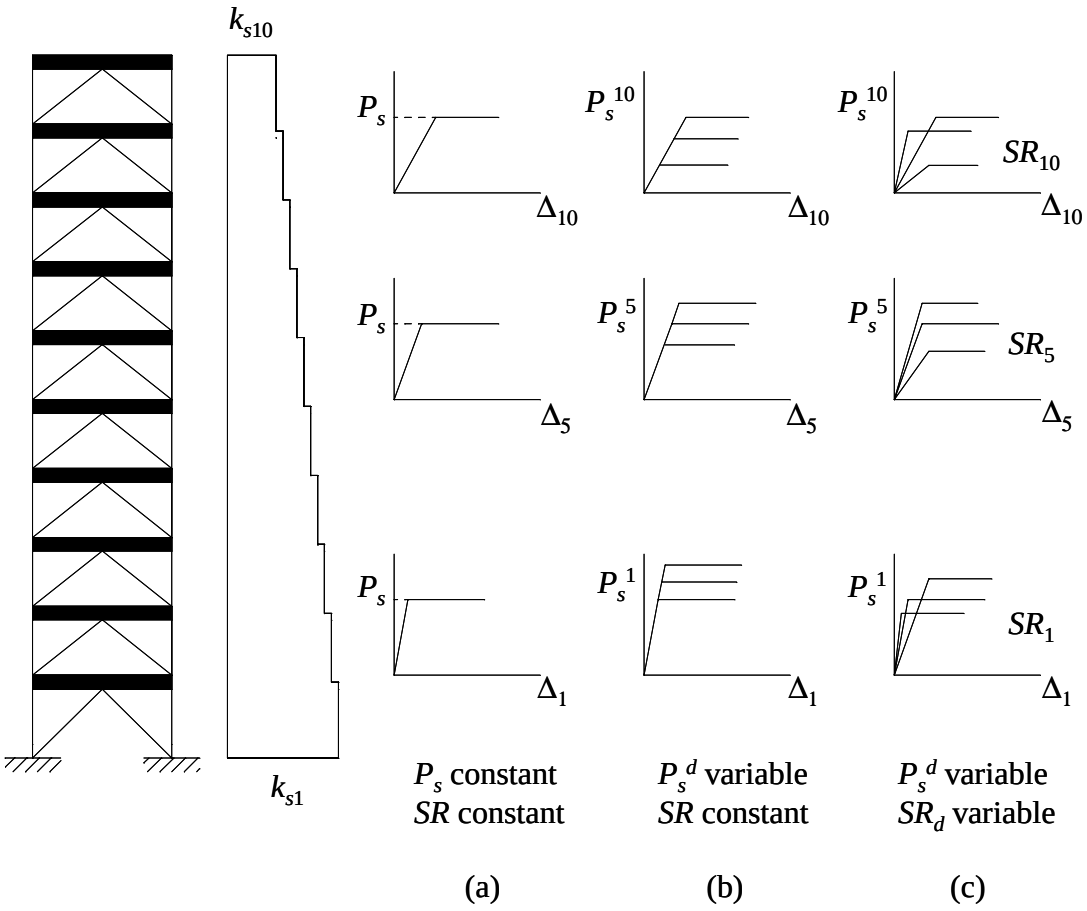

Figure 6.4: Possible combinations of design parameters of the friction device-assemblages at different stories, (a) uniform distribution of slip-load P_s and stiffness ratio SR, (b) constant stiffness ratio SR and variable slip-load P_s^d, (c) variables slip-load P_s^d and stiffness ratio SR_d.

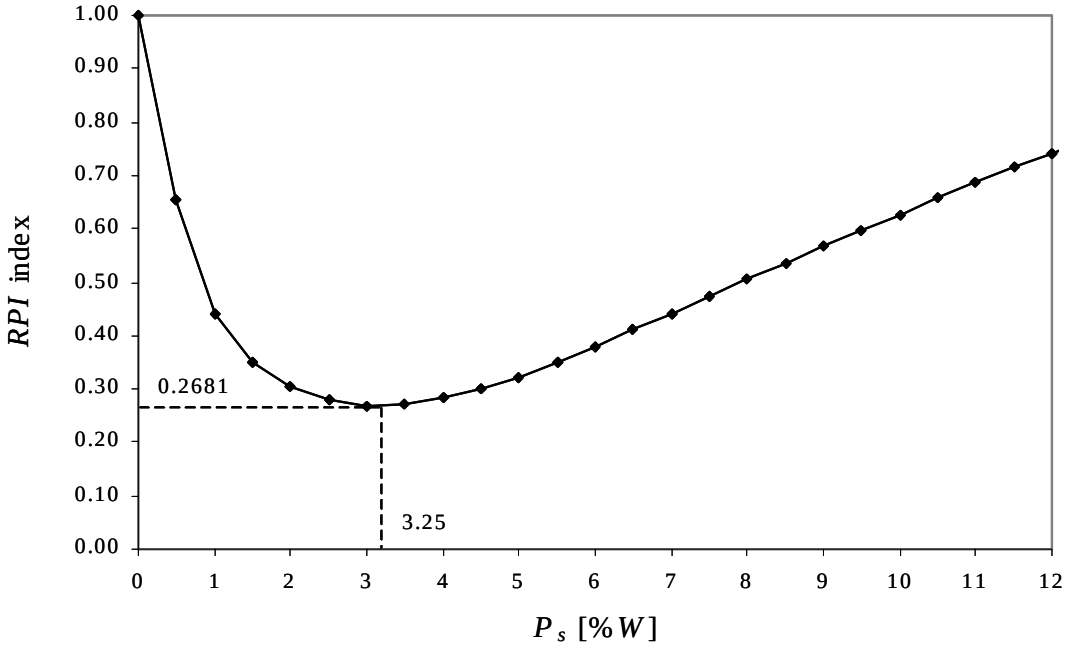

Figure 6.5: Optimum slip-load study for uniform distribution.

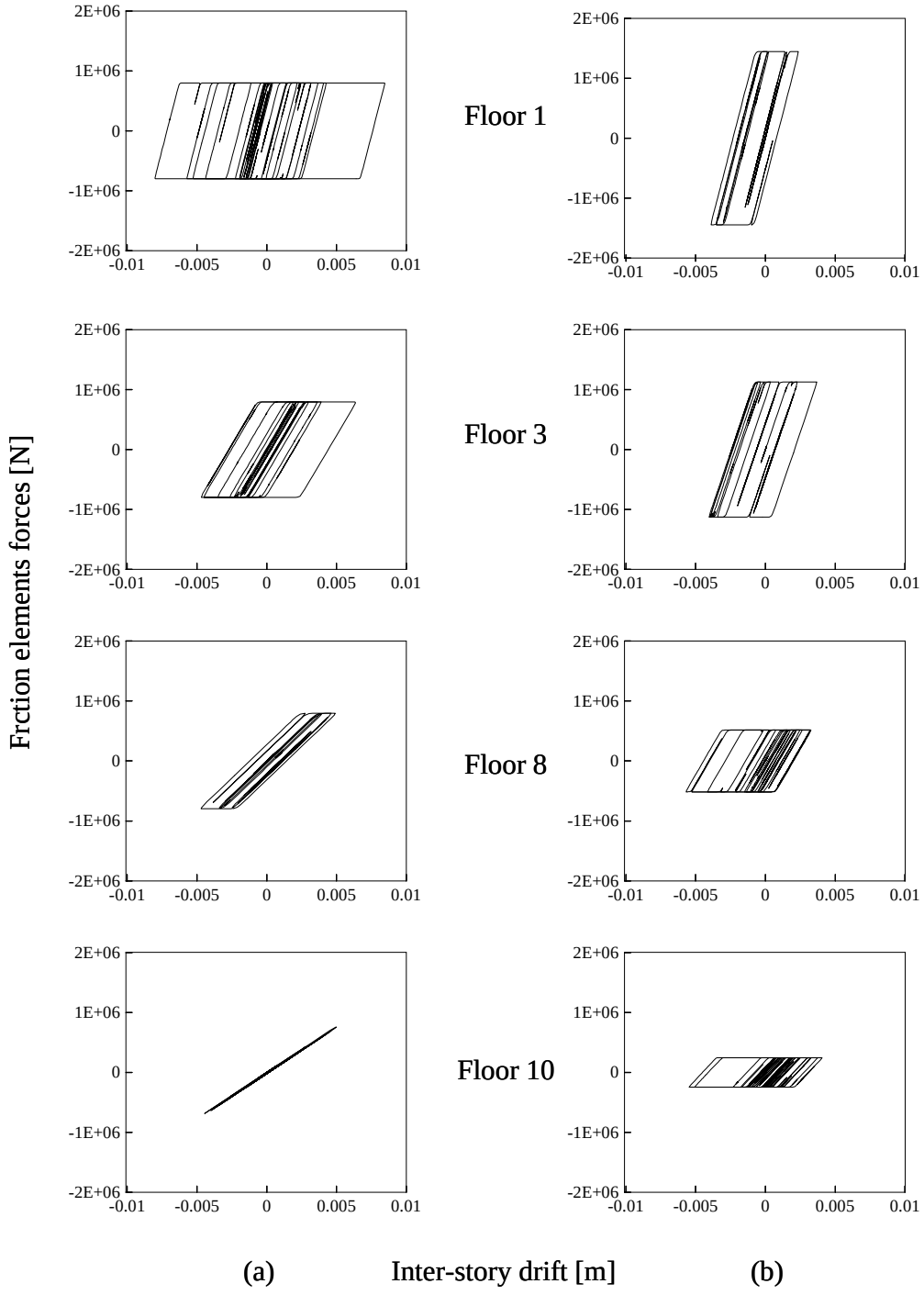

Figure 6.6: Comparison of force-deformation responses for friction elements obtained for the San Fernando earthquake, (a) uniform slip-load distribution, (b) genetic algorithm slip-load distribution.

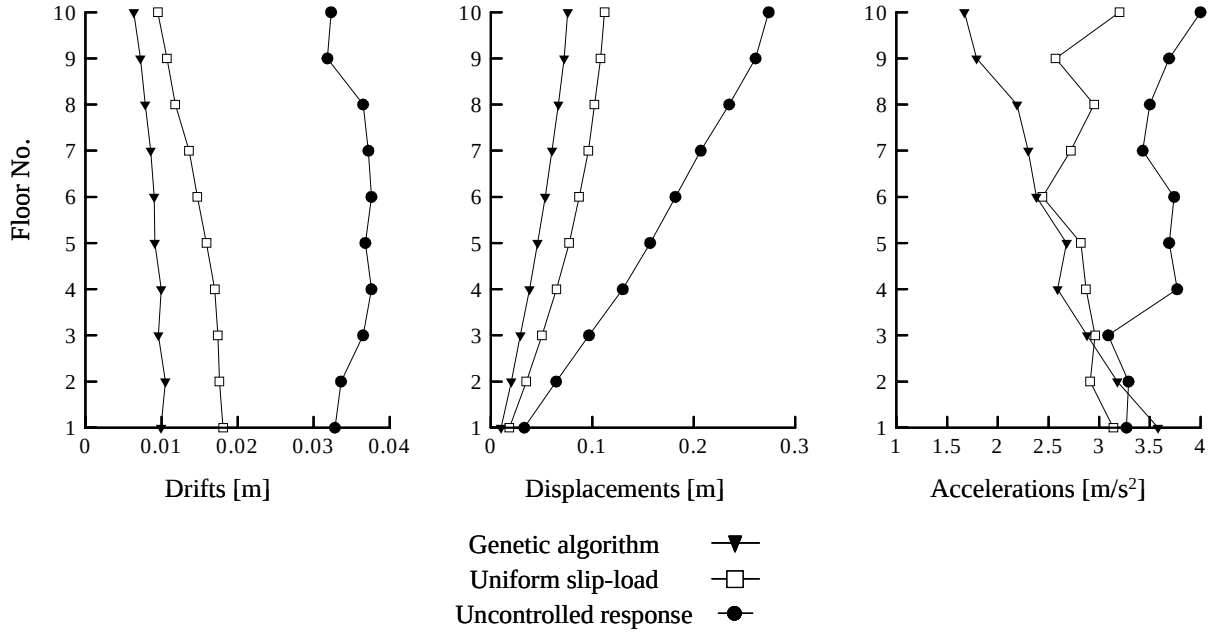

Figure 6.7: Comparison of maximum response quantities along the building height averaged over the four artificially generated accelerograms for distributions of damper parameters obtained by different approaches (*RPI* index of Eq. 6.15).

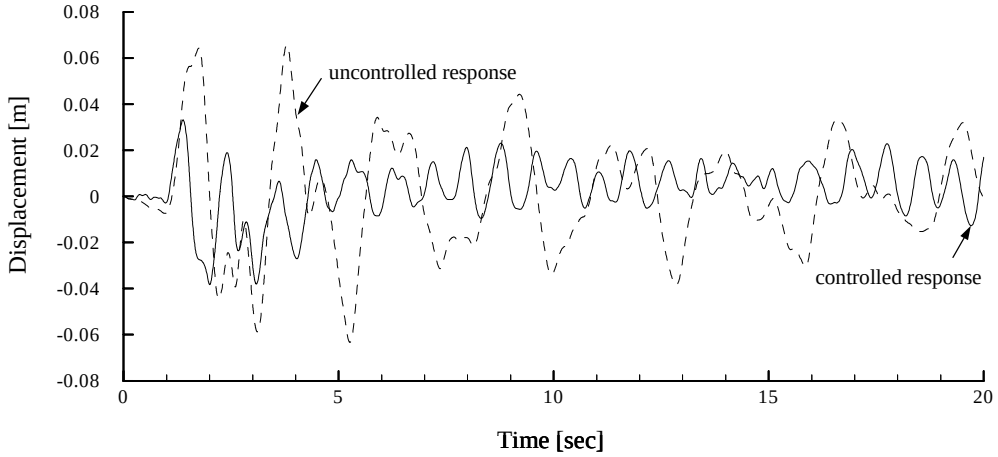

(a)

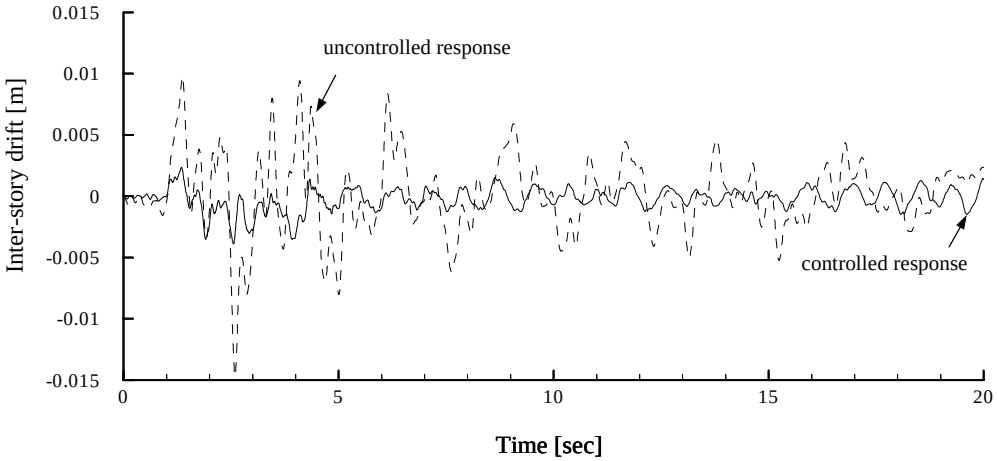

(b)

Figure 6.8: Comparison of uncontrolled and controlled responses for the San Fernando acceleration record, (a) top floor displacement, (b) 1st story drift.

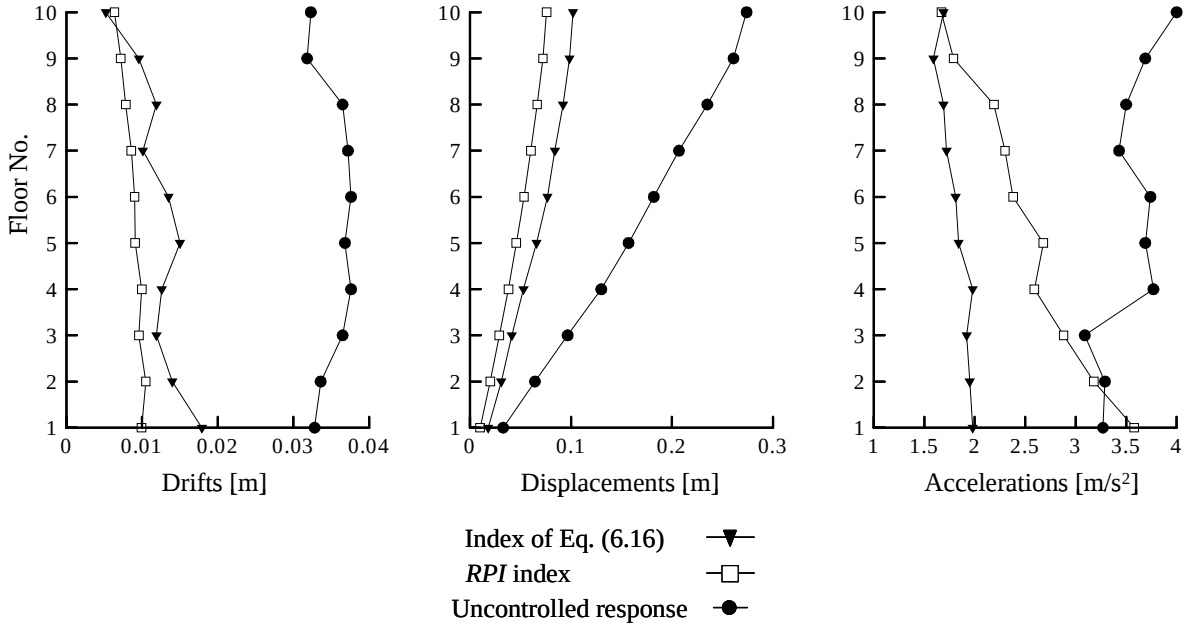

Figure 6.9: Comparison of maximum response quantities along the building height averaged over the four artificially generated accelerograms for distributions of damper parameters obtained using different performance indices.

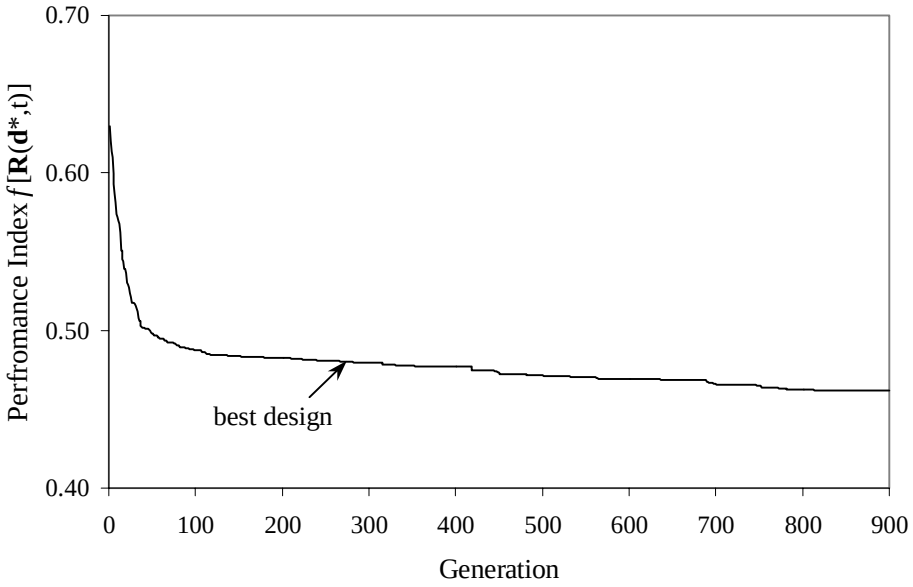

Figure 6.10: Optimization history for maximum response reduction using genetic algorithm.

Chapter 7

Summary, Conclusions and Future Work

7.1 Summary

The supplementary energy dissipation devices are known to be effective in reducing the earthquake-induced response of structural systems. Optimal sizing and placement of these protective systems is of practical interest. The main objective of this study, therefore, has been to formulate a general framework for the optimal design of passive energy dissipation devices for seismic structural applications. To accomplish this objective, the research activities involved the implementation of appropriate optimization strategies, the establishment of meaningful performance indices, and the development of accurate and efficient analytical and numerical techniques for seismic response calculations.

Among the different energy dissipation devices currently available, the fluid and solid viscoelastic devices, and the metallic yielding and friction hysteretic devices were selected in this study. An overview of the special characteristics of these dampers, along with the research issues relevant to their optimal use for seismic rehabilitation and structural performance enhancement were briefly introduced in Chapter 1.

The general formulation of the structural optimal design problem was presented in Chapter 2. Two different treatments of the optimal design problem have been contemplated. A gradient projection technique was presented for the optimal solution of problems in which the parameters of the damping devices can be considered as continuous. On the other hand, a genetic algorithm approach was presented for the solution of problems involving the placement

of a given number of devices with predetermined mechanical properties, or a discrete representation of the properties of the devices. This chapter also included a basic description of the structural building models and ground motion representation considered in this study. The main assumption made for the numerical and analytical developments of subsequent chapters has been that the addition of passive devices to the framing system allowed the main structural elements (beams and columns) to remain within their elastic range of action and free of damage under earthquake disturbances.

Chapters 3 and 4 were devoted to the optimal design of linear viscoelastically-damped building structures. The fluid viscoelastic devices, considered in Chapter 3, and the solid viscoelastic devices, studied in Chapter 4, were characterized by linear velocity dependent mechanical models consisting of various arrangements of linear springs and viscous dashpots. The concept of performance-based design of structures was introduced in Chapter 3. This methodology not only facilitated the determination of the level of damping or number of devices required to satisfy a stipulated design goal, but also provided the optimal distribution of the required amount of damping or number of devices within a building frame. The numerical procedures for calculation of the required response quantities and gradient information for search direction and sensitivities analysis were simplified from the assumed linear behavior of the structural system. A generalized modal based random vibration approach was developed for estimation of the maximum response quantities of the structural system. This technique permits the analysis of linear structures with overdamped modes and closely spaced frequencies, and is able to treat any linear structural system with arbitrary linear damping characteristics as long as it can be expressed as a set of first-order differential equations. An approach to evaluate the sensitivity of the optimum solution and the performance function was also described. Numerical results were presented to show the applicability and usefulness of the optimization approaches. The presented examples considered both continuous and discrete representation of the mechanical properties of the devices as well as different forms of performance indices and types of building structures. Comparisons of the design solutions obtained for the same problem using the gradient projection technique and the genetic algorithm approach were provided to evaluate the convergence characteristics of these optimization procedures.

Chapters 3 and 4 were dedicated to the optimal design of linear viscoelastically-damped structures. The linearity of the system response facilitated the analysis and subsequent application of the optimization procedures. The incorporation of devices with highly hysteretic behavior, on the other hand, introduced localized nonlinearities that rendered the response of the overall system as nonlinear. Consequently, a time domain method of analysis has to be implemented for the determination of the required response quantities. Chapter 5, dedicated to the optimal design of yielding metallic devices, presented the problems arising in the optimization process when considering time history analyses involving earthquake acceleration records. The presence of multiple local minima solutions and the cumbersome calculation of gradient information required in the gradient-based approach motivated the use of a genetic algorithm approach to solve the optimal design problem. The optimal design of friction devices, considered in Chapter 6, presented similar characteristics and design challenges. Therefore, these two chapters followed the same design approach. The mechanical parameters governing the behavior of the devices were first identified, and a hysteretic model was then validated for proper response calculations of the combined structural system. A number of alternate performance indices were defined. Several sets of numerical results were obtained according to the system responses and energy criteria.

7.2 Conclusions

Specific conclusions for different dissipation devices are given in the chapters where their numerical results are described. Here only the broad conclusions of this study are summarized as follows:

- The problem of designing energy dissipation devices for the retrofit and seismic protection of existing building structures can be conveniently solved using an optimization-based design approach.
- The gradient projection approach is a useful and highly efficient technique for the solution of problems involving a linear viscoelastically-damped structures and a stochastic characterization of the input ground motion.

- Genetic algorithm is a powerful technique that performs with comparable effectiveness for linear and nonlinear devices. The approach can be conveniently used for problems in which the design variables can be considered as discrete such as the optimal placement of devices in a building or the selection of the mechanical properties of the devices from a list of permissible values. The approach is flexible inasmuch as it can work with any performance function established to obtain the desired results. Since the approach utilizes several possible solution simultaneously in search for the optimal solution, it is most likely to converge to a globally optimal solution.
- Numerical results have shown that all energy dissipation devices are quite effective in reducing the structural dynamic response. Using the proposed optimization-based approach, these devices can be optimally placed and designed to reduce certain response quantities such as story deformations, base shear and floor accelerations or to achieve a desired structural performance objective.
- Results also indicate that different performance objectives can lead to different optimal designs. For example, the acceleration-based performance index design could be different from that of the drift-based performance index design. However, depending upon the relationship between the different performance functions, the optimal design for one performance objective may also be reasonably near optimal for other performance objectives.

7.3 Future Research

In this study, the application of a general optimization-based design framework has been presented for a broad class of problems involving different types of energy dissipation devices, structural building models, and ground motion characterizations. Lot more can be done with this approach for the design of passive control systems for seismic structural protection. In this regard, the following topics are recommended for future studies:

- Determination of the most adequate device or combination of devices for a particular structural application and intensity level of seismic excitation.

- Incorporation in the analysis of the possible inelastic behavior of the main structural members.
- Application of the general framework to the design of other types of devices, such as the Shape Memory Structural dampers, Energy Dissipating Restraints (EDR), and dynamic vibration absorbers.
- Development and application of statistical linearization techniques for the analysis and optimal design of nonlinear devices.
- Use of more refined models of structures and devices. Study of the influence of the flexibility of bracings in the design of linear viscoelastically-damped structures.
- Development of simplified procedures, software tools and design methodologies for the direct use of practitioners engineers.
- Implementation of an experimental program to validate the results predicted by the numerical analysis.

Appendix

A.1 Partial Fraction Coefficients

The partial fraction coefficients required in Eqs. (3.54) to (3.56) are defined as:

$$W_{lijk} = -\left\{\left(\Omega^2 - \Omega^{-2}\right)\mu_{lijk} - 2\left[1 - \Omega^2 + 2\left(\beta_j^2\,\Omega^2 - \beta_k^2\right)\right]\eta_{lijk}\right\} / \delta_{jk} \tag{A.1}$$

$$Q_{lijk} = \left\{\left(\Omega^2 - \Omega^{-2}\right)\eta_{lijk} - 2\,\Omega^{-2}\left[1 - \Omega^2 + 2\left(\beta_k^2\,\Omega^2 - \beta_j^2\right)\mu_{lijk}\right]\right\} / \left(\omega_j^2\,\delta_{jk}\right) \tag{A.2}$$

$$A_{lijk} = \alpha_j\left(-\{\mathbf{g}_{li}\}_k + 2\,\{\mathbf{a}_{li}\}_k\,\alpha_j\right) / \gamma_{jk} \tag{A.3}$$

$$B_{lijk} = -\omega_k^2\left[2\{\mathbf{a}_{li}\}_k\,\omega_k^2 + \{\mathbf{g}_{li}\}_k\left(\alpha_j + 2\,\omega_k\,\beta_k\right)\right] / \gamma_{jk} \tag{A.4}$$

$$C_{lijk} = \left[\{\mathbf{g}_{li}\}_k\,\alpha_j + 2\{\mathbf{a}_{li}\}_k\,\omega_k\left(\omega_k + 2\,\alpha_j\,\beta_k\right)\right] / \gamma_{jk} \tag{A.5}$$

with

$$\Omega = \omega_j / \omega_k \tag{A.6}$$

$$\begin{aligned}\eta_{lijk} = {} & \{\mathbf{g}_{li}\}_j\{\mathbf{g}_{li}\}_k\left(1 - 4\,\beta_j^2 + 4\,\beta_j\,\beta_k\,\Omega - \Omega^2\right) + \\ & 4\,\omega_j^2\{\mathbf{a}_{li}\}_j\{\mathbf{a}_{li}\}_k\left(1 - \Omega^2\right) + 4\,\omega_j\left(\{\mathbf{a}_{li}\}_j\{\mathbf{g}_{li}\}_k - \{\mathbf{a}_{li}\}_k\{\mathbf{g}_{li}\}_j\right)\left(\beta_k\,\Omega - \beta_j\right)\end{aligned} \tag{A.7}$$

$$\begin{aligned}\mu_{lijk} = {} & \{\mathbf{g}_{li}\}_j\{\mathbf{g}_{li}\}_k\left(\Omega^2 - 1\right) + 4\,\omega_j^2\{\mathbf{a}_{li}\}_j\{\mathbf{a}_{li}\}_k\left[\left(1 - 4\,\beta_j^2\right)\Omega^2 + 4\,\beta_j\,\beta_k\,\Omega - 1\right] + \\ & 4\,\omega_j\,\Omega\left(\{\mathbf{a}_{li}\}_j\{\mathbf{g}_{li}\}_k - \{\mathbf{a}_{li}\}_k\{\mathbf{g}_{li}\}_j\right)\left(\beta_j\,\Omega - \beta_k\right)\end{aligned} \tag{A.8}$$

$$\delta_{jk} = 16\left(\beta_j^2 + \beta_k^2 - \beta_j^4 - \beta_k^4\right) + 4\left(\Omega^2 + \Omega^{-2}\right)\left[1 - 2\left(\beta_j^2 + \beta_k^2 - 2\,\beta_j^2\,\beta_k^2\right)\right] - \Omega^{-4} - \Omega^4 - 6 \tag{A.9}$$

$$\gamma_{jk} = \omega_k^2 + \alpha_j^2 + 2\,\alpha_j\,\omega_k\,\beta_k \tag{A.10}$$

A.2 Gradients Calculations Formulas

In this section, the partial derivative formulas needed to calculate the gradients in Eq. (3.54) are provided. They are obtained by direct application of the chain rule of differentiation. Here, they are presented in compact forms, suitable for programming.

By denoting with $\nabla(\ )$ the row vector gradient of a given quantity and considering the scalar product of vectors, the derivatives of the response components $\boldsymbol{S}_{1i}$, $\boldsymbol{S}_{2i}$ and $\boldsymbol{S}_{3i}$ with respect to the d^{th} design variable are obtained from the chain rule of differentiation as:

$$\mathbf{S}_{1i,d} = \nabla \mathbf{S}_{1i} \cdot \left[\{\mathbf{e}_{li}\}_{j,d}, \{\mathbf{e}_{li}\}_{k,d}, \alpha_{j,d}, \alpha_{k,d}, J_{lj,d}, J_{lk,d} \right]^T \tag{A.11}$$

$$\mathbf{S}_{2i,d} = \nabla \mathbf{S}_{2i} \cdot \left[\{\mathbf{e}_{li}\}_{j,d}, A_{lijk,d}, B_{lijk,d}, C_{lijk,d}, J_{lj,d}, I_{1lk,d}, I_{2lk,d} \right]^T \tag{A.12}$$

$$\mathbf{S}_{3i,d} = \nabla \mathbf{S}_{3i} \cdot \left[\{\mathbf{g}_{li}\}_{j,d}, \{\mathbf{g}_{li}\}_{k,d}, \{\mathbf{a}_{li}\}_{j,d}, \{\mathbf{a}_{li}\}_{k,d}, \Omega_{,d}, Q_{lijk,d}, W_{lijk,d}, I_{1lj,d}, I_{1lk,d}, I_{2lj,d}, I_{2lk,d} \right]^T \tag{A.13}$$

where

$$A_{lijk,d} = \nabla A_{lijk} \cdot \left[\alpha_{j,d}, \{\mathbf{g}_{li}\}_{k,d}, \{\mathbf{a}_{li}\}_{k,d}, \omega_{k,d}, \beta_{k,d} \right]^T \tag{A.14}$$

$$B_{lijk,d} = \nabla B_{lijk} \cdot \left[\alpha_{j,d}, \{\mathbf{g}_{li}\}_{k,d}, \{\mathbf{a}_{li}\}_{k,d}, \omega_{k,d}, \beta_{k,d} \right]^T \tag{A.15}$$

$$C_{lijk,d} = \nabla C_{lijk} \cdot \left[\alpha_{j,d}, \{\mathbf{g}_{li}\}_{k,d}, \{\mathbf{a}_{li}\}_{k,d}, \omega_{k,d}, \beta_{k,d} \right]^T \tag{A.16}$$

$$Q_{lijk,d} = \nabla Q_{lijk} \cdot \left[\{\mathbf{g}_{li}\}_{j,d}, \{\mathbf{g}_{li}\}_{k,d}, \{\mathbf{a}_{li}\}_{j,d}, \{\mathbf{a}_{li}\}_{k,d}, \Omega_{,d}, \omega_{j,d}, \beta_{j,d}, \beta_{k,d} \right]^T \tag{A.17}$$

$$W_{lijk,d} = \nabla W_{lijk} \cdot \left[\{\mathbf{g}_{li}\}_{j,d}, \{\mathbf{g}_{li}\}_{k,d}, \{\mathbf{a}_{li}\}_{j,d}, \{\mathbf{a}_{li}\}_{k,d}, \Omega_{,d}, \omega_{j,d}, \beta_{j,d}, \beta_{k,d} \right]^T \tag{A.18}$$

$$J_{lj,d} = \nabla J_{lj} \cdot \left[\omega_{j,d}, \beta_{j,d} \right]^T; \quad I_{1lj,d} = \nabla I_{1lj} \cdot \left[\omega_{j,d}, \beta_{j,d} \right]^T; \quad I_{2lj,d} = \nabla I_{2lj} \cdot \left[\omega_{j,d}, \beta_{j,d} \right]^T \tag{A.19}$$

$$\{\mathbf{g}_{li}\}_{j,d} = \nabla \{\mathbf{g}_{li}\}_{j} \cdot \left[\{\mathbf{a}_{li}\}_{j,d}, \{\mathbf{b}_{li}\}_{j,d}, \omega_{j,d}, \beta_{j,d} \right]^T \tag{A.20}$$

$$\{\mathbf{a}_{li}\}_{j,d} = \mathrm{Re}\left[\{\mathbf{q}_{li}\}_{j,d} \right]; \qquad \{\mathbf{b}_{li}\}_{j,d} = \mathrm{Im}\left[\{\mathbf{q}_{li}\}_{j,d} \right] \tag{A.21}$$

$$\Omega_{,d} = \frac{\left(\omega_k\, \omega_{j,d} - \omega_j\, \omega_{k,d}\right)}{\omega_k^2} \tag{A.22}$$

Finally, the derivatives of the performance indexes given by Eqs. (3.80) and (3.81) can be calculated as

$$\left[\, f_1(\mathbf{d})\right]_{,d} = \frac{\left\{E\left[\mathbf{R}_i(\mathbf{d},t)\right]\right\}_{,d}}{E\left[R_{oi}\right]}, \qquad d = 1,\ldots,n_l \tag{A.23}$$

$$\left[\, f_2(\mathbf{d})\right]_{,d} = \frac{\left\{E\left[\mathbf{R}(\mathbf{d},t)\right]\right\}\cdot\left\{E\left[\mathbf{R}(\mathbf{d},t)\right]\right\}_{,d}}{\left\|E\left[\mathbf{R}_o\right]\right\|\left\|E\left[\mathbf{R}(\mathbf{d},t)\right]\right\|}, \qquad d = 1,\ldots,n_l \tag{A.24}$$

For post-optimality analysis, the quantities $f_{,dp}(\mathbf{d}^*)$ can be obtained as

$$\left[\, f_1(\mathbf{d})\right]_{,dp} = \frac{\left\{E\left[\mathbf{R}_i(\mathbf{d},t)\right]\right\}_{,dp} - f_{1,d}\left\{E\left[\mathbf{R}_{oi}\right]\right\}_{,p}}{E\left[\mathbf{R}_{oi}\right]}, \qquad d = 1,\ldots,n_l \tag{A.25}$$

$$\begin{aligned}\left[\, f_2(\mathbf{d})\right]_{,dp} = {} & \frac{\left\{E\left[\mathbf{R}(\mathbf{d},t)\right]\right\}_{,p}\cdot\left\{E\left[\mathbf{R}(\mathbf{d},t)\right]\right\}_{,d} + \left\{E\left[\mathbf{R}(\mathbf{d},t)\right]\right\}\cdot\left\{E\left[\mathbf{R}(\mathbf{d},t)\right]\right\}_{,dp}}{\left\|E\left[\mathbf{R}_o\right]\right\|\left\|E\left[\mathbf{R}(\mathbf{d},t)\right]\right\|} \\ & - \frac{f_{2,d}\left\langle f_2^{-1}\left\{E\left[\mathbf{R}(\mathbf{d},t)\right]\right\}\cdot\left\{E\left[\mathbf{R}(\mathbf{d},t)\right]\right\}_{,p} + f_2\left\{E\left[\mathbf{R}_o\right]\right\}\cdot\left\{E\left[\mathbf{R}_o\right]\right\}_{,p}\right\rangle}{\left\|E\left[\mathbf{R}_o\right]\right\|\left\|E\left[\mathbf{R}(\mathbf{d},t)\right]\right\|}\end{aligned} \tag{A.26}$$

where $\left\{E\left[\mathbf{R}(\mathbf{d},t)\right]\right\}_{,p}$, and $\left\{E\left[\mathbf{R}(\mathbf{d},t)\right]\right\}_{,dp}$ are obtained for variations in the input disturbance parameters as:

$$\left\{E\left[\mathbf{R}_i(\mathbf{d},t)\right]\right\}_{,p} = \frac{\left\{E\left[\mathbf{R}_i^2(\mathbf{d},t)\right]\right\}_{,p}}{2\,E\left[\mathbf{R}_i(\mathbf{d},t)\right]}; \quad \left\{E\left[\mathbf{R}_i(\mathbf{d},t)\right]\right\}_{,dp} = \frac{\left\{E\left[\mathbf{R}_i^2(\mathbf{d},t)\right]\right\}_{,dp}}{2\left\{E\left[\mathbf{R}_i(\mathbf{d},t)\right]\right\}_{,d}} \tag{A.27}$$

with

$$\left\{E\left[\mathbf{R}_i^2(\mathbf{d},t)\right]\right\}_{,p} = \left(\mathbf{S}_{1i} + \mathbf{S}_{2i} + \mathbf{S}_{3i}\right)_{,p}; \qquad \left\{E\left[\mathbf{R}_i^2(\mathbf{d},t)\right]\right\}_{,dp} = \left(\mathbf{S}_{1i} + \mathbf{S}_{2i} + \mathbf{S}_{3i}\right)_{,dp} \tag{A.28}$$

and

$$\begin{aligned}\mathbf{S}_{1i,p} = \nabla\mathbf{S}_{1i}\cdot\left[0,0,0,0,J_{lj,p},J_{lk,p}\right]^T; \quad \mathbf{S}_{2i,p} = \nabla\mathbf{S}_{2i}\cdot\left[0,0,0,0,J_{lj,p},I_{1lk,p},I_{2lk,p}\right]^T \\ \mathbf{S}_{3i,p} = \nabla\mathbf{S}_{3i}\cdot\left[0,0,0,0,0,0,0,I_{1lj,p},I_{1lk,p},I_{2lj,p},I_{2lk,p}\right]^T\end{aligned} \tag{A.29}$$

$$\mathbf{S}_{1i,dp} = \left(\nabla \mathbf{S}_{1i}\right)_{,p} \cdot \left[\left\{\mathbf{e}_{li}\right\}_{j,d}, \left\{\mathbf{e}_{li}\right\}_{k,d}, \alpha_{j,d}, \alpha_{k,d}, J_{lj,d}, J_{lk,d} \right]^T + \nabla \mathbf{S}_{1i} \cdot \left[0,0,0,0, J_{lj,dp}, J_{lk,dp} \right]^T \quad \text{(A.30)}$$

$$\begin{aligned} \mathbf{S}_{2i,dp} = \left(\nabla \mathbf{S}_{2i}\right)_{,p} \cdot \left[\left\{\mathbf{e}_{li}\right\}_{j,d}, A_{lijk,d}, B_{lijk,d}, C_{lijk,d}, J_{lj,d}, I_{1lk,d}, I_{2lk,d} \right]^T + \\ \nabla \mathbf{S}_{2i} \cdot \left[0,0,0,0, J_{lj,dp}, I_{1lk,dp}, I_{2lk,dp} \right]^T \end{aligned} \quad \text{(A.31)}$$

$$\begin{aligned} \mathbf{S}_{3i,dp} = \left(\nabla \mathbf{S}_{3i}\right)_{,p} \cdot \left[\left\{\mathbf{g}_{li}\right\}_{j,d}, \left\{\mathbf{g}_{li}\right\}_{k,d}, \left\{\mathbf{a}_{li}\right\}_{j,d}, \left\{\mathbf{a}_{li}\right\}_{k,d}, \Omega_{,d}, Q_{lijk,d}, W_{lijk,d}, I_{1lj,d}, I_{1lk,d}, I_{2lj,d}, I_{2lk,d} \right]^T + \\ \nabla \mathbf{S}_{3i} \cdot \left[0,0,0,0,0,0,0, I_{1lj,dp}, I_{1lk,dp}, I_{2lj,dp}, I_{2lk,dp} \right]^T \end{aligned} \quad \text{(A.32)}$$

$$\begin{aligned} J_{j,dp} = \left(\nabla J_{lj}\right)_{,p} \cdot \left[\omega_{j,d}, \beta_{j,d} \right]^T; \quad I_{1lj,dp} = \left(\nabla I_{1lj}\right)_{,p} \cdot \left[\omega_{j,d}, \beta_{j,d} \right]^T \\ I_{2lj,dp} = \left(\nabla I_{2lj}\right)_{,p} \cdot \left[\omega_{j,d}, \beta_{j,d} \right]^T \end{aligned} \quad \text{(A.33)}$$

References

[1] Abbas, H. and Kelly, J. M., (1993). "A Methodology for Design of Viscoelastic Dampers in Earthquake-Resistant Structures," *Report No. UCB/EERC 93/09*, Earthquake Engineering Research Center, University of California at Berkeley, Berkeley, CA.

[2] Aguirre, M. and Sánchez, A. R., (1992). "Structural Seismic Damper," *Journal of Structural Engineering*, 118, 1158-1171.

[3] Aiken, I. D. and Kelly, J. M., (1990). "Earthquake Simulator Testing and Analytical Studies of Two Energy-Absorbing Systems for Multistory Structures," *Report No. UCB/EERC-90/03*, Earthquake Engineering Research Center, University of California at Berkeley, Berkeley, CA.

[4] Aprile, A., Inaudi, J. A., and Kelly, J. M., (1997). "Evolutionary Model of Viscoelastic Dampers for Structural Applications," *Journal of Engineering Mechanics*, 123(6), 551-560.

[5] Ashour, S. A. and Hanson, R. D., (1987). "Elastic Seismic Response of Buildings with Supplemental Damping," *Report No. UMCE 87-1*, University of Michigan, Ann Arbor, MI.

[6] Austin, M. A. and Pister, K. S., (1983). "Optimal Design of Friction-Based Frames Under Seismic Loading," *Report No. UCB/EERC 83-10*, Earthquake Engineering Research Center, University of California at Berkeley, Berkeley, CA.

[7] Austin, M. A. and Pister, K. S., (1985). "Design of Seismic-Resistant Friction-Braced Frames," *Journal of Structural Engineering*, 111, 2751-2769.

[8] Bagley, R. L. and Torvik, P. J., (1983). "Fractional Calculus - A Different Approach to the Analysis of Viscoelastically Damped Structures," *AIAA Journal*, 21(5), 741-748.

[9] Balling, R. J., Ciampi, V., Pister, K. S., and Polak, E., (1981). "Optimal Design of Seismic-Resistant Planar Steel Frames," *Report No. UCB/EERC 81-20*, Earthquake Engineering Research Center, University of California at Berkeley, Berkeley, CA.

[10] Bergman, D. M. and Goel, S. C., (1987). "Evaluation of Cyclic Testing of Steel-Plate Devices for Added Damping and Stiffness," *Report No. UMCE 87-10*, University of Michigan, Ann Harbor, MI.

[11] Bergman, D. M. and Hanson, R. D., (1993). "Viscoelastic Mechanical Damping Devices Tested at Real Earthquake Displacements," *Earthquake Spectra*, 9(3), 389-418.

[12] Bertero, V. V., (1989). "Experimental and Analytical Studies of Promising Techniques for the Repair and Retroffiting of Buildings", *Lessons Learned from the 1985 Mexico Earthquake*, EERI.

[13] Bhatti, M. A., (1979). "Optimal Design of Localized Nonlinear Systems with Dual Performance Criteria Under Earthquake Excitations," *Report No. UCB/EERC 79-15*, Earthquake Engineering Research Center, University of California at Berkeley, Berkeley, CA.

[14] Bhatti, M. A. and Pister, K. S., (1981a). "A Dual Criteria for Optimal Design of Earthquake-Resistant Structural Systems," *Earthquake Engineering and Structural Dynamics*, 9, 557-572.

[15] Bhatti, M. A. and Pister, K. S., (1981b). "Transient Response Analysis of Structural Systems with Nonlinear Behavior," *Computers and Structures*, 13, 181-188.

[16] Blume, J. A., Newmark, N. M., and Corning, L. H., (1961). *Design of Multistory Reinforced Concrete Buildings for Earthquake Motions*, Portland Cement Association, Skokie, Illinois.

[17] Bracci, J. M., Lobo, R. F., and Reinhorn, A. M., (1993). "Seismic Retrofit of Reinforced Concrete Structures Using Damping Devices", *ATC-17-1 Seminar on Seismic Isolation, Passive Energy Dissipation, and Active Control*, San Francisco, CA, 569-580.

[18] Camp, C. V., Pezeshk, S., and Cao, G., (1998). "Optimized Design of Two-Dimensional Structures Using Genetic Algorithm," *Journal of Structural Engineering*, 124(5), 551-559.

[19] Chan, E., (1997). "Optimal Design of Buildings Structures Using Genetic Algorithms," *Report No. EERL 97-06*, Earthquake Engineering Research Laboratory, California Institute of Technology, Pasadena, CA.

[20] Chang, K. C., Soong, T. T., Lai, M. L., and Nielsen, (1993). "Viscoelastic Dampers as Energy Dissipation Devices for Seismic Applications," *Earthquake Spectra*, 9(3), 371-388.

[21] Chang, K. C., Soong, T. T., Lai, M. L., and Nielsen, E. J., (1993). "Development of a Design Procedure for Structures with Added Viscoelastic Dampers", *ATC-17-1 Seminar on Seismic Isolation, Passive Energy Dissipation, and Active Control*, San Francisco, CA, 473-484.

[22] Chang, K. C., Soong, T. T., Oh, S. T., and Lai, M. L., (1991). "Seismic Response of a 2/5 Scale Steel Structure with Added Viscoelastic Dampers," *Report No. NCEER 91-0012*, National Center for Earthquake Engineering Research, University of New York at Buffalo, Buffalo, NY.

[23] Chang, K. C., Soong, T. T., Oh, S. T., and Lai, M. L., (1992). "Effect of Ambient Temperature on Viscoelastically Damped Structure," *Journal of Structural Engineering*, 118(7), 1955-1973.

[24] Chang, K. C., Soong, T. T., Oh, S. T., and Lai, M. L., (1995). "Seismic Behavior of Steel Frame with Added Viscoelastic Dampers," *Journal of Structural Engineering*, 121(10), 1418-1426.

[25] Chen, G. S., Bruno, R. J., and Salama, M., (1991). "Optimal Placement of Active/Passive Members in Truss Structures Using Simulated Annealing," *AIAA Journal*, 29, 1327-1334.

[26] Cheng, F. Y. and Li, D., (1998). "Genetic Algorithm Development for Multiobjective Optimization of Structures," *AIAA Journal*, 36(6), 1105-1112.

[27] Cherry, S. and Filiatrault, A., (1993). "Seismic Response Control of Buildings Using Friction Dampers," *Earthquake Spectra*, 9, 447-466.

[28] Ciampi, V., De Angelis, M., and Paolacci, F., (1995). "Design of Yielding or Friction-Based Dissipative Bracings for Seismic Protection of Buildings," *Engineering Structures*, 17, 381-391.

[29] Colajanni, P. and Papia, M., (1995). "Seismic Response of Braced Frames With and Without Friction Dampers," *Engineering Structures*, 17, 129-140.

[30] Colajanni, P. and Papia, M., (1997). "Hysteretic Behavior Characterization of Friction-Damped Braced Frames," *Journal of Structural Engineering*, 123(8), 1020-1028.

[31] Constantinou, M. C., Mokha, A., and Reinhorn, A. M., (1990). "Teflon Bearings in Base Isolation. II: Modeling," *Journal of Structural Engineering*, 116(2), 455-474.

[32] Constantinou, M. C., Soong, T. T., and Dargush, G. F., (1998). *Passive Energy Dissipation Systems for Structural Design and Retrofit*, Monograph No. 1, Multidisciplinary Center for Earthquake Engineering Research, Buffalo, NY.

[33] Constantinou, M. C. and Symans, M. D., (1993a). "Experimental and Analytical Investigation of Seismic Response of Structures with Supplemental Fluid Dampers," *Report No. NCEER 92-0032*, National Center for Earthquake Engineering Research, University of New York at Buffalo, Buffalo, NY.

[34] Constantinou, M. C. and Symans, M. D., (1993b). "Experimental Study of Seismic Response of Structures with Supplemental Fluid Dampers," *The Structural Design of Tall Buildings*, 2, 93-132.

[35] Constantinou, M. C. and Symans, M. D., (1993c). "Seismic Response of Structures with Supplemental Damping," *The Structural Design of Tall Buildings*, 2, 77-92.

[36] Constantinou, M. C., Symans, M. D., Tsopelas, P., and Taylor, D. P., (1993). "Fluid Viscous Dampers in Applications of Seismic Energy Disipation and Seismic Isolation", *ATC-17-1 Seminar on Seismic Isolation, Passive Energy Dissipation, and Active Control*, San Francisco, CA, 581-592.

[37] Constantinou, M. C. and Tadjbakhsh, I. G., (1983). "Optimum Design of a First Story Damping System," *Computers and Structures*, 17, 305-310.

[38] Crosby, P., Kelly, J. M., and Singh, Y., (1994). "Utilizing Viscoelastic Dampers in the Seismic Retrofit of a Thirteen Story Steel Frame Building", *12th Structures Congress*, Atlanta, GA, 1286-1291.

[39] Dargush, G. F. and Soong, T. T., (1995). "Behavior of Metallic Plate Dampers in Seismic Passive Energy Dissipation Systems," *Earthquake Spectra*, 11, 545-568.

[40] Davis, L., (1991). *Handbook of Genetic Algorithms*, Van Nostrand Reinhold, New York, N.Y.

[41] De Silva, C. W., (1981). "An algorithm for the Optimal Design of Passive Vibration Controllers for Flexible Systems," *Journal of Sound and Vibration*, 75, 495-502.

[42] Elsesser, E., (1997). "Historic Upgrades in San Francisco", *Civil Engineering*, 50-53.

[43] Federal Emergency Management Agency - FEMA, (1997). "NEHRP Guidelines and Commentary for the Seismic Rehabilitation of Buildings," *Reports No. 273 and 274*, Building Seismic Council, Washington, DC.

[44] Fierro, E. A. and Perry, C. L., (1993). "San Francisco Retrofit Design Using Added Damping and Stiffness (ADAS) Elements", *ATC-17-1 Seminar on Seismic Isolation, Passive Energy Dissipation, and Active Control*, San Francisco, CA, 593-604.

[45] Filiatrault, A. and Cherry, S., (1987). "Performance Evaluation of Friction Damped Braced Steel Frames Under Simulated Earthquake Loads," *Earthquake Spectra*, 3, 57-78.

[46] Filiatrault, A. and Cherry, S., (1988). "Comparative Performance of Friction Damped Systems and Base Isolation Systems for Earthquake Retrofit Systems for Earthquake Retrofit and Aseismic Design," *Earthquake Engineering and Structural Dynamics*, 16, 389-416.

[47] Filiatrault, A. and Cherry, S., (1989a). "Efficient Numerical Modeling for the Design of Friction Damped Braced Steel Plane Frames," *Canadian Journal of Civil Engineering*, 16, 211-218.

[48] Filiatrault, A. and Cherry, S., (1989b). "Parameters Influencing the Design of Friction Damped Structures," *Canadian Journal of Civil Engineering*, 16, 753-766.

[49] Filiatrault, A. and Cherry, S., (1990). "Seismic Design Spectra for Friction-Damped Structures," *Journal of Structural Engineering*, 116, 1334-1355.

[50] FitzGerald, T., Anagnos, T., Goodson, M., and Zsutty, T., (1989). "Slotted Bolted Connections in Aseismic Design for Concentrically Braced Connections," *Earthquake Spectra*, 5, 383-391.

[51] Foti, D., Bozzo, L., and Lopez-Almansa, F., (1998). "Numerical Efficiency Assessment of Energy Dissipators for Seismic Protection of Buildings," *Earthquake Engineering and Structural Dynamics*, 27, 543-556.

[52] Foutch, D. A., Wood, S. L., and Brady, P. A., (1993). "Seismic Retrofit of Nonductile Reinforced Concrete Using Viscoelastic Dampers", *ATC-17-1 Seminar on Seismic Isolation, Passive Energy Dissipation, and Active Control*, San Francisco, CA, 605-616.

[53] Fujita, K., Kokubo, E., Nakatogowa, T., Shibata, H., Kunieda, M., Hara, F., Suzuki, K., Ichihashi, I., Yoshimura, H., Zaitsu, T., and Ono, T., (1991). "Development of Friction Damper as a Seismic Support for the Piping System in Nuclear Power Plants", *ASME, Pressure Vessels and Piping*, San Diego.

[54] Furuya, H. and Haftka, R. T., (1995). "Placing Actuators on Space Structures by Genetic Algorithms and Effectiveness Indices," *Structural Optimization*, 9, 69-75.

[55] Furuya, O., Hamazaki, H., and Fujita, S., (1998). "Proper Placement of Energy Absorbing Devices for Reduction of Wind-Induced Vibration in High-Rise Buildings," *Journal of Wind Engineering and Industrial Aerodynamics*, 931-942.

[56] Gen, M. and Cheng, R., (1997). *Genetic Algorithms and Engineering Design*, John-Wiley & Sons, New York, N.Y.

[57] Ghafory-Ashtiany, M. and Singh, M. P., (1981). "Seismic Response of Structural System with Random Parameters," *Report No. VPI-E81.15*, Virginia Polytechnic Institute and State University, Blacksburg, VA.

[58] Gluck, N., Reinhorn, A. M., Gluck, J., and Levy, R., (1996). "Design of Supplemental Dampers for Control of Structures," *Journal of Structural Engineering*, 122(12), 1394-1399.

[59] Goel, S. C., Hanson, R. D., and Wight, J. K., (1989). "Strengthening of Existing Buildings for Earthquake Survival", *Lessons Learned from the 1985 Mexico Earthquake*, Ed. Bertero, V. V., EERI, 166-171.

[60] Goldberg, D. E., (1989a). *Genetic Algorithms in Search, Optimization and Machine Learning*, Addison-Wesley, Reading, MA.

[61] Goldberg, D. E., (1989b). *Genetic Algorithms in Search, Optimization and Machine Learning*, Addison-Wesley, Reading, MA.

[62] Graesser, E. J. and Cozzarelli, F. A., (1991). "A Multidimensional Hysteretic Model for Plastically Deforming Metals in Energy Absorbing Devices," *Report No. NCEER 91-0006*, National Center for Earthquake Engineering Center, University of New York at Buffalo, Buffalo, NY.

[63] Grigorian, C. E. and Popov, E. P., (1994). "Energy Dissipation with Slotted Bolted Connections," *Report No. UCB/EERC 94-02*, Earthquake Engineering Research Center, University of California at Berkeley, Berkeley, CA.

[64] Grigorian, C. E. and Popov, E. P., (1999). "Slotted Bolted Connections for Energy Dissipation," *ATC-17-1 Seminar on Seismic Isolation, Passive Energy Dissipation, and Active Control*, San Francisco, CA, 545-556.

[65] Grigorian, C. E., Yang, T., and Popov, E. P., (1993). "Slotted Bolted Connection Energy Dissipators," *Earthquake Spectra*, 9(3), 491-504.

[66] Gürgöze, M. and Müller, P. C., (1992). "Optimal Positioning of Dampers in Multi-Body Systems," *Journal of Sound and Vibration*, 158(3), 517-530.

[67] Hadi, M. N. and Arfiadi, Y., (1998). "Optimum Design of Absorber for MDOF Structures," *Journal of Structural Engineering*, 124, 1272-1280.

[68] Haftka, R. T. and Gürdal, Z., (1992). *Elements of Structural Optimization*, Kluwer Academic, Dordrecht.

[69] Haftka, R. T. and Kamat, M. P., (1985). *Elements of Structural Optimization*, Martinus Nijhoff, Dordrecht, The Netherlands.

[70] Hahn, G. D. and Sathiavageeswaran, K. R., (1992). "Effects of Added-Damper Distribution on the Seismic Response of Buildings," *Computers and Structures*, 43, 941-950.

[71] Hanson, R., (1993). "Supplemental Damping for Improved Seismic Performance," *Earthquake Spectra*, 9(3), 319-334.

[72] Hanson, R. D., Aiken, I., Nims, D. K., Richter, P. J., and Bachman, R., (1993). "State-of-the-Art and State-of-the-Practice in Seismic Energy Dissipation", *ATC-17-1 Seminar on Seismic Isolation, Passive Energy Dissipation, and Active Control*, San Francisco, CA, 449-471.

[73] Hendsbee, D., (1993). "Retrofit of a Concrete Frame Building Using Added Damping", *ATC-17-1 Seminar on Seismic Isolation, Passive Energy Dissipation, and Active Control*, San Francisco, CA, 617-626.

[74] Higgins, C. and Kasai, K., (1998). "Full-Scale Real-Time Seismic Testing and Analysis of a Viscoelastically Damped Steel Frame," *6th U.S. National Conference on Earthquake Engineering*, Seattle, WA.

[75] Hindmarsh, A. C., (1983). "ODEPACK, A Systematized Collection of ODE Solvers", *Scientific Computing*, Ed. Stepleman, R. S., North-Holland, Amsterdam, 55-64.

[76] Holland, J. H., (1975). *Adaptation in Natural and Artificial Systems*, University of Michigan Press, Ann Arbor, MI.

[77] Housner, G. W., Bergman, L. A., Caughey, T. K., Chassiakos, A. G., Claus, R. O., Masri, S. F., Skelton, R. E., Soong, T. T., Spencer, B. F., and Yao, J. T. P., (1997). "Structural Control: Past, Present, and Future," *Journal of Engineering Mechanics*, 123(9), 897-971.

[78] Hsu, S. Y. and Fafitis, A., (1992). "Seismic Analysis Design of Frames with Viscoelastic Connections," *Journal of Structural Engineering*, 118(9), 2459-2474.

[79] Inaudi, J. A., (1997). "Analysis of Hysteretic Damping Using Analytical Signals," *Journal of Engineering Mechanics*, 123(7), 743-745.

[80] Inaudi, J. A. and De la Llera, J. C., (1993). "Dynamic Analysis of Nonlinear Structures Using State-Space Formulation and Partitioned Integration Schemes," *Report No. UCB/EERC-92/18*, Earthquake Engineering Research Center, University of California at Berkeley, Berkeley, CA.

[81] Inaudi, J. A. and Kelly, J. M., (1995a). "Linear Hysteretic Damping and the Hilbert Transform," *Journal of Engineering Mechanics*, 121(5), 626-632.

[82] Inaudi, J. A. and Kelly, J. M., (1995b). "Modal Equations of Linear Structures with Viscoelastic Dampers," *Earthquake Engineering and Structural Dynamics*, 24, 145-151.

[83] Inaudi, J. A., Kelly, J. M., and To, C. W., (1993). "Statistical Linearization Method in the Preliminary Design of Structures with Energy Dissipating Restraints," *ATC-17-1*

Seminar on Seismic Isolation, Passive Energy Dissipation, and Active Control, San Francisco, CA, 509-520.

[84] Inaudi, J. A. and Makris, N., (1996). "Time-Domain Analysis of Linear Hysteretic Damping," *Earthquake Engineering and Structural Dynamics*, 25, 529-545.

[85] Inaudi, J. A., Nims, D. K., and Kelly, J. M., (1993). "On the Analysis of Structures with Energy Dissipating Restraints," *Report No. UCB/EERC 93-13*, Earthquake Engineering Research Center, University of California at Berkeley, Berkeley, CA.

[86] Inaudi, J. A., Zambrano, A., and Kelly, J. M., (1993). "On the Analysis of Structures with Viscoelastic Dampers," *Report No. UCB/EERC 93-06*, Earthquake Engineering Research Center, University of California at Berkeley, Berkeley, CA.

[87] Japan Building Center, (1993). "Technological Development of Earthquake-Resistant Structures," *Report of the Expert Comitee on Advanced Technology for Building Structures*, A. A. Balkema Publishers, Brookfield, VT.

[88] Jara, J. M., Gomez-Soberon, C., Vargas, E., and Gonzalez, R., (1993). "Seismic Performance of Buildings with Energy Dissipating Systems", *ATC-17-1 Seminar on Seismic Isolation, Passive Energy Dissipation, and Active Control*, San Francisco, CA, 663-674.

[89] Jenkins, W. M., (1997). "On the Application of Natural Algorithms to Structural Design Optimization," *Engineering Structures*, 19(4), 302-308.

[90] Kanai, K., (1961). "An Empirical Formula for the Spectrum of Strong Earthquake Motions," *Bulletin Earthquake Research Institute, University of Tokyo*, 39, 85-95.

[91] Kanitkar, R., Harms, M., Lai, M.-L., and Crosby, P., (1998). "Linear and Non-Linear Analysis of a Four Story Structure Using Viscoelastic Dampers," *6th U.S. National Conference on Earthquake Engineering*, Seattle, WA.

[92] Kasai, K., Fu, Y., and Watanabe, A., (1998). "Passive Control Systems for Seismic Damage Mitigation," *Journal of Structural Engineering*, 124(5), 501-512.

[93] Kasai, K., Munshi, J. A., Lai, M. L., and Maison, B. F., (1993). "Viscoelastic Damper Hysteretic Model: Theory, Experiment, and Application", *ATC-17-1 Seminar on Seismic Isolation, Passive Energy Dissipation, and Active Control*, San Francisco, CA, 521-532.

[94] Keel, C. J. and Mahmoodi, P., (1986). "Designing of Viscoelastic Dampers for Columbia Center Building", *Building Motion in Wind*, Eds. Isyumov, N. and Tschanz, ASCE, New York, NY, 66-82.

[95] Kelly, J. M., (1993). *Earthquake-Resistant Design with Rubber*, Springer-Verlag, London.

[96] Kelly, J. M., Skinner, R. I., and Heine, A. J., (1972). "Mechanism of Energy Absorption in Special Devices for Use in Earthquake Resistant Structures," *Bulletin of N.Z.Society for Eartquake Engineering*, 5(3).

[97] Keshtkar, H. E., Hanson, R. D., and Scott, R. A., (1991). "Optimum Design of Earthquake Resistant Modular Structures," *Report No. UMCE 91-14*, Department of Civil Engineering, University of Michigan, Ann Arbor, MI.

[98] Kim, Y. and Ghaboussi, J., (1999). "A New Method of Reduced Order Feedback Control Using Genetic Algorithms," *Earthquake Engineering and Structural Dynamics*, 28, 193-212.

[99] Lai, M. L., Chang, K. C., Soong, T. T., Hao, D. S., and Yeh, Y. C., (1995). "Full-Scale Viscoelastically Damped Steel Frame," *Journal of Structural Engineering*, 121(10), 1443-1447.

[100] Lai, S.-S. P., (1982). "Statistical Characterization of Strong Ground Motions Using Power Spectral Density Functions," *Bulletin of the Seismological Society of America*, 72(1), 259-274.

[101] Lin, R. C., Liang, Z., Soong, T. T., and Zhang, R. H., (1988). "An Experimental Study of Seismic Structural Response with Added Viscoelastic Dampers," *Report No.*

NCEER 88-0018, National Center for Earthquake Engineering Research, University of New York at Buffalo, Buffalo, NY.

[102] Lin, R. C., Liang, Z., Soong, T. T., and Zhang, R. H., (1991). "An Experimental Study on Seismic Behavior of Viscoelastically Damped Structures," *Engineering Structures*, 13, 75-83.

[103] Lundén, R., (1980). "Optimum Distribution of Additive Damping for Vibrating Frames," *Journal of Sound and Vibration*, 72, 391-402.

[104] Mahmoodi, P., (1969). "Structural Dampers," *Journal of the Structural Division ASCE*, 95, 1661-1672.

[105] Makris, N., (1997). "Causal Hysteretic Element," *Journal of Engineering Mechanics*, 123(11), 1209-1214.

[106] Makris, N., (1998a). "Viscous Heating of Fluid Dampers. I: Small-Amplitude Motions," *Journal of Engineering Mechanics*, 124(11), 1210-1216.

[107] Makris, N., (1998b). "Viscous Heating of Fluid Dampers. II: Large-Amplitude Motions," *Journal of Engineering Mechanics*, 124(11), 1217-1223.

[108] Makris, N. and Constantinou, M. C., (1991). "Fractional Derivative Model for Viscous Dampers," *Journal of Structural Engineering*, 117(9), 2708-2724.

[109] Makris, N. and Constantinou, M. C., (1993). "Models of Viscoelasticity with Complex-Order Derivatives," *Journal of Engineering Mechanics*, 119(7), 1453-1464.

[110] Makris, N., Constantinou, M. C., and Dargush, G. F., (1993). "Analytical Model of Viscoelastic Fluid Dampers," *Journal of Structural Engineering*, 119(11), 3310-3325.

[111] Makris, N., Dargush, G. F., and Constantinou, M. C., (1993). "Dynamic Analysis of Generalized Viscoelastic Fluids," *Journal of Engineering Mechanics*, 119(8), 1663-1679.

[112] Makris, N., Dargush, G. F., and Constantinou, M. C., (1995). "Dynamic Analysis of Viscoelastic Fluid Dampers," *Journal of Engineering Mechanics*, 121(10), 1114-1121.

[113] Makris, N., Inaudi, J. A., and Kelly, J. M., (1999). "Macroscopic Models with Complex Coefficients and Causality," *Journal of Engineering Mechanics*, 122(6), 566-573.

[114] Makris, N., Roussos, Y., Whittaker, A. S., and Kelly, J. M., (1997). "Viscous Heating of Fluid Dampers During Seismic and Wind Excitations - Analytical Solutions and Design Formulae," *Report No. UCB/EERC 97-11*, Earthquake Engineering Research Center, University of California at Berkeley, Berkeley, CA.

[115] Martinez, R., (1993). "Experiences on the Use of Supplementary Energy Dissipators on Building Structures," *Earthquake Spectra*, 9, 581-626.

[116] McMahon, M. T., (1998). "A Distributed Genetic Algorithm with Migration for the Design of Composite Laminate Structures", Virginia Polytechnic Institute and State University, Blacksburg, VA.

[117] McMahon, M. T., Watson, L. T., Soremekun, G. A., Gürdal, Z., and Haftka, R. T., (1998). "A Fortran 90 Genetic Algorithm Module for Composite Laminate Structure Design," *Engineering with Computers*, 14, 260-273.

[118] Meirovitch, L., (1997). *Principles and Techniques of Vibrations*, Prentice-Hall, Upper Saddle River, NJ.

[119] Michalewicz, Z., (1992). *Genetic Algorithms + Data Structures = Evolution Programs*, Springer-Verlag, New York, NY.

[120] Milman, M. H. and Chu, C. C., (1994). "Optimization Methods for Passive Damper Placement and Tuning," *Journal of Guidance, Control and Dynamics*, 17, 848-856.

[121] Miranda, E., Alonso, J., and Lai, M. L., (1998). "Performance-Based Design of a Building in Mexico City Using Viscoelastic Devices," *6th U.S. National Conference on Earthquake Engineering*, Seattle, WA.

[122] Murthy, D. V. and Haftka, R. T., (1988). "Derivatives of Eigenvalues and Eigenvectors of a General Complex Matrix," *International Journal for Numerical Methods in Engineering*, 26, 293-311.

[123] Nakashima, M., Saburi, K., and Tsuji, B., (1996). "Energy Input and Dissipation Behavior of Structures with Hysteretic Dampers," *Earthquake Engineering and Structural Dynamics*, 25, 483-496.

[124] Namita, Y., Shibata, H., Hara, F., Ichihashi, I., Matsuda, T., Yoshinaga, T., Kunieda, M., Suzuki, K., Liyama, K., and Murota, M., (1991). "Development of Energy Absorber and its Applications to Piping Systems in Nuclear Power Plants", *ASME, Pressure Vessels and Piping Conference*, San Diego, CA.

[125] Natke, H. G., (1993). "Topological Structural Optimization under Dynamic Loads", *Optimization of Structural Systems and Applications*, Eds. Hernandez, S. and Brebbia, C. A., Computational Mechanics Publications, Southampton, 67-78.

[126] Nims, D., Richter, P., and Bachman, R., (1993). "The Use of the Energy Dissipating Restraint for Seismic Hazard Mitigation," *Earthquake Spectra*, 9, 467-489.

[127] Nims, D. K., Inaudi, J. A., Richter, P. J., and Kelly, J. M., (1993). "Application of the Energy Dissipating Restraint to Buildings", *ATC-17-1 Seminar on Seismic Isolation, Passive Energy Dissipation, and Active Control*, San Francisco, CA, 627-638.

[128] Niwa, N., Kobori, T., Takahasi, M., Hatada, T., and Kurino, H., (1995). "Passive Seismic Response Controlled High-Rise Building with High Damping Device," *Earthquake Engineering and Structural Dynamics*, 24, 655-671.

[129] Onoda, J. and Hanawa, Y., (1993). "Actuator Placement Optimization by Genetic and Improved Simulated Annealing Algorithms," *AIAA Journal*, 31, 1167-1169.

[130] Özdemir, H., (1976). "Nonlinear Transient Dynamic Analysis of Yielding Structures," Thesis/Dissertation, University of California at Berkeley, Berkeley, CA.

[131] Pall, A. S. and Marsh, C., (1982). "Response of Friction Damped Braced Frames," *Journal of Structural Engineering*, 108(ST6), 1313-1323.

[132] Pall, A. S., Marsh, C., and Fazio, P., (1980). "Friction Joints for Seismic Control of Large Panel Structures," *Journal of the Prestressed Concrete Institute*, 25(6), 38-61.

[133] Pall, A. S. and Pall, R., (1993). "Friction-Dampers Used for Seismic Control of New and Existing Buildings in Canada," *ATC-17-1 Seminar on Seismic Isolation, Passive Energy Dissipation, and Active Control*, San Francisco, CA, 675-686.

[134] Pall, A. S., Vezina, S., and Pall, R., (1993). "Friction-Dampers for Seismic Control of Canadian Space Agency Headquarters," *Earthquake Spectra*, 9(3), 547-557.

[135] Pasquin, C., Charania, H., Steele, R., Pall, R., and Pall, A. S., (1999). "Friction-Dampers for Seismic Control of Selkirk Water Front Offices, Victoria," *6th U.S. National Conference on Earthquake Engineering*, Seattle, WA.

[136] Pekau, O. A. and Guimond, R., (1991). "Controlling Seismic Response of Eccentric Structures by Friction Dampers," *Earthquake Engineering and Structural Dynamics*, 20, 505-521.

[137] Pekcan, G., Mander, J. B., and Chen, S. S., (1995). "The Seismic Response of a 1:3 Scale Model R.C. Structure with Elastomeric Spring Dampers," *Earthquake Spectra*, 11(2), 249-267.

[138] Perry, C. L., Fierro, E. A., Sedarat, H., and Scholl, R. E., (1993). "Seismic Upgrade in San Francisco Using Energy Dissipation Devices," *Earthquake Spectra*, 9(3), 559-579.

[139] Petzold, L. R., (1983). "Automatic Selection of Methods for Solving Stiff and Nonstiff Systems of Ordinary Differential Equations," *SIAM Journal of Scientific and Statistical Computation*, 4, 136-148.

[140] Pong, W. S., Tsai, C. S., and Lee, G. C., (1994). "Seismic Study of Building Frames with Added Energy-Absorbing Devices," *Report No. NCEER 94-0016*, National Center for Earthquake Engineering Research, University of New York at Buffalo, Buffalo, NY.

[141] Rai, D. C., (1999). "Supplemental Damping for Seismic Strengthening: a Case Study," *Engineering Structures*, 21, 603-614.

[142] Ramber, W., (1943). "Description of Stress-Strain Curves by Three Parameters," *Technical Note 902*.

[143] Rao, S. S., (1996). *Engineering Optimization*, John Wiley & Sons, New York, NY.

[144] Rao, S. S. and Pan, T. S., (1991). "Optimal Placement of Actuators in Actively Controlled Structures Using Genetic Algorithms," *AIAA Journal*, 29, 942-943.

[145] Ray, D., Pister, K. S., and Chopra, A. K., (1974). "Optimum Design of Earthquake-Resistant Shear Buildings," *Report No. UCB/EERC 74-3*, Earthquake Engineering Research Center, University of California at Berkeley, Berkeley, CA.

[146] Ray, D., Pister, K. S., and Polak, E., (1976). "Sensitivity Analysis for Hysteretic Dynamic Systems: Theory and Applications," *Report No. EERC 76-12*, Earthquake Engineering Research Center, University of California at Berkeley, Berkeley, CA.

[147] Reinhorn, A. M., Li, C., and Constantinou, M. C., (1995). "Experimental and Analytical Investigation of Seismic Retrofit of Structures with Supplemental Damping: Part 1 - Fluid Viscous Damping Devices," *Report No. NCEER 95-0001*, National Center for Earthquake Engineering Research, University of New York at Buffalo, Buffalo, NY.

[148] Ribakov, Y. and Gluck, J., (1999). "Optimal Design of ADAS Damped MDOF Structures," *Earthquake Spectra*, 15(2), 317-330.

[149] Robinson, W. H. and Greenback, L. R., (1976). "An Extrusion Energy Absorber Suitable for the Protection of Structures During an Earthquake," *International Journal of Earthquake Engineering and Structural Dynamics*, 4.

[150] Roik, K., Dorka, U., and Dechent, P., (1988). "Vibration Control of Structures Under Earthquake Loading by Three-Stage Friction-Grip Elements," *Earthquake Engineering and Structural Dynamics*, 16, 501-521.

[151] Rosen, J. B., (1960). "The Gradient Projection Method for Nonlinear Programming, Part I: Linear Constraints," *SIAM Journal*, 8, 181-217.

[152] Ruiz, S., Urrego, O., and Silva, F., (1995). "Influence of the Spatial Distribution of Energy-Dissipating Bracing Elements on the Seismic Response of Multistorey Frames," *Earthquake Engineering and Structural Dynamics*, 24, 1511-1525.

[153] Samali, B. and Kwok, K. C., (1995). "Use of Viscoelastic Dampers in Reducing Wind- and Earthquake- Induced Motion of Building Structures," *Engineering Structures*, 17, 639-654.

[154] Scholl, R. E., (1993). "Design Criteria for Yielding and Friction Energy Dissipators", *ATC-17-1 Seminar on Seismic Isolation, Passive Energy Dissipation, and Active Control*, San Francisco, CA, 485-496.

[155] Seleemah, A. A. and Constantinou, M. C., (1997). "Investigation of Seismic Response of Buildings with Linear and Nonlinear Fluid Viscous Dampers," *Report No. NCEER 97-0004*, National Center for Earthquake Engineering Research, University of New York at Buffalo, Buffalo, NY.

[156] Shen, K. L. and Soong, T. T., (1995). "Modeling of Viscoelastic Dampers for Structural Applications," *Journal of Engineering Mechanics*, 121(6), 694-700.

[157] Shen, K. L. and Soong, T. T., (1996). "Design of Energy Dissipation Devices Based on Concept of Damage Control," *Journal of Structural Engineering*, 122(1), 76-82.

[158] Shibata, H., Hara, F., Ichihashi, I., Satoh, A., Furukawa, S. I., Kunieda, M., Suzuki, K., Fukuda, T., Takata, K., and Kobayashi, H., (1991). "Development of Elastic-Plastic Damper as a Seismic Support for the Piping System in Nuclear Power Plants", *ASME, Pressure Vessels and Piping Conference*, San Diego, CA.

[159] Shukla, A. K. and Datta, T. K., (1999). "Optimal Use of Viscoelastic Dampers in Building Frames for Seismic Force," *Journal of Structural Engineering*, 125(4), 401-409.

[160] Singh, M. P., Chang, T. S., and Suárez, L. E., (1992). "A Response Spectrum Method for Seismic Design Evaluation of Rotating Machines," *Journal of Vibration and Acoustics*, 114, 454-460.

[161] Skinner, R. I., Beck, R. I., and Bycroft, G. N., (1975). "A Practical System for Isolating Structures from Earthquake Attack," *Earthquake Engineering and Structural Dynamics*, 3.

[162] Skinner, R. I., Kelly, J. M., and Heine, A. J., (1975). "Hysteretic Dampers for Earthquake Resistant Structures," *Earthquake Engineering and Structural Dynamics*, 3.

[163] Skinner, R. I., Robinson, W. H., and McVerry, G. H., (1993). *An Introduction to Seismic Isolation*, John-Wiley & Sons, Chichester, England.

[164] Sobieszcanski-Sobieski, J., Barthelemey, J. F., and Riley, K. M., (1982). "Sensitivity of Optimum Solutions of Problem Parameters," *AIAA Journal*, 20, 1291-1299.

[165] Soong, T. T. and Dargush, G. F., (1997). *Passive Energy Dissipation Systems in Structural Engineering*, John-Wiley & Sons, New York, NY.

[166] Stiemer, S. F., Godden, W. G., and Kelly, J. M., (1981). "Experimental Behavior of a Spatial Piping System with Steel Energy Absorbers Subjected to Simulated Differential Seismic Input," *Report No. UCB/EERC 81-09*, Earthquake Engineering Research Center, University of California at Berkeley, Berkeley, CA.

[167] Su, Y. and Hanson, R., (1990). "Seismic Response of Building Structures with Mechanical Damping Devices," *Report No. UMCE 90-2*, University of Michigan, Ann Arbor, MI.

[168] Sumitomo Metal Industries, (1987). "Friction Damper for Earthquake Response Control," *In-House Report 1987-12*.

[169] Tajimi, H., (1960). "A Statistical Method of Determining the Maximum Response of a Building Structure During an Earthquake", *Proceeding of II World Conference in Earthquake Engineering*, Tokyo, 781-797.

[170] Takewaki, I., (1997). "Optimal Damper Placement for Minimum Transfer Functions," *Earthquake Engineering and Structural Dynamics*, 26, 1113-1124.

[171] Takewaki, I., (1999). "Optimal Damper Placement for Building Structures Including Surface Ground Amplifications", *13th ASCE Engineering Mechanics Division Conference*.

[172] Takewaki, I. and Yoshitomi, S., (1998). "Effects of Support Stiffnesses on Optimal Damper Placement for a Planar Building Frame," *The Structural Design of Tall Buildings*, 7, 323-336.

[173] Takewaki, I., Yoshitomi, S., Uetani, K., and Tsuji, M., (1999). "Non-Monotonic Optimal Damper Placement Via Steepest Direction Search," *Earthquake Engineering and Structural Dynamics*, 28, 655-670.

[174] Tena-Colunga, A., (1997). "Mathematical Modelling of the ADAS Energy Dissipation Device," *Engineering Structures*, 19, 811-821.

[175] Tena-Colunga, A., Del Valle, E., and Perez, M., (1996). "Issues on the Seismic Retrofit of a Building near Resonant Response and Structural Pounding," *Earthquake Spectra*, 12, 567-597.

[176] Tena-Colunga, A. and Vergara, A., (1997). "Comparative study on the Seismic Retrofit of a Mid-Rise Steel Building: Steel bracing vs. Energy Dissipation," *Earthquake Engineering and Structural Dynamics*, 26, 637-655.

[177] Terenzi, G., (1999). "Dynamics of SDOF Systems with Nonlinear Viscous Damping," *Journal of Engineering Mechanics*, 125(8), 956-963.

[178] Tremblay, R. and Stiemer, S. F., (1993). "Energy Dissipation Through Friction Bolted Connections in Concentrically Braced Steel Frames," *ATC-17-1 Seminar on Seismic Isolation, Passive Energy Dissipation, and Active Control*, San Francisco, CA, 557-568.

[179] Tsai, C. S., (1993). "Innovative Design of Viscoelastic Dampers for Seismic Mitigation," *Nuclear Engineering and Design*, 139, 165-182.

[180] Tsai, C. S., (1994). "Temperature Effect of Viscoelastic Dampers During Earthquakes," *Journal of Structural Engineering*, 120(7), 394-409.

[181] Tsai, C. S. and Lee, H. H., (1993). "Applications of Viscoelastic Dampers to High-Rise Buildings," *Journal of Structural Engineering*, 119(4), 1222-1233.

[182] Tsai, C. S. and Tsai, K. C., (1995). "TPEA Device as Seismic Damper for High-Rise Buildings," *Journal of Engineering Mechanics*, 121, 1075-1081.

[183] Tsai, K., Chen, H., Hong, C., and Su, Y., (1993). "Design of Steel Triangular Plate Energy Absorbers for Seismic-Resistant Construction," *Earthquake Spectra*, 9(3), 505-528.

[184] Tsai, K. C., Li, J-W., Hong, C. P., Chen, H. W., and Su, Y. F., (1993). "Welded Steel Triangular-Plate Device for Seismic Energy Dissipation", *ATC-17-1 Seminar on Seismic Isolation, Passive Energy Dissipation, and Active Control*, San Francisco, CA, 687-698.

[185] Tsopelas, P. and Constantinou, M. C., (1994). "NCEER-Taisei Corporation Research Program on Sliding Seismic Isolation System for Bridges: Experimental and Analytical Study of a System Consisting of Sliding Bearings and Fluid Restoring Force/Damping Devices," *Report No. NCEER 94-0002*, National Center for Earthquake Engineering Research, University of New York at Buffalo, Buffalo, NY.

[186] Tsuji, M. and Nakamura, T., (1996). "Optimum Viscous Dampers for Stiffness Design of Shear Buildings," *The Structural Design of Tall Buildings*, 5, 217-234.

[187] Uang, C. M. and Bertero, V., (1988). "Use of Energy as a Design Criterion in Earthquake Resistant Design," *Report No. UCB/EERC-86/10*, Earthquake Engineering Research Institute, University of California, Berkeley, CA.

[188] Vanderplaats, G. N. and Yoshida, N., (1985). "Efficient Calculation of Optimum Design Sensitivity," *AIAA Journal*, 23, 1798-1805.

[189] Wang, B. P. and Pilkey, W. D., (1981). "Optimal Damper Location in the Vibration Control of Large Space Structures", *AIAA Symposium on Dynamics and Control of Large Flexible Spacecraft*, Blacksburg, VA, 379-392.

[190] Wen, Y. K., (1980). "Equivalent Linearization of Hysteretic Systems Under Random Excitation," *Journal of Applied Mechanics, ASME*, 47(EM2), 150-154.

[191] Whittaker, A., Aiken, I., Bergman, D. M., Clark, P., Cohen, J., Kelly, J. M., and Scholl, R., (1993). "Code Requirements for the Design and Implementation of Passive Energy Dissipation", *ATC-17-1 Seminar on Seismic Isolation, Passive Energy Dissipation, and Active Control*, San Francisco, CA, 497-508.

[192] Whittaker, A., Bertero, V., Thompson, C., and Alonso, J., (1989). "Earthquake Simulator Tests of Steel Plate Added Damping and Stiffness Elements," *Report No. UCB/EERC 89-02*, Earthquake Engineering Research Center, University of California at Berkeley, Berkeley, CA.

[193] Whittaker, A., Bertero, V., Thompson, C., and Alonso, J., (1991). "Seismic Testing of Steel Plate Energy Dissipation Devices," *Earthquake Spectra*, 7, 563-604.

[194] Wu, B., Ou, J. P., and Soong, T. T., (1997). "Optimal Placement of Energy Dissipation Devices for Three-Dimensional Structures," *Engineering Structures*, 19, 113-125.

[195] Xia, C. and Hanson, R., (1992). "Influence of ADAS Element Parameters on Building Seismic Response," *Journal of Structural Engineering*, 118, 1903-1918.

[196] Xia, C., Hanson, R., and Wight, J., (1990). "A Study of ADAS Element Parameters and Their Influence on Earthquake Response of Building Structures," *Report No. UMCE 90-12*, University of Michigan, Ann Arbor, MI.

[197] Yang, T-S. and Popov, E. P., (1995). "Experimental and Analytical Studies of Steel Connections and Energy Dissipators," *Report No. UCB/EERC 95-13*, Earthquake Engineering Research Center, University of California at Berkeley, Berkeley, CA.

[198] Youssef, N. and Guh, T. J., (1993). "Seismic Retrofit of Structures with Passive Energy Dissipation Devices", *ATC-17-1 Seminar on Seismic Isolation, Passive Energy Dissipation, and Active Control*, San Francisco, CA, 639-650.

[199] Zhang, R. H. and Soong, T. T., (1989). "Seismic Response of Steel Frame Structures with Added Viscoelastic Dampers," *Earthquake Engineering and Structural Dynamics*, 18, 389-396.

[200] Zhang, R. H. and Soong, T. T., (1992). "Seismic Design of Viscoelastic Dampers for Structural Applications," *Journal of Structural Engineering*, 118(5), 1375-1392.

Vita

Luis M. Moreschi was born on November 15, 1966, in the city of San Luis, Argentina. He earned a Bachelor of Science degree in Civil Engineering from National University of San Juan, Argentina, in 1992. In May 1995, he received a Master of Science degree in Civil Engineering from University of Puerto Rico at Mayagüez. After working for a year as a structural engineer, he joined the Engineering Science and Mechanics Department at Virginia Polytechnic Institute and State University (Virginia Tech) to continue his graduate studies. He received a Doctor of Philosophy degree in Engineering Mechanics on July 10, 2000.

Luis M. Moreschi

July, 2000